UNIVERSITY OF MINNESOTA
ST. ANTHONY FALLS LABORATORY

Project Report No. 492

Wind velocity profiles and shear stresses downwind from a canopy: Experiments in a wind tunnel

by

Angel L.S. Perez, Dane A. Jaster,
James Thill, Fernando Porte-Agel and Heinz Stefan

Prepared for
National Center for Earth Surface Dynamics

May 2007
Minneapolis, Minnesota

Abstract

We are interested in the shear stresses exerted by wind on a lake surface, especially if a lake has a small surface area. We have therefore begun to study the development of the atmospheric boundary layer over a small lake surrounded by a vegetation canopy of trees or cattails. Wind tunnel experiments have been performed to simulate the transition from a canopy to a flat solid surface. In the first experiment we used several layers of chicken wire with a total height of 5cm, a porosity of 98.8% and a length of 2.4m (8 ft) in flow direction to represent the vegetation canopy, and the floor of the wind tunnel consisting of plywood was used to represent the lake. The chicken wire represents a porous step that ends at x=0. This experimental set-up was considered to be a crude representation of a canopy of tress or other vegetation that ends at the shore of a lake. In a second experiment we used an array of pipe cleaners inserted in a styrofoam board to represent the canopy. The porosity of that canopy was 78%. In a third experiment we used a solid step which could be a simplified representation of a high bank or buildings on the upwind side of the lake.

Wind velocity profiles were measured downstream from the end of the canopy or step at distances up to x=7m. Using the velocity profile at x=0, the absolute roughnesses of the two canopies were determined to be 1.3 cm and 0.5 cm, respectively, and the displacement heights were determined to be 2.3 cm and 6.6 cm. The roughness of the wind tunnel floor downstream from the canopy was determined to be 0.00001m =0.01mm.

Three distinct layers were identified in the measured velocity profiles downstream from the canopy: the surface layer in response to the shear on the wind tunnel floor, an outer layer far above the canopy, and a mixing/blending layer in between. With sufficient distance downwind from the canopy the mixing layer should disappear, and the remaining two layers should form the well-known logarithmic velocity profile. In other words the memory of the canopy should become erased from the velocity profile with sufficient distance downstream. The shear stress on the wind tunnel floor was found to approximately double from x=0 to about x/h=100. Changes of mass fluxes, momentum fluxes and energy fluxes integrated with height above the wind tunnel floor were related to the distance from the edge of the canopy (x=0). The aerodynamically rough and porous canopy made the velocity profiles and the associated fluxes substantially different from those downstream from a solid step. One significant difference was the absence of a separated flow region downstream from the highly porous canopy. Instead, the velocity profile coming out of the rougher and more permeable canopy was linear with distance above the wind tunnel floor. Essentially the velocities profiles differ because of two attributes: the canopy roughness (z_0) and the canopy porosity. We believe that the (initial) shape of the each velocity profile at the end of the canopy is given by the canopy roughness, while the velocity profiles downwind from the canopy are shaped by both roughness and the porosity of the canopy.

The three experiments performed, the data obtained, and results of a first data analysis will be described in this report in three parts (A,B and C).

Independent (input) variables in the three experiments

Canopy porosity	0%	78%	98%
Height of canopy, h (m)	0.0508	0.075	0.05
Wind tunnel velocity setting (m/s)	10	10	15
Reference velocity U_r (m/s)*	8.95	9.46	13.09
Displacement height in canopy d (m)	0.0508	0.066	0.023
Absolute roughness of canopy z_{0i}(m)	0.00001	0.005	0.013
Absolute roughness of wind tunnel floor z_{0s} (m)	0.00001	0.00001	0.00001

*U_r is the velocity measured at the end of the canopy at a height z=6h above the wind tunnel floor. (h=height of the canopy)

Porosity	$\ln\left(\frac{z_{0i}}{z_{0s}}\right)$	d/h	U* (m/s)	τ^* (N/m^2)	U* / U_r
0%	0	1	2.2	6.3	0.25
78%	6.215	0.88	2.3	7.6	0.24
98%	7.170	0.46	2.65	9.2	0.20
100%	0	0	n/a	n/a	n/a

Table of Contents of Parts A, B and C

Part A contains all sections listed
Parts B and C contain abbreviated sections 2 through 4.1

List of Figure Titles

Part A contains the complete set of figures listed below. Part B and Part C contain a selective number of these figures. Figure titles are identical in all three parts.

Part A. Chicken wire experiment

Summary of independent experimental variables for data set #1 (chicken wire)

Height of canopy (chicken wire): h = 0.05m or 5.0cm
Velocity setting in wind tunnel: 15 m/s
Velocity profiles taken at: x=0.0m, 0.2m, 0.4m, 0.6m, 1.1m, 1.8m, 2.76m, 5.4m

Reference velocity at x=0m and height z= 6h: U_{ref} = 13.09 m/s
Reference height: h = 0.05m or 5.0cm

Computed canopy porosity: ε = 98.0%
Computed canopy roughness: z_{0c} = 0.013 m
Computed canopy displacement height: d = 0.023 m
Computed canopy shear velocity: U* = 1.73 m/s

Computed surface roughness downstream from canopy: z_{0s} = 0.00001 m

1. Introduction

The surface mixed layer (SML) of lakes is the most dynamic zone within the limnological system. Turbulent mixing in the SML is the primary facilitating mechanism of transport of momentum, heat, and mass from the air-water interface into the water. The rate of transport of momentum, heat, and mass across the surface of a lake is known to depend on the wind stress on the water surface.

Surface mixed layer deepening destroys stratification. Stratification is known to limit gas transfer (most notably, O_2) in the water column of lakes and reservoirs and to affect the sediment chemistry (Condie and Webster 2001; Hocking and Patterson 1994; Portielje and Lijklema 1995; Kolb and Heineman 1995). In engineered aquatic systems constructed for contaminant removal, such as stormwater detention ponds and wetlands, stratification is generally considered undesirable (Lawrence and Breen 1998). Surface layer turbulent mixing, and its effects on stratification, is a crucial underpinning of our understanding of many ecological, geochemical, and physical processes that occur in lakes. Forced convection induced by wind stress on the water surface, and free thermal convection induced by heat loss from the water to the atmosphere are the main processes that generate SML turbulence. Of these, the effect of wind stress is much less well understood (Wüest and Lorke 2003).

While arguably among the most important forces in the hydrodynamic balance of the limnological system, wind stress on the surface of a small water body is not well documented. Direct observations of wind over or near lakes are not only uncommon but also questionable because of uncertainty about the spatial inhomogeneity of the instantaneous and time averaged wind field. More common are measurements at local weather stations, typically several kilometers from the lake of interest. Often these measurements bear little predictable correlation with wind speeds directly over lakes. This lack of observation

necessitates that numerical lake models for water quality calibrate wind speed by an unknown parameter referred to as the "wind sheltering coefficient" (Hondzo and Stefan, 1993). The calibrated wind speed is unlikely to represent wind speed at a particular point in space and time; rather the calibration provides an areally and temporally averaged wind speed that minimizes the mean residual between the model results and data. While practical for zero or one-dimensional lake models, this approach neglects meaningful and significant details of non-uniform wind speed distributions over lakes that are likely to be important for the construction of physically realistic three-dimensional lake models (e.g. Edinger 2001, Wang and Hutter 1998; Wang, Hutter, and Bäuerle 2001; Wang 2003).

Momentum transfer at a lake surface

The transport of momentum across the air-water interface generally occurs from the atmosphere to the water. As the wind impinges on the water surface, the water surface generates a drag on the wind, slowing the wind nearest the water surface. Because water is a Newtonian fluid, the drag force accelerates the water surface. As the shear stress on the water surface accumulates, instabilities form and quickly become "cat's paws" (Dorman and Mollo-Christensen 1973) and capillary-gravity waves. The added roughness of the capillary wave field imposes a larger drag between the wind and the water, thereby enhancing momentum transport and requiring an additional energy input to maintain the waves (Belcher and Hunt 1998; Wüest and Lorke 2003). At wind speeds of a few meters per second, the capillary wave field reaches a state of saturation, after which increasing the wind stress does not generate more or larger capillary waves (Mourad, Thompson, and Vandemark 2000). Beyond capillary wave saturation, further transport of momentum into the water surface layer serves to generate larger waves that are superimposed on the capillary wave field.

The preceding description of the momentum transport (τ) from wind to water suggests that the momentum is transported via two distinct pathways (surface boundary layer shear stress, τ_{SBL}, and wave formation/maintenance shear stress,

τ_{WAVE}) at the water surface (Anis and Moum 1995; Terray et al. 1996; Burchard 2001; Wüest and Lorke 2003).

The shear stress is partitioned as

$$\tau = \tau_{SBL} + \tau_{WAVE} \quad \left[F / L^2\right] \tag{1.1}$$

and can be parameterized as

$$\tau = C_D \rho_a \overline{U}^2 \quad \left[F / L^2\right] \tag{1.2}$$

In the previous equation, C_D is an empirical drag coefficient, ρ_a is the density of air, and $\overline{U}$ is the time averaged streamwise wind velocity at some specified height above the water surface. The drag coefficient is a function of wave roughness, which is a rather complicated function of both wind speed and the state of wave development or wave age A_W. The wave age is simply the ratio of wave phase speed c_p to either the wind velocity or to roughly 30 times the air shear velocity $U*$.

$$A_W = \frac{c_p}{\overline{U}} \approx \frac{c_p}{30U*} \tag{1.3}$$

By this association of C_D with A_W and with $\overline{U}$, a relationship between C_D and $\overline{U}_{10}$ (wind speed measured at 10 m height) can be established. As A_W gets larger (i.e. the waves "mature" or get "older"), the waves approach an equilibrium at which the restoring force that tends to damp the waves is just balanced by τ_{WAVE}. The large energy carried by each wave is generally dissipated by wave breaking in shallow water or against the shoreline and contributes little to the generation of turbulent mixing in the lake surface layer except near shore. For immature wave fields (those farther upwind of more mature wave fields), the momentum of individual waves is smaller and more difficult to consistently maintain. Therefore, the balance between restoring forces and τ_{WAVE} is much more sporadic, as the waves are continuously formed and destroyed (by breaking) on small scales at a high frequency. The net effect of the smaller wave breaking is to convert a large portion of τ_{WAVE} into turbulence producing energy that is used to mix the surface layer (Banner and Phillips 1974; Banner and Peregrine 1993; Thorpe 1995; Melville 1996). It is important to note, in Figure 3.1, that the data shown

represent a relationship that is valid only for mature wave fields (i.e. $A_W \approx 1.14$ to 2.0). For "younger" wave fields, the waves are still accelerating (and breaking frequently) with respect to the mean wind forcing. Because much of the wind stress is partitioned into wave development and breaking, the aerodynamic drag coefficient associated with younger waves is higher than that associated with more mature waves that are traveling with a phase speed of the order of the wind speed. Consequently, the case of well-developed waves represents a lower bound on the drag coefficient associated with a given wind speed (Wüest and Lorke 2003). In small and medium lakes, wind speed is generally low, i.e. < 5 m/s, representing the greatest variability in drag coefficients. Because of sheltering and limited fetch, wave fields on lakes are often immature. In addition to spatial wind speed variability, these interactions are the primary complications in determining momentum transfer from the atmosphere into the lake surface boundary layer.

In this paper, we present results from a wind tunnel experiment designed to study the transition from a vegetation canopy to a water surface (Figure 1.1). The purpose of the experiment was to measure and analyze the velocity profiles and surface shear stresses downstream from the canopy for potential use in lake water quality models.

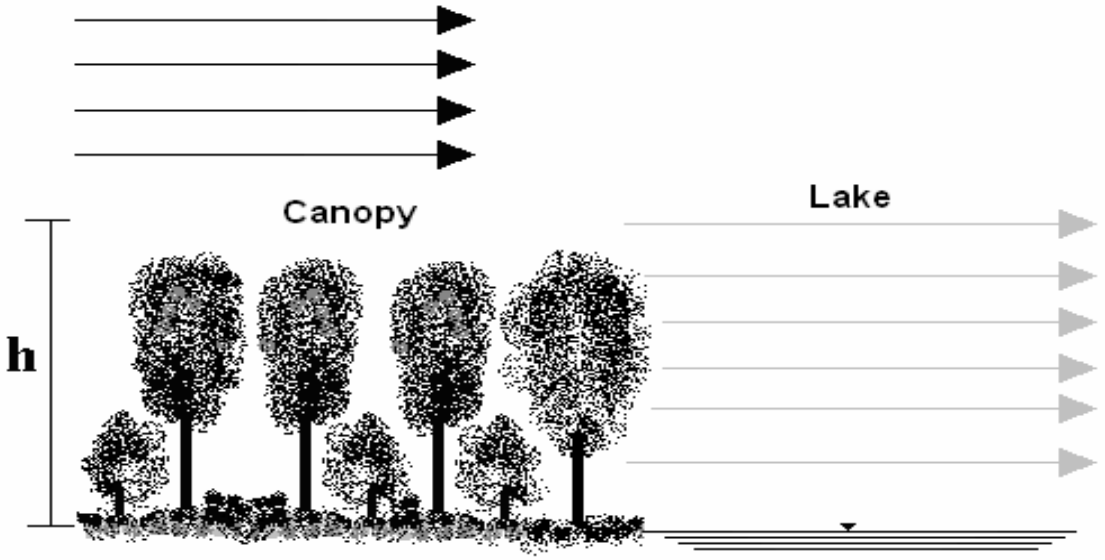

Figure 1.1. Schematic view of a tree canopy around a lake

2. Wind tunnel experiment

The experiment was conducted in the boundary layer wind tunnel of the Saint Anthony Falls Laboratory at the University of Minnesota. The tunnel can be operated in both open and closed (recirculating) circuit and it allows for control of the air temperature and mean wind velocity up to a maximum of 30 m/s. The test section is 1.7 m wide, 1.8 m high, and 16 m long (Figure 2.1). More details on the wind tunnel characteristics are given by Farell and Iyengar (1999). In this study, the tunnel was operated in closed circuit and the average velocity was 15 m/s.

The canopy was simulated by a layer of dense chicken wire placed over the wind tunnel floor (Figure 2.2). The porosity of the wire was determined to be 98.0 %. This model canopy covered the total width of the wind tunnel and extended over a length of 1.2m (4 ft) in the flow direction. The canopy had a height of *approximately* 5 cm.

The floor of the wind tunnel consisted of painted plywood, and represented a smooth surface. The experiment was run at an air temperature of 28^{o}C. The Reynolds number based on model canopy height of 0.05 m was therefore approximately Re = (15)(0.05)(67000) = 50 000. Based on wind tunnel height of H = 1.6 m it would have been Re = 1 800 000. A Pitot tube was used to measure the time-averaged wind velocity at different positions in the boundary layer. The Pitot tube had 3mm outer diameter and was mounted on a traversing mechanism that allowed vertical positioning above the wind tunnel floor. Measurements were made along the centerline of the wind tunnel test section, i.e. 0.85m from the lateral walls. At each position of the Pitot tube an average velocity over seconds was recorded, and stored in the data base used in the analysis. In particular, vertical profiles of wind velocity were collected over the chicken wire mesh near the transition and also at seven different positions downwind of the transition (0.2 m, 0.4 m, 0.6 m, 1.1 m, 1.8 m, 2.76 m and 5.4 m).

Figure 2.1. Test section of the St. Anthony Falls Laboratory wind tunnel (looking upwind)

Figure 2.2: Canopy represented by chicken wire mesh, 98% porosity, 5cm height

3. Data analysis and results

3.1 Velocity data

The data were analyzed using Microsoft Excel. The wind velocity profiles in the transition from a canopy to a lake surface are expected to be a hybrid between a separated flow and a logarithmic profile. Figures 3.1 and 3.2 show the measured velocities plotted against the vertical position (distance to the wind tunnel floor) using both linear and semi logarithmic scales.

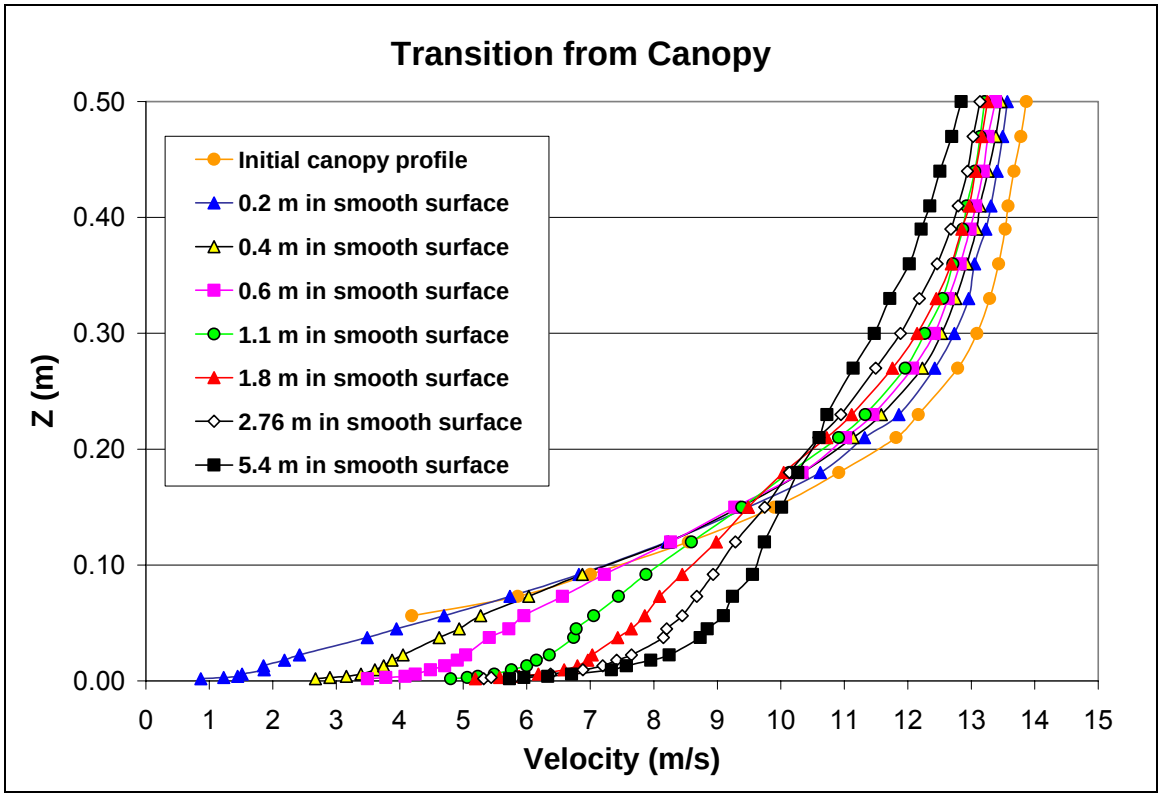

Figure 3.1: Velocity profiles in Cartesian coordinates

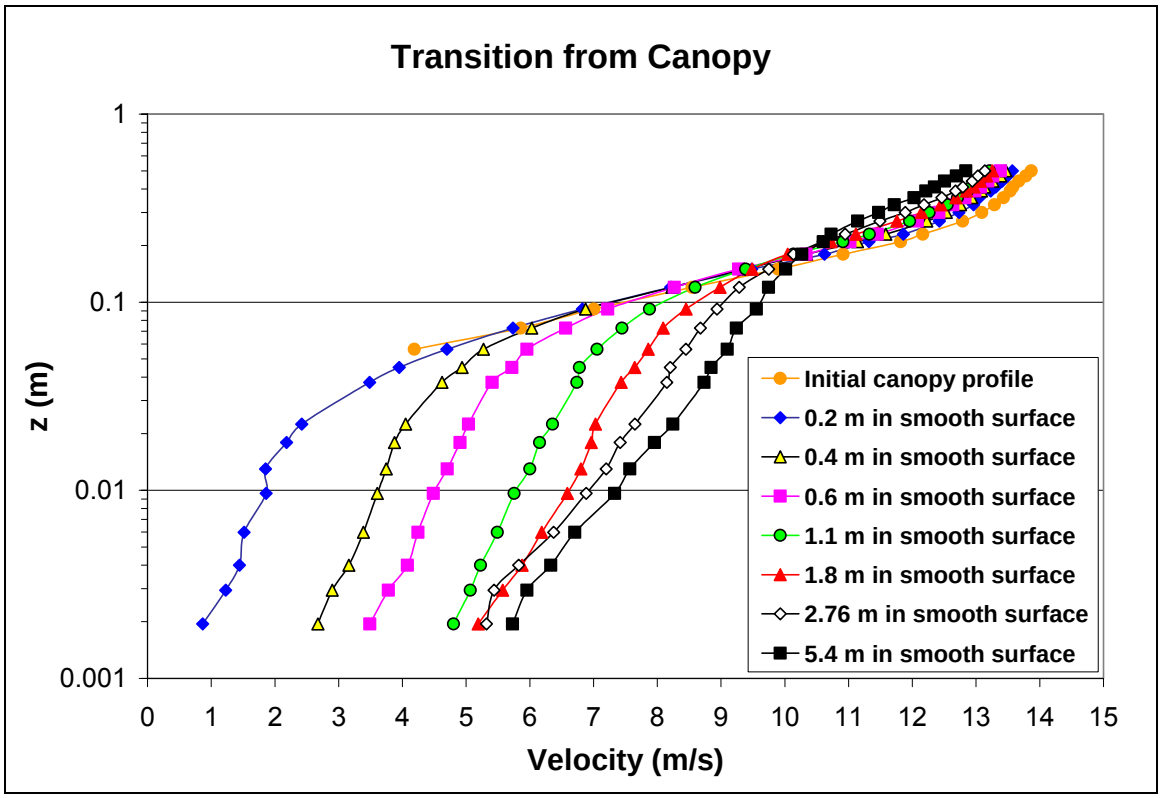

Figure 3.2 Semi-logarithmic plot of velocity profiles

In the analysis the wind velocity profiles were divided into three layers: a surface (boundary) layer, a blending layer and an outer layer. The surface layer is affected by the roughness of the lakes surface. The outer layer is far above the canopy. The blending layer is between the outer layer and the surface layer. In the blending layer momentum is transferred from the outer layer to the surface layer.

3.2 Surface (boundary) layer: Surface roughness, surface shear stress and surface layer thickness downwind from the canopy

The surface (boundary) layer was analyzed first. This layer is affected by the shear stress acting on the wind from the water surface. In this layer a logarithmic velocity profile fits the data.

The shear velocity U_* and the roughness length z_0 of the wind tunnel surface can be found using the Prandtl-von Karman equation

$$\frac{U}{U_*} = \frac{1}{\kappa} \ln\left(\frac{z}{z_0}\right) \tag{3.1}$$

In this equation, U(z) is the wind velocity, U_* is the shear velocity, k is the von Karman constant (0.4), z is the height, and z_0 is the aerodynamic roughness height. The above equation can be rewritten as

$$U = \frac{U_*}{k}(\ln z) - \frac{U_*}{k}\ln(z_0) \tag{3.2}$$

Equation 3.2 resembles a straight line equation given by the function

$$y = ax + b \tag{3.3}$$

where $y = U$, $a = \frac{U_*}{k}$, $b = -\frac{U_*}{k}\ln(z_0)$ and $x = \ln(z)$.

Since "a" is the slope of the line, one can find U_* from the slope of a semi - logarithmic velocity profile plot. "b" is the intercept of the straight line at x = 0. We can therefore find z_0 graphically by extrapolating the straight line drawn through the wind speed data on a semi-log graph to the height where U = 0. The absolute roughness of the wind tunnel floor z_0 was determined to be roughly 0.00001 m (Figure 3.3). It should be recalled that the wind tunnel floor represents the water surface of the lake which will have a different roughness. This value of z_0 is consistent with previous data collected in the same wind tunnel.

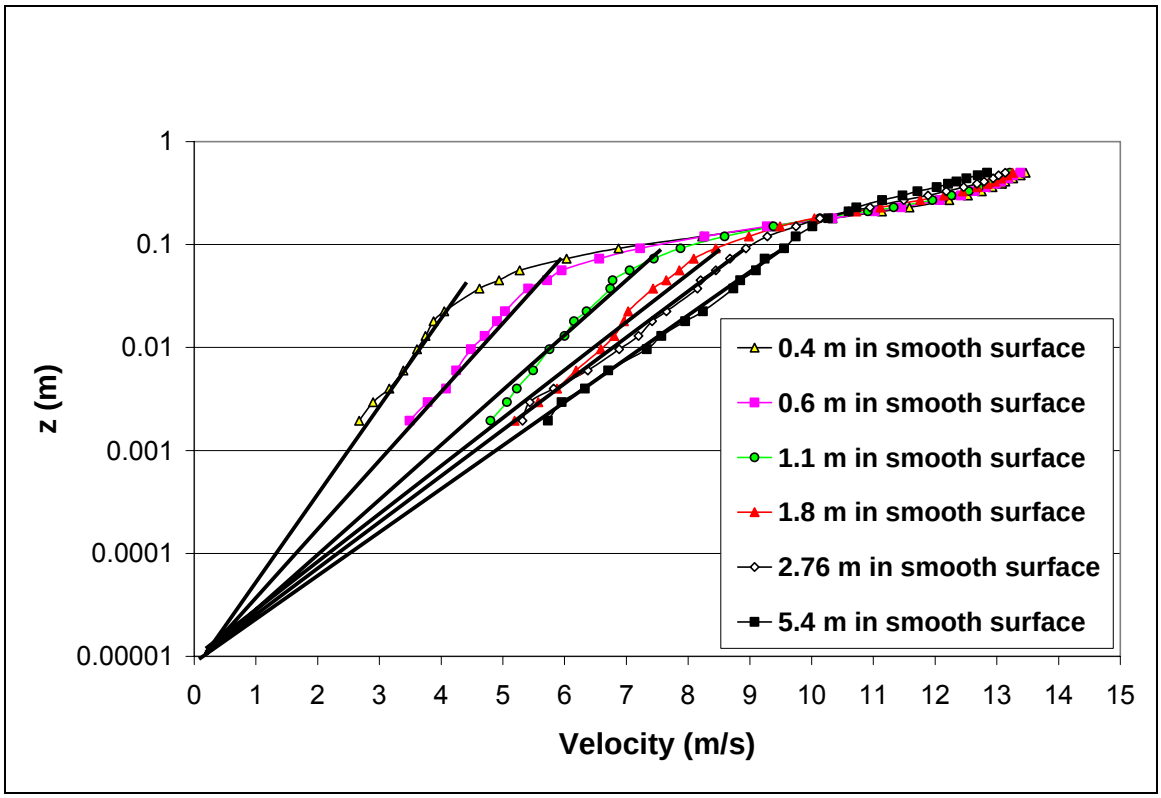

Figure 3.3 Determination of surface roughness (z_{0s}) downstream from canopy

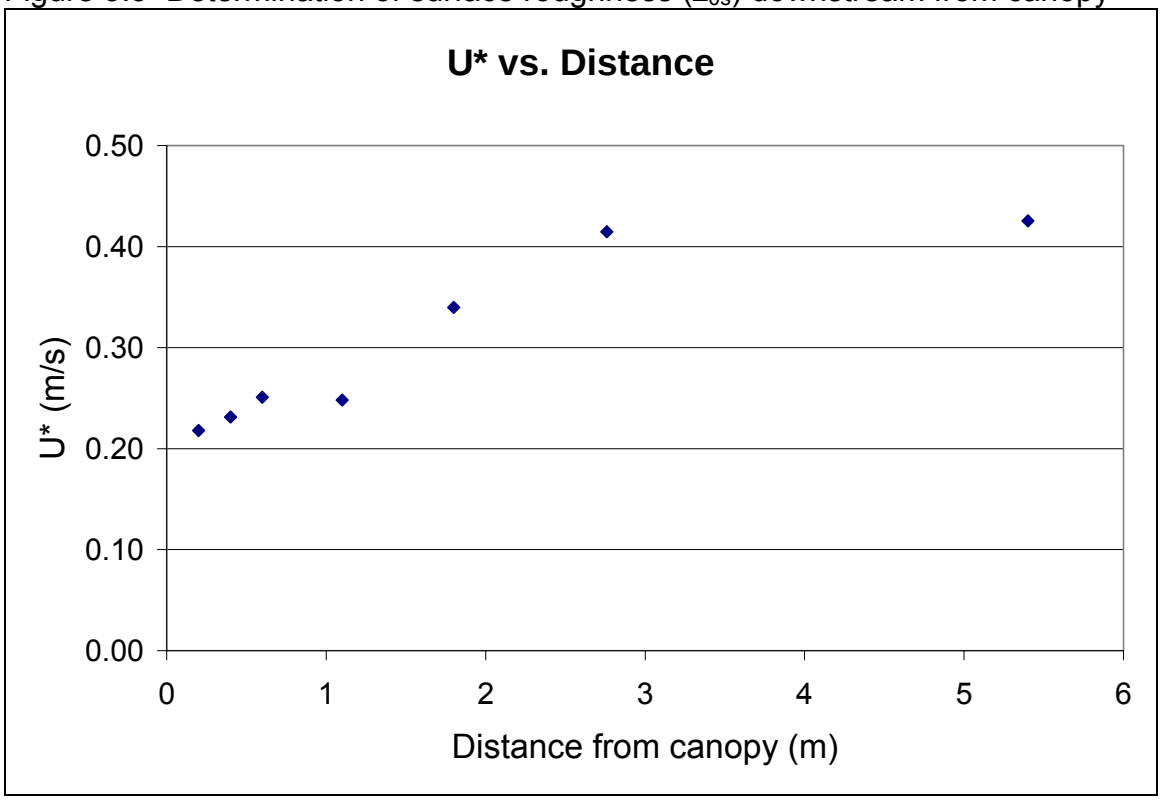

Figure 3.4 Shear velocity (U_*) vs. distance from canopy

The shear velocity U_*, also determined from Figure 3.3 increases as the distance downwind from the edge of the canopy is increased (Figure 3.4). This velocity increase is associated with the increase in wind velocity across the surface. In the immediate wake of the canopy the water surface is sheltered from the wind, but the wind velocity on the surface increases with distance from the shelter.

Because shear stress is difficult to measure directly, the shear velocity is used to estimate shear stress as

$$\tau = \rho U_*^2 \tag{3.4}$$

In the previous formula, τ is the shear stress, ρ is the density of air (1.29 kg/m^3), and U_* is the shear velocity. From the computed values for U_*, the shear stress was determined. Figure 3.5 displays the shear stress values. The shear stress increases as the distance from the canopy is increased, similarly to the shear velocity. Wind in the outer layer pushes across the blending layer into the slower lower surface layer creating extra shear.

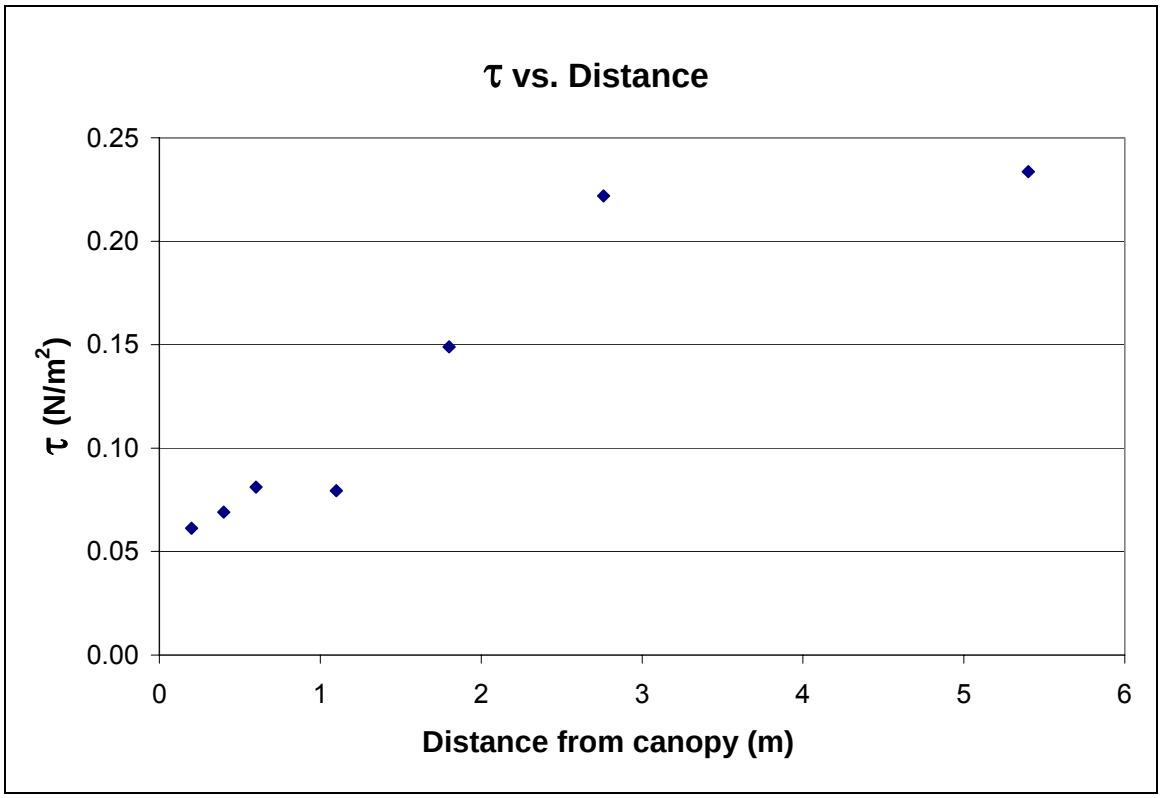

Figure 3.5 Surface shear stress (τ) vs. distance from canopy

With increasing distance from the canopy, the surface layer seems to be growing in thickness. The upper end or thickness of the surface layer (y1) was determined from the semi-logarithmic plots of the velocity profiles (Figure 3.2). The ln(z)-values of the first six velocity measurements above the wind tunnel floor were plotted in Cartesian coordinates, and a straight line was fitted. Where the linear fit to the semi-logarithmic velocity profile deviated by a value of 0.02 m/s, the surface layer was assumed to end. The corresponding point was identified by the height y1 in Figure 3.6. Similarly a straight line was fitted to the data points in the blending layer on the semi-logarithmic plot of the velocity profiles. Where the linear fit deviated from the actual velocity profile by a value of 0.02 m/s, the blending layer was assumed to end. That point was identified by the height y2 in Figure 3.7. Results of y1 and y2 are plotted in Figure 3.8 vs. distance. The thickness y1 of the surface layer has a value of 0 at the end of the canopy and increases linearly with distance. It reaches a maximum height of 0.2

m above the surface at a distance of about 6 m; this is equivalent to 4h where h = 0.05m is the height of the canopy. y2 also asymptotically approaches 0.2m. The diminishing distance between y1 and y2 is noteworthy; it indicates that the transition from the surface layer to the blending layer vanishes at about 6m or 120h, where h is the height of the canopy.

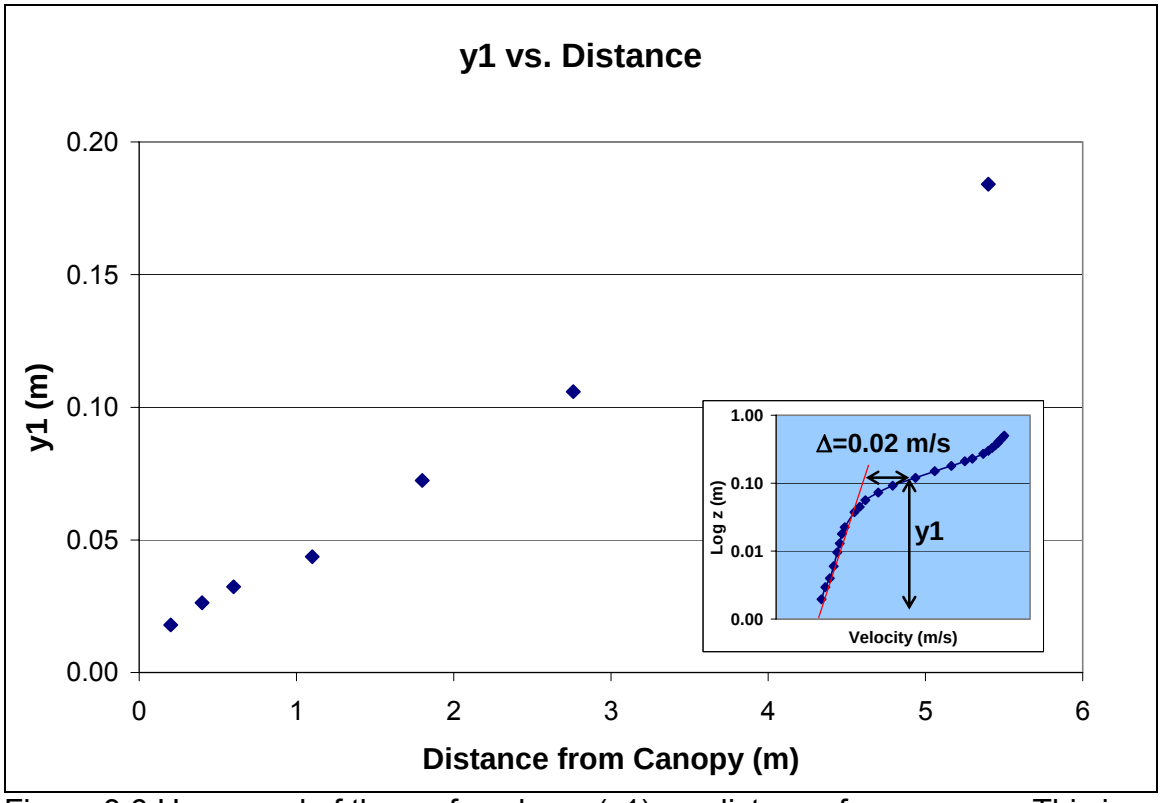

Figure 3.6 Upper end of the surface layer (y1) vs. distance from canopy. This is the **thickness of the surface layer**

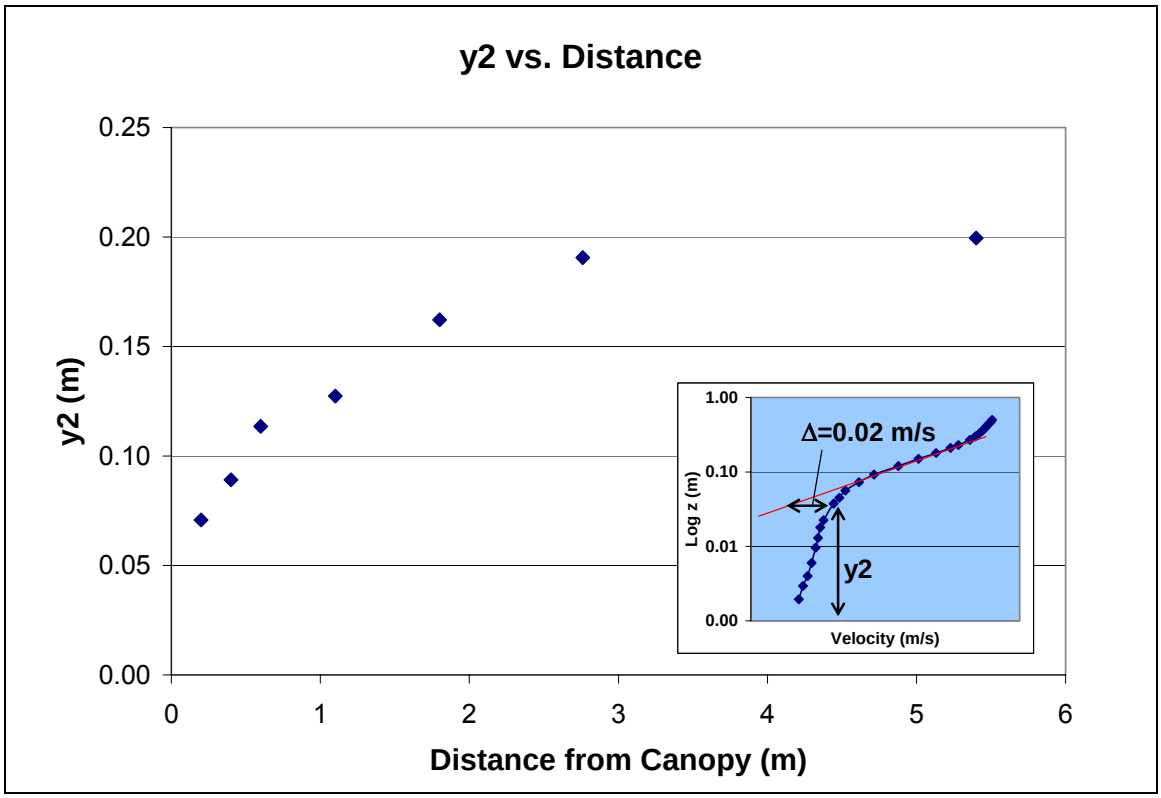

Figure 3.7 Lower end of blending layer (y2) vs. distance from canopy

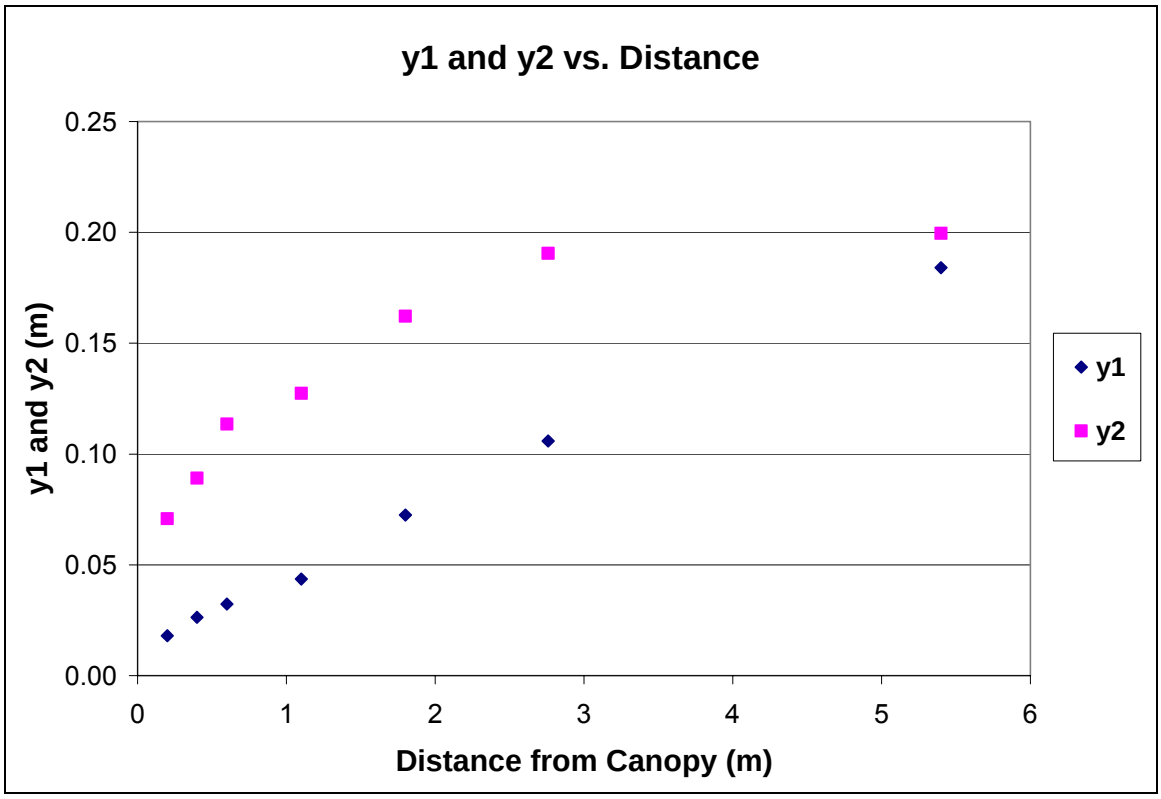

Figure 3.8 Upper end of surface layer (y1) and lower end of blending layer (y2) vs. distance from canopy

L

3.3 Mixing (transition, blending) layer: location and thickness of the mixing/blending layer downwind from the canopy

In the mixing/blending layer, wind velocities make a transition from the low velocities of the surface layer to the high velocities in the outer layer. The surface layer begins to blend into the mixing layer where the logarithmic velocity profiles deviate from their linear trend. In the mixing/transition/blending layer the measured velocity profile no longer follows a logarithmic law. Therefore the Cartesian velocity profiles are used to determine the thickness of the mixing/blending layer.

Two linear portions can be seen in the Cartesian plots of each velocity profile in Figure 3.1. Linear equations were fitted to the data points that compose each linear portion. Two points (y3 and y4) were determined for each profile where the linear fits to the Cartesian velocity profile deviated by a value of 0.02 m/s from the actual data. The linear fit for y4 was determined using the very last four data points, while the previous four points were used to determine y3. The height y3 identifies the upper end of the mixing layer (Figure 3.9) and y4 gives the lower end of the outer layer (Figure 3.10).

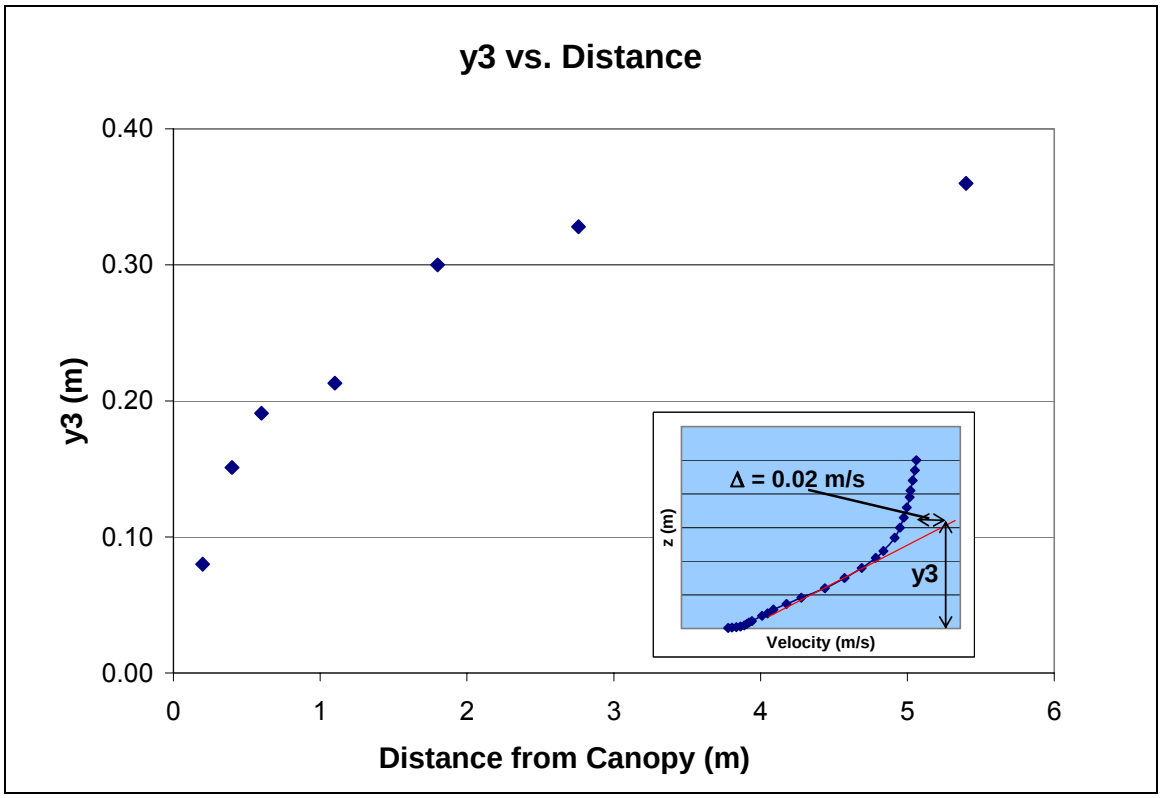

Figure 3.9 Upper end of the blending layer (y3) vs. distance from canopy

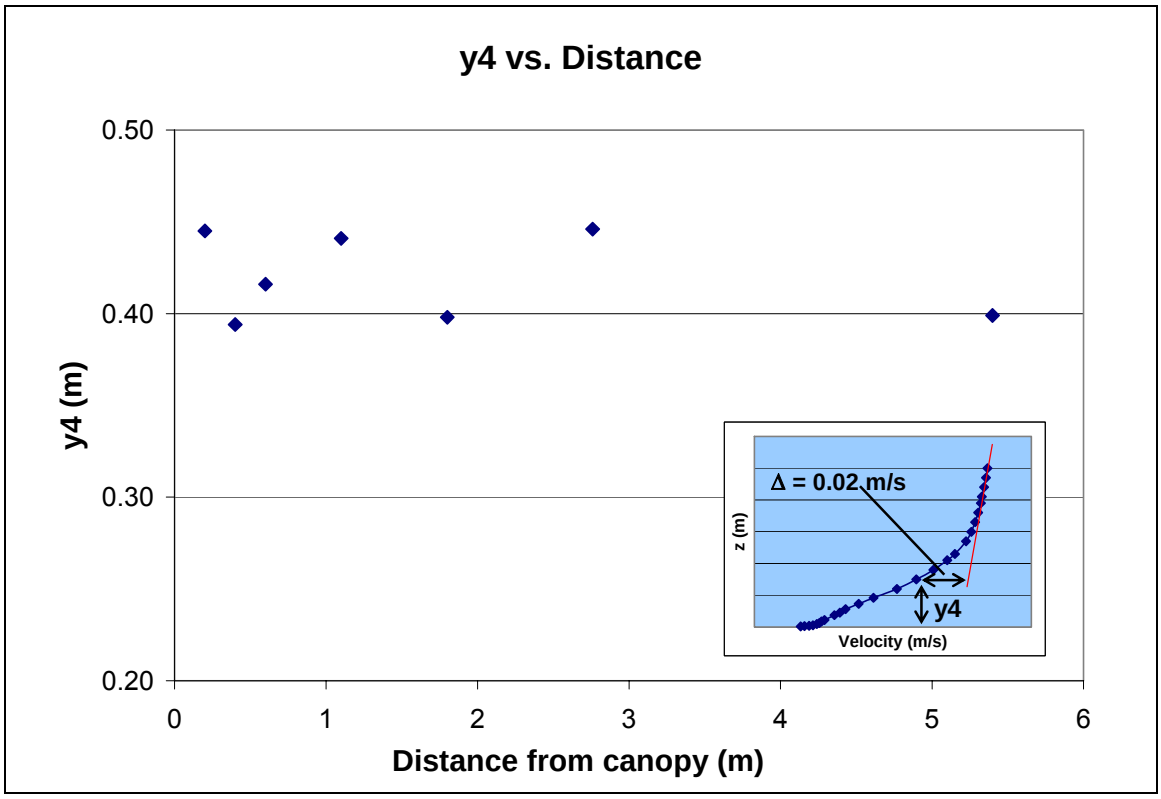

Figure 3.10 Lower end of outer layer (y4) vs. distance from canopy

As the distance from the canopy increases, the distance y3 increases but appears to converge to a height of about 0.40 m (Figure 3.9). The distance y4 shows no dependence on distance from the canopy; it is fairly constant between 0.40m and 0.45m (Figure 3.10). Results from Figures 3.9 and 3.10 have been combined in Figure 3.11. The values of y3 and y4 converge to an approximate value of 0.40 m above the wind tunnel floor; this is equivalent to 8h where h = 0.05m is the height of the canopy. The distance y4 is approximately the beginning of the outer layer.

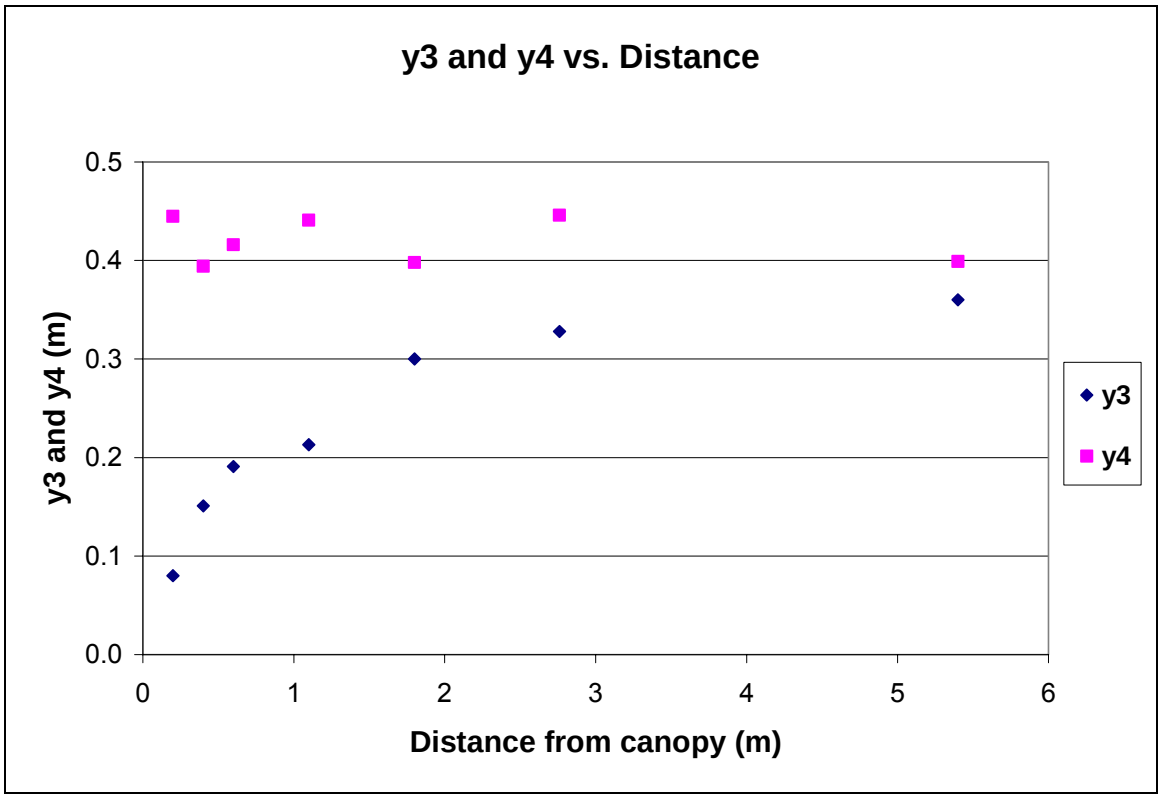

Figure 3.11 Upper end of the blending layer (y3) and lower end of the outer layer (y4) vs. distance from canopy

The thickness of the mixing/blending layer is the distance between y2 and y3 which have been plotted vs. distance from the canopy in Figure 3.12. This thickness begins at zero because at the edge of the canopy there is no mixing or

blending layer. Beyond the canopy, a surface layer develops, and the outer layer begins to transfer momentum into the surface layer through the mixing/blending layer. Downwind, as the distance from the canopy increases, the mixing layer thickens and attains a value of about 0.2 m or 4h at a distance x = 55h. One would expect the mixing layer to disappear further downwind.

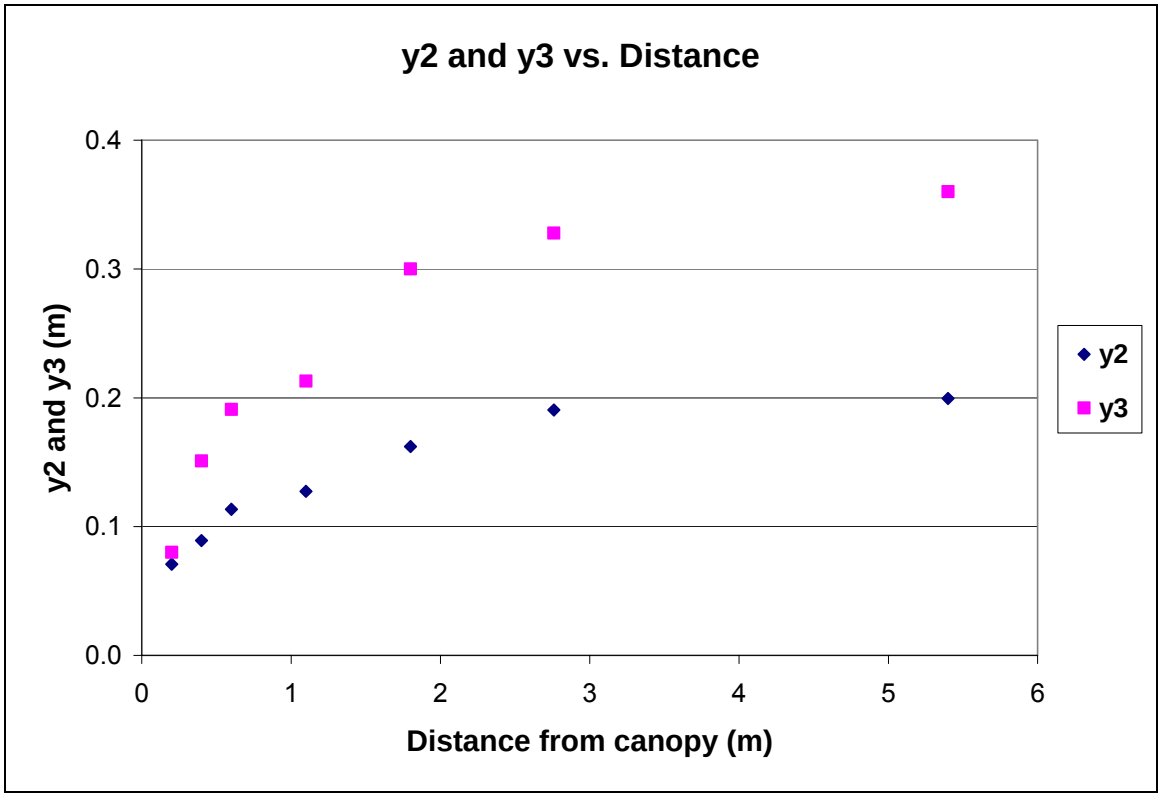

Figure 3.12 Upper (y3) and lower (y2) end of the mixing/blending layer vs. distance from the canopy. The distance between y2 and y3 is the **thickness of the mixing/blending layer**

In Figure 3.13 the heights y1 and y4, i.e. the upper end of the surface layer and the lower end of the outer layer, respectively, are plotted. As the thickness y1 of the surface layer grows, the distance between y1 and y4 diminishes. This occurs as the thickness between y2 and y3 increases. The point where both plots have the same thickness of 0.20m occurs at about 4m or 80h away from the canopy (Figure 3.14). At this point the mixing/blending layer has reached its maximum thickness. Beyond this point, the blending layer diminishes in thickness until it

completely disappears. At that distance the canopy has lost its effect and the wind velocity profiles consists of a surface layer and an outer layer only, i.e. the wind velocity profile matches the classical boundary layer profile, and has lost its memory of the canopy. Unfortunately, our measurements extended only to a distance x=5.4m or 108h. The expected loss of the mixing layer thickness cannot be seen in Figure 3.12 but is apparent in Figure 3.13.

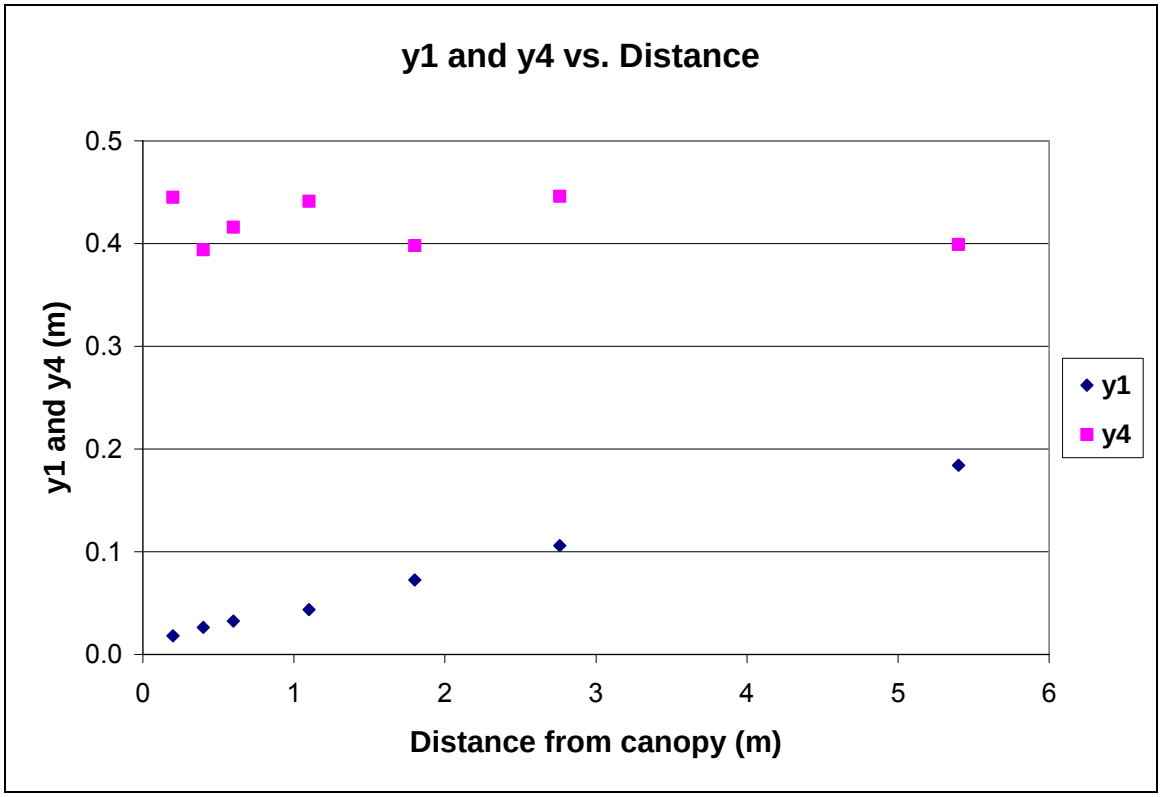

Figure 3.13 Upper end of surface layer (y1) and lower end of outer layer (y4) vs. distance from canopy

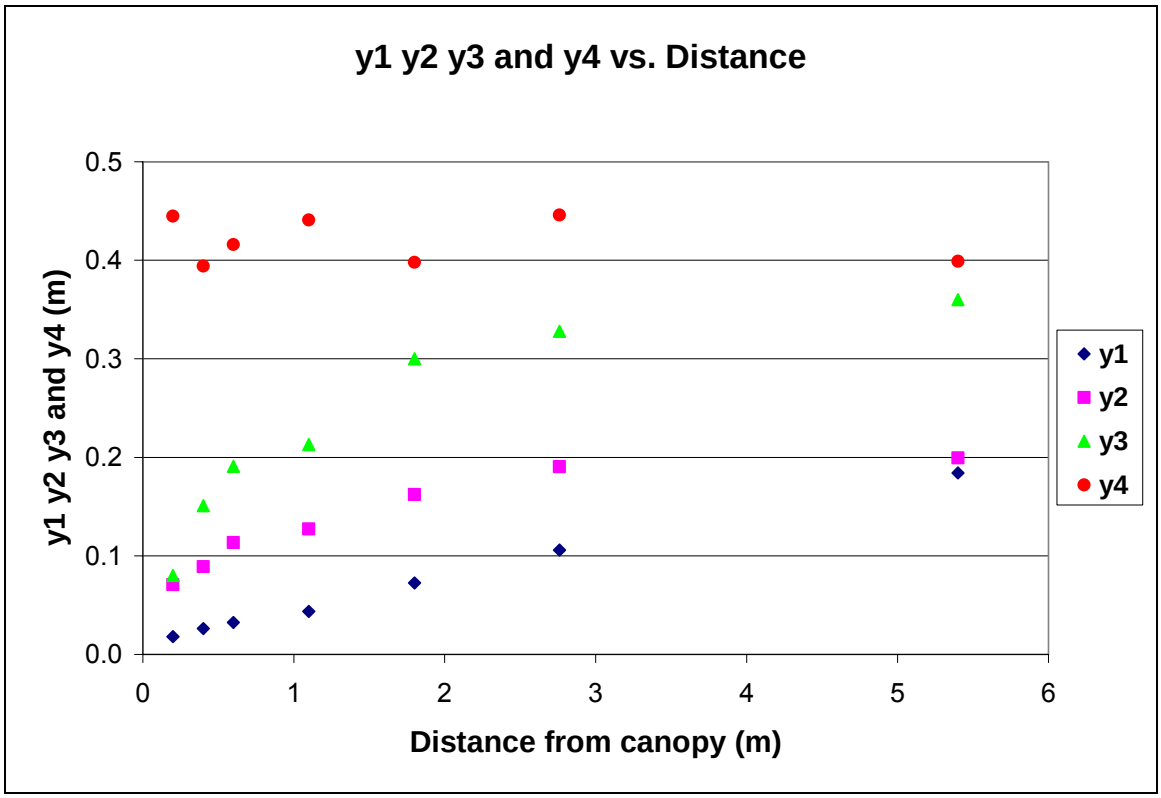

Figure 3.14 Upper and lower boundaries of the surface layer, the mixing layer and the outer layer

3.4 Outer (free stream) layer

Above the surface (boundary) layer and the mixing/blending layer, there is the outer/free stream layer. In a wind field without upper boundary the free stream velocity would not vary, but in a wind tunnel wind tunnel test section, some variation in free stream velocity has to occur because of the continuity requirement. Figure 3.1 shows the deviations in the free stream velocity. The height y4 at which the outer or free stream layer begins, has a fairly constant value y4=0.4m.

Another interpretation of the measured velocity profiles is obtained by plotting iso-velocity lines down-stream from the canopy (Figures 3.15). Streamlines will be shown as iso-mass lines later in Figure 3.26. The transport of mass and momentum from the outer layer (essentially above z = 0.4m height) towards the

lower boundary at z = 0 is evident in Figure 3.16. It can be recalled that the height of the canopy is 0.05m.

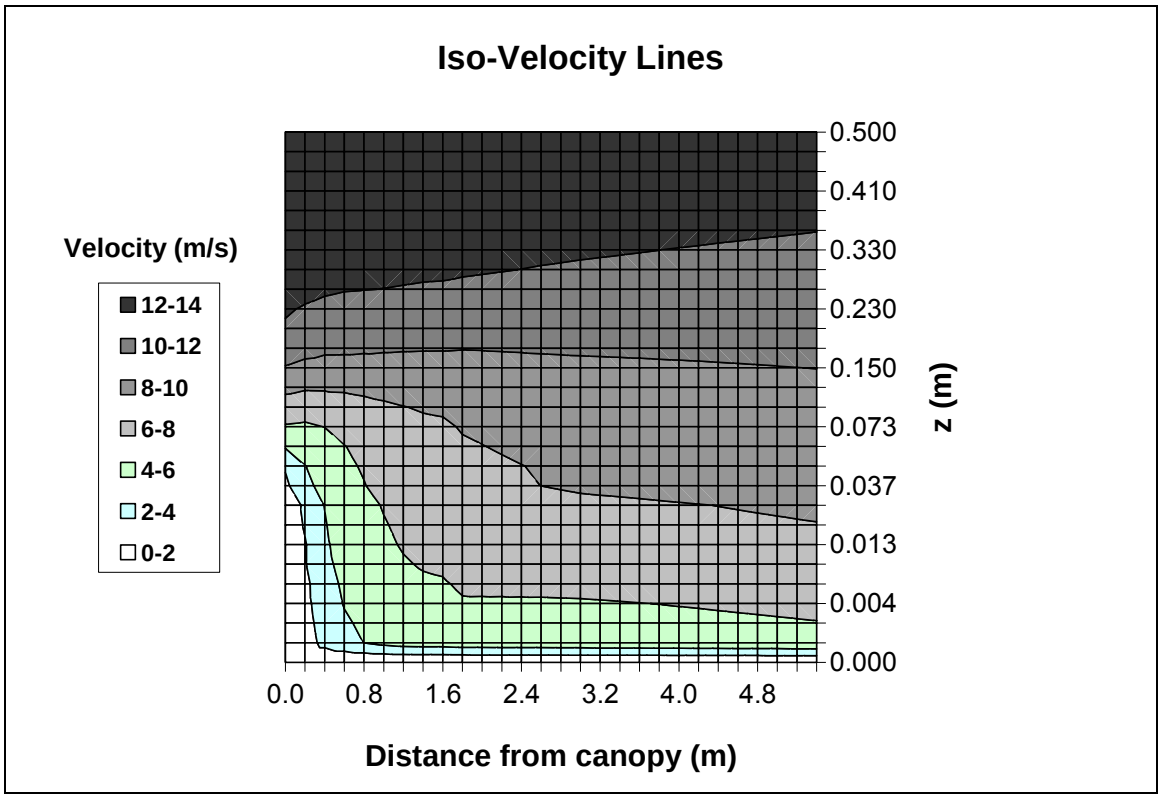

Figure 3.15. Iso-velocity lines plotted at 2 m/s intervals

3.5 Mass, momentum and energy flow downwind from the canopy

The entire flow field can also be characterized by the horizontal fluxes of mass, momentum and energy (power), both local and cumulative, above the ground surface. The cumulative fluxes are defined as follows:

Mass: $m = \rho \int u \, dz$

Momentum: $M = \rho \int u^2 \, dz$

Energy (power): $E = \rho \int u^3 \, dz$

These cumulative fluxes have been calculated from the velocity profiles and plotted as profiles at different distances from the canopy in Figures 3.16, 3.17 and 3.18. The density of air was taken to be 1.239 kg/m^3.

Flow regions near the ground surface are gaining in mass, momentum and energy flow as the distance from the canopy increases. Mass, momentum and energy are transferred from the outer layer to the surface layer. To see this transfer more clearly, the **change** in cumulative flow with distance from the end of the canopy was determined and plotted in Figures 3.29, 3.20 and 3.21. On these figures we can identify the thickness of the layer above the ground that is gaining mass or momentum or energy with distance. These thicknesses have been plotted in Figure 3.22 against distance from the canopy. We can also identify the thickness of the layer that has gained the most mass or momentum or energy. These layer thicknesses correspond to the maxima on Figures 3.19 to 3.21, and have been plotted in Figure 3.23.

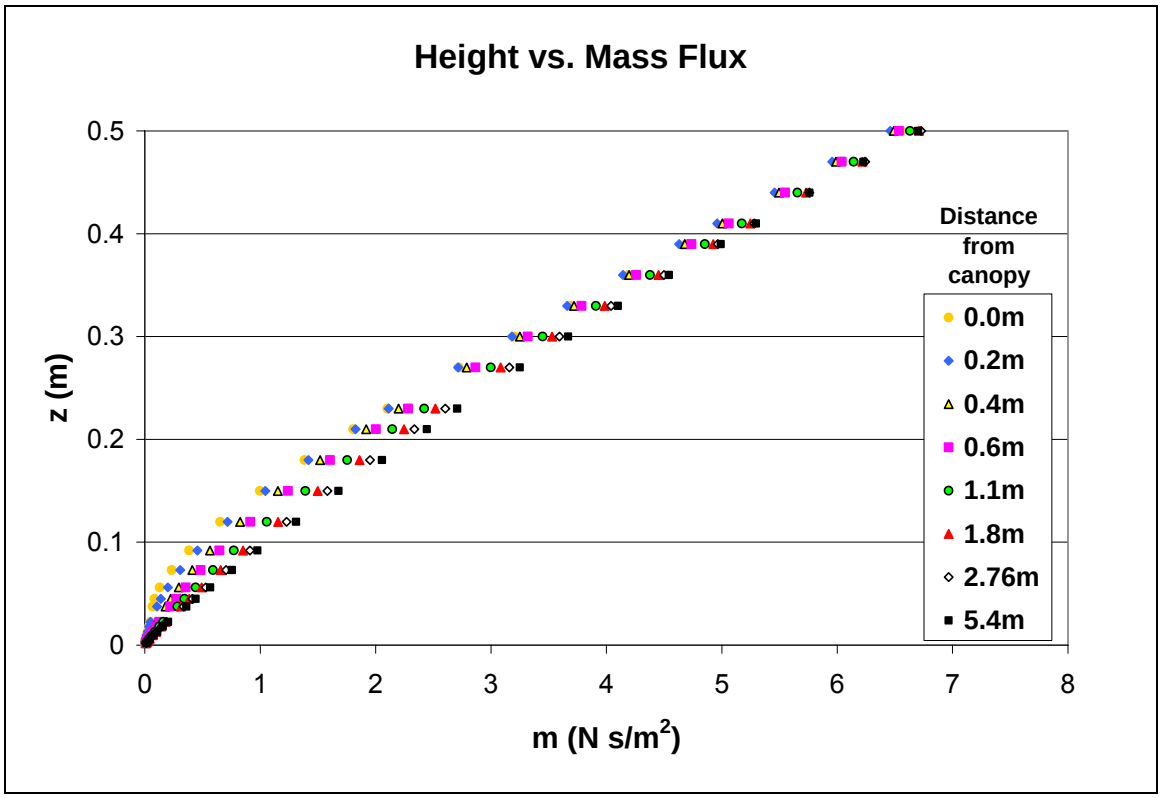

Figure 3.16 Cumulative mass flow downwind from the canopy

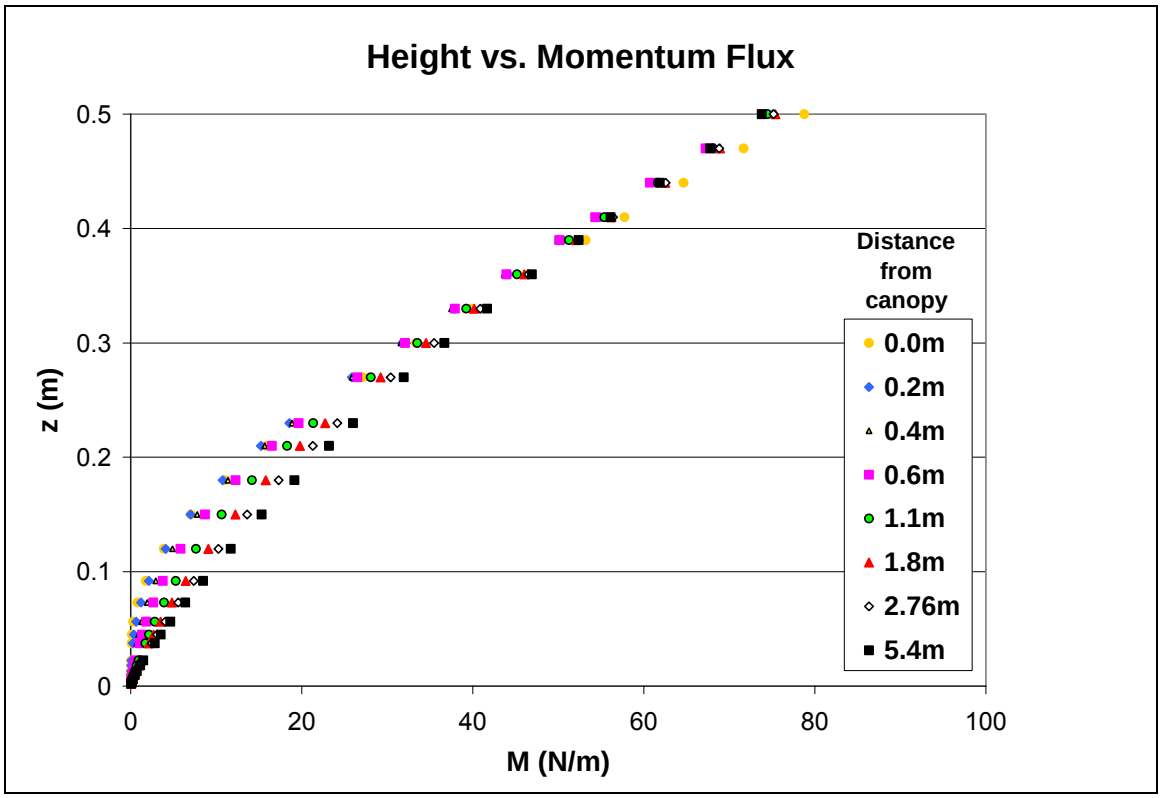

Figure 3.17. Cumulative momentum flow downwind from the canopy

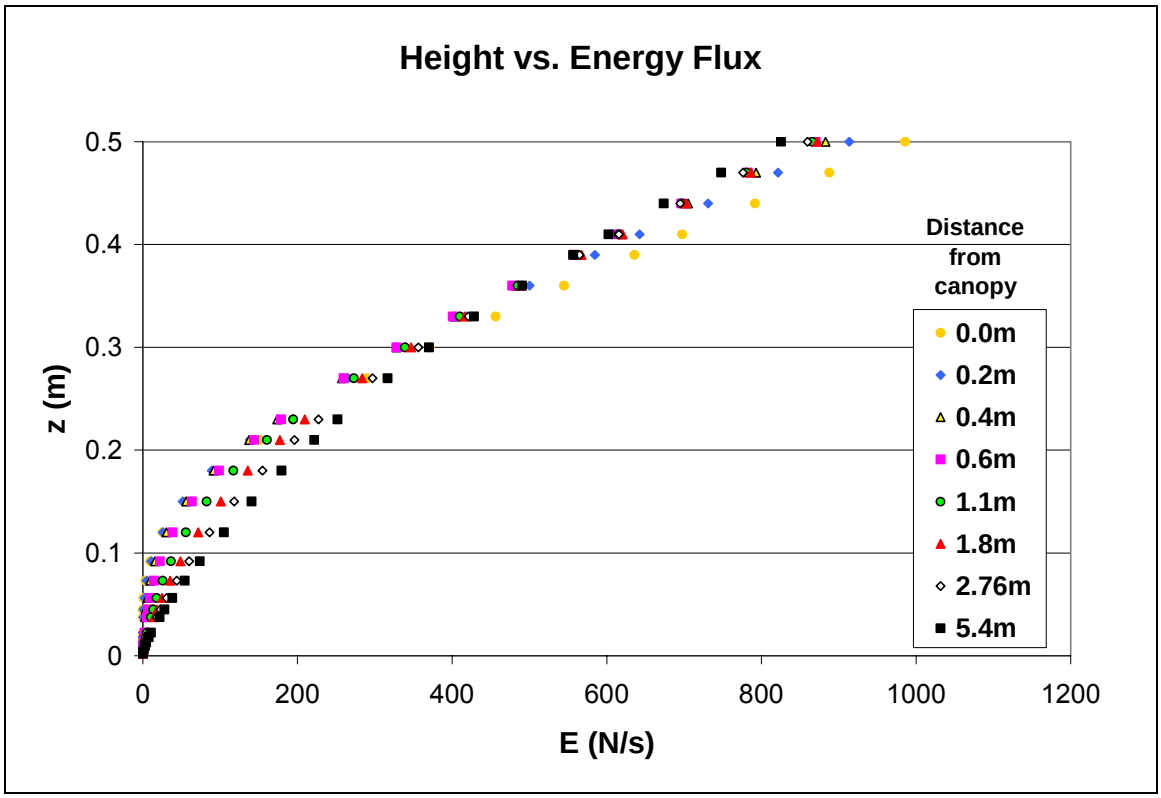

Figure 3.18 Cumulative energy flow downwind from the canopy

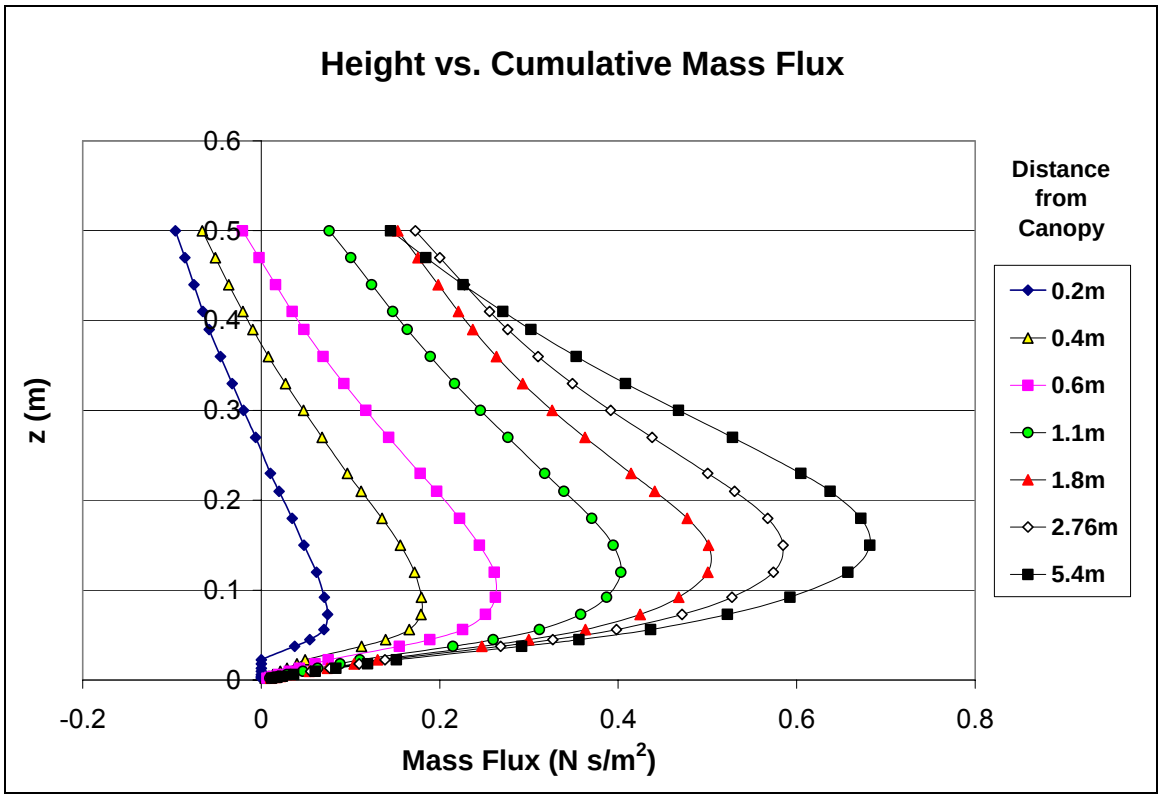

Figure 3.19 Change in cumulative mass flow downwind from the canopy. Increases in cumulative mass flow from the edge of the canopy (x=0) to a distance (x) from the canopy have been plotted.

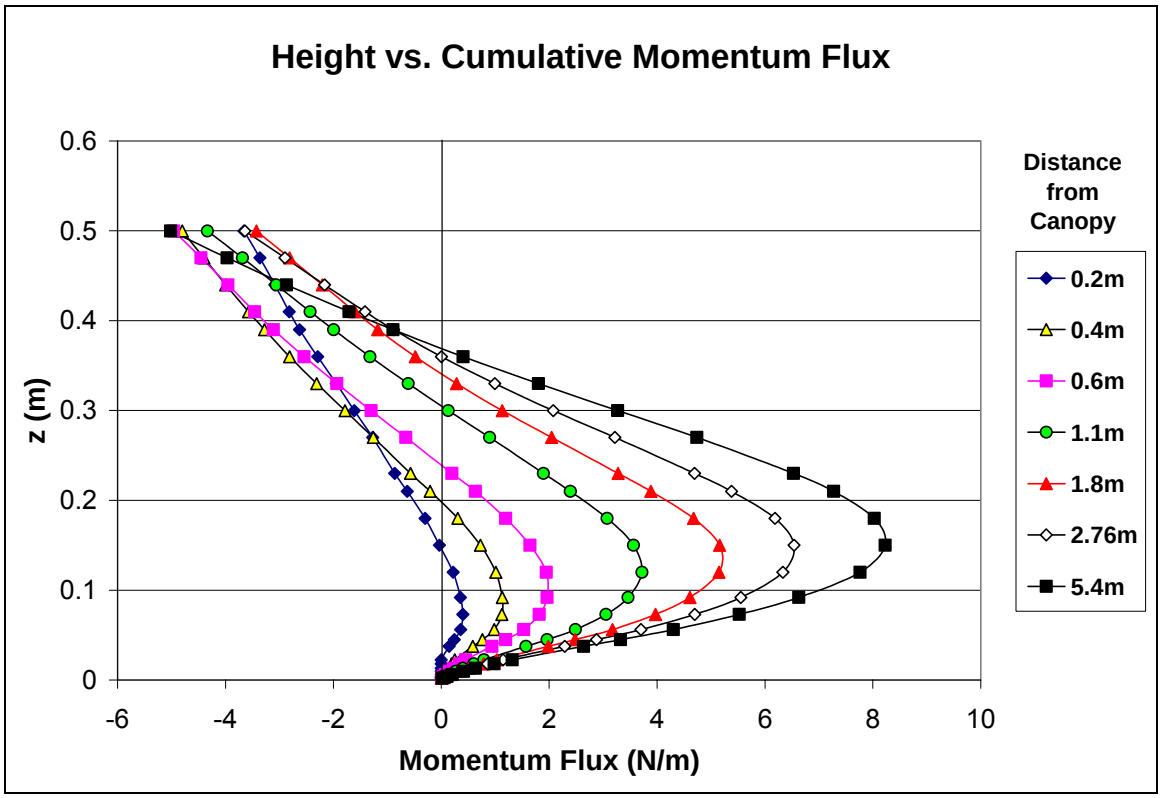

Figure 3.20 Change in cumulative momentum flow downwind from the canopy

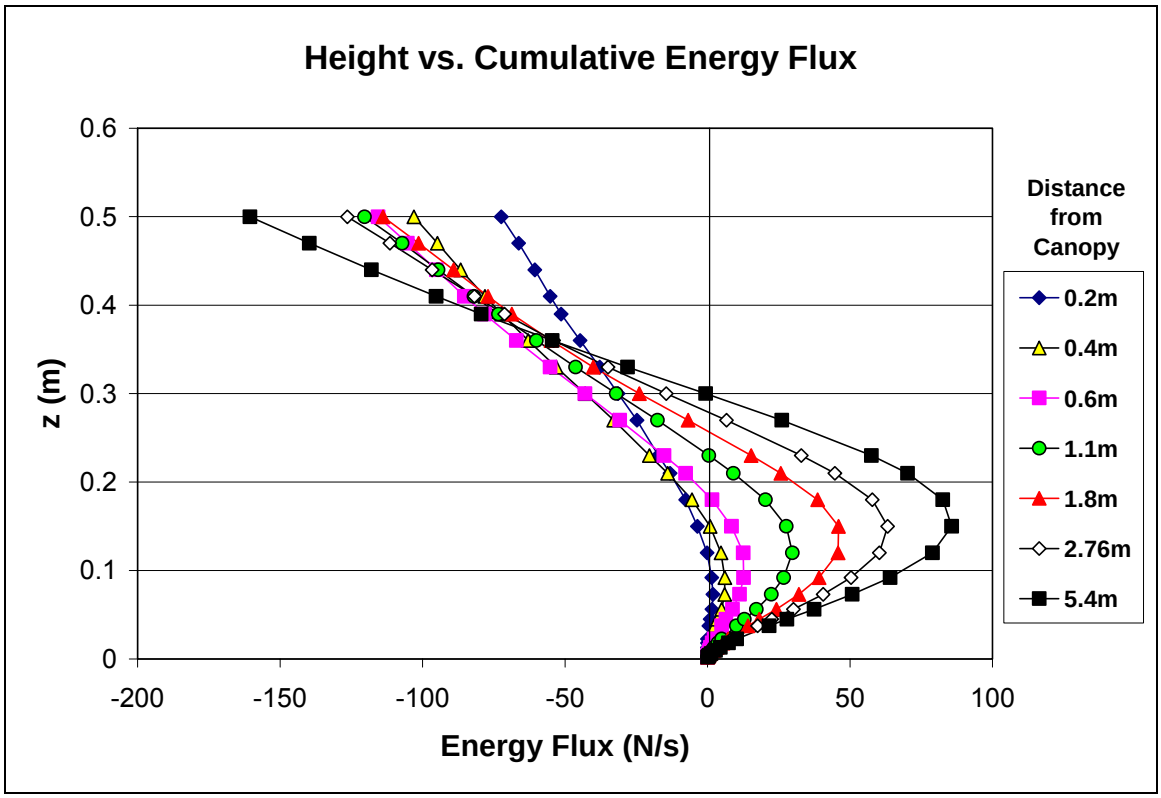

Figure 3.21 Change in cumulative energy flow downwind from the canopy

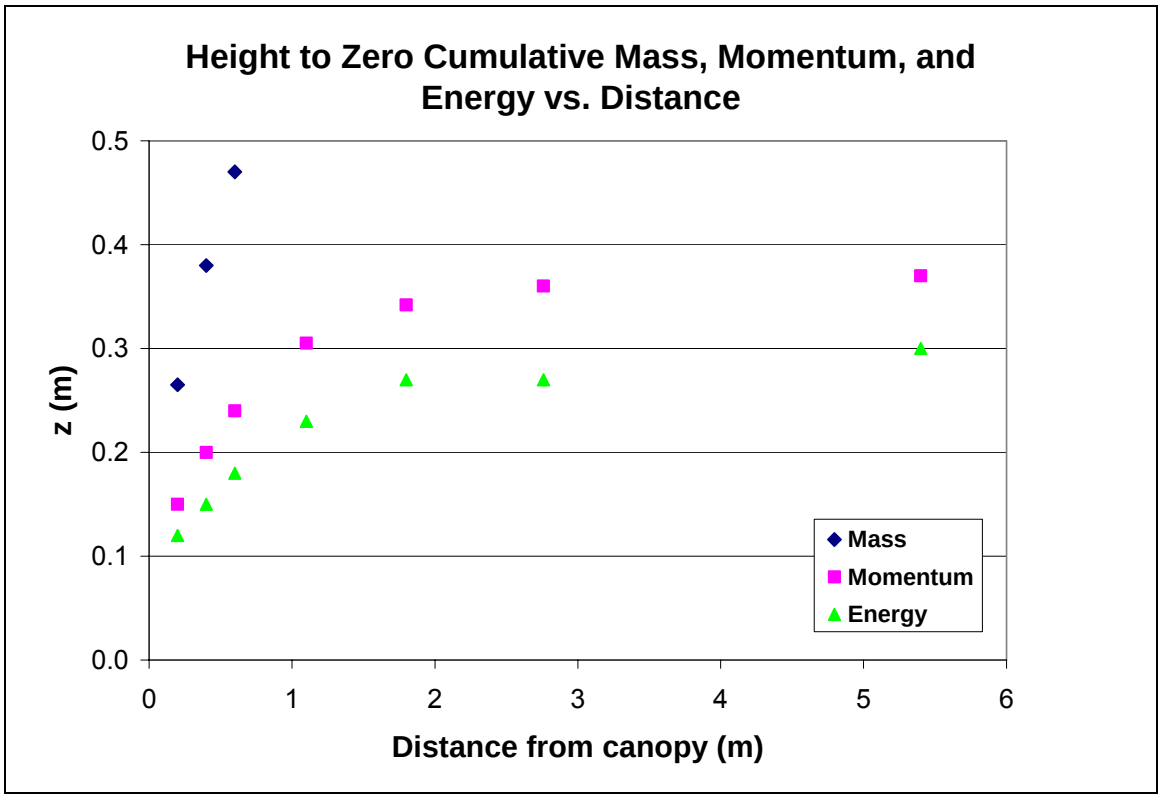

Figure 3.22 Heights of no change in cumulative flow of mass, momentum and energy between the edge of the canopy (x=0) and a distance (x) downwind from the canopy

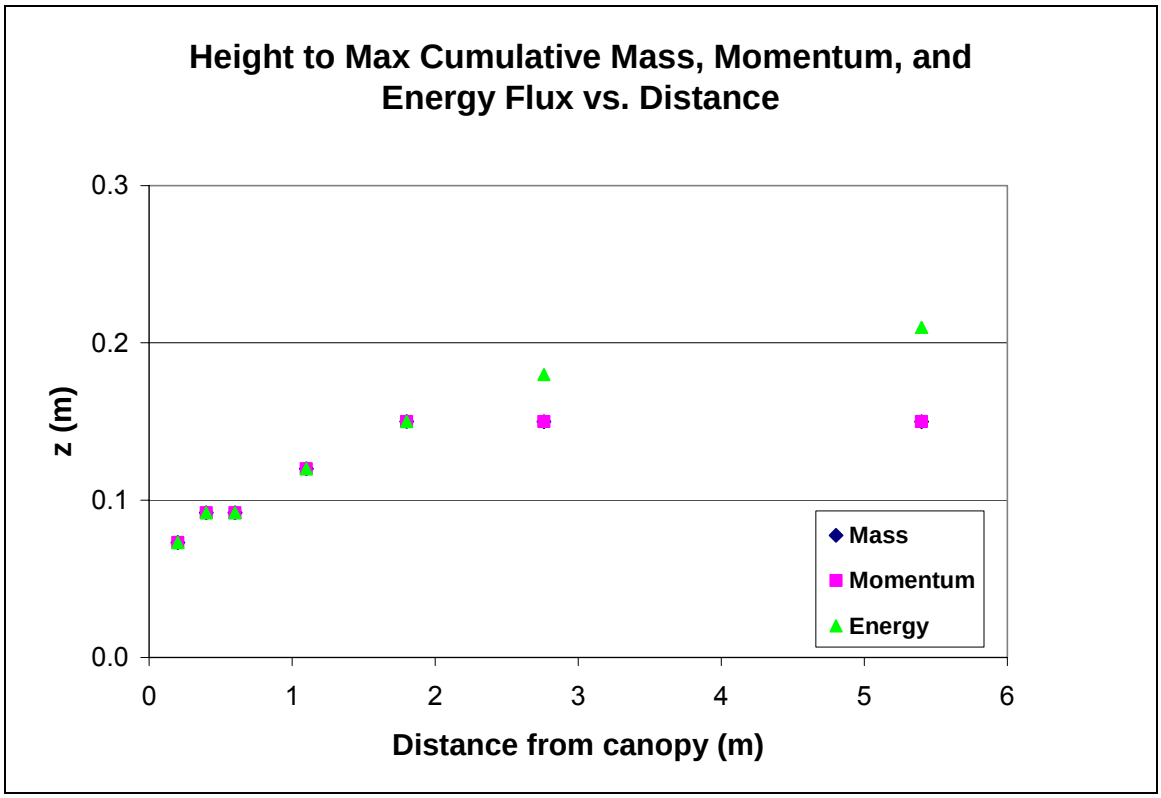

Figure 3.23 Heights of maximum change in cumulative flow of mass, momentum and energy

3.6 Shear stress distribution in the wind field downwind from the canopy.

Of particular interest is the loss or gain of momentum because it relates directly to the shear stresses both on the ground surface and in the air. The momentum balance for a control volume between two measured velocity profiles 1 and 2 can be written as

$$M_2 - M_1 = \tau(z)\,\Delta x - \tau(0)\,\Delta x + (m_2 - m_1)\,(\bar{u}(z)) \qquad (3.5)$$

where M_1, m_1 and M_2, m_2 are the momentum and mass fluxes defined above. $\bar{u}(z) = (u_1(z) + u_2(z))/2$ is the average velocity between the two measurement sections 1 and 2 and at elevation z. With the exception of $\tau(z)$ all parameters in this equation are known from measurements or can be calculated from measurements. We can therefore solve equation (3.5) for $\tau(z)$.

Calculated profiles of $\tau(z)$ have been plotted (Figure 3.24). There are changes in shear stresses within the wind field. Downwind from the canopy, the shear stresses increase because momentum is provided into the system from the outer layer, and transferred through the blending layer. Downwind from the canopy, the shear stresses within the wind field first increase with distance from the ground, then decrease. The shear stresses change most significantly and rapidly within a short distance from the canopy. In the short transition from x=0 to x=0.2m the shear stress has its maximum value at about the canopy height (Figure 3.24). Away from the canopy the shear stress throughout the wind field becomes relatively constant. Furthest downwind (x=5.4m) the calculated shear stress in the wind field is approximately constant (0.23 N/m^2) at all heights (Figure 3.5 and 3.24) illustrating that the memory of the canopy has been essentially lost.
Some shear stresses have negative values, i.e. they act in the reverse direction. The height at which the shear stress has a maximum down-stream of the canopy is shown in Figure 3.25. It rises from the canopy height h=5cm to about 4h over a distance x=108h. Immediately downwind of the canopy a zero shear stress occurs in the wind field at a height that has been plotted in figure 3.26. By definition there is no shear force exerted between the air layers above and below that height, although momentum is still transferred by influx of mass from above.

In Figure 3.27, the iso-mass flow lines are plotted. Immediately after the canopy, mass is transported from the outer layer into the blending layer, and from there into the surface layer. The majority of the transfer of mass into the blending layer starts immediately after the canopy and ends at a distance of about 2.6m, or 52h, downwind from the canopy. After this region, the effects of the canopy are still visible, but small in value.

In Figure 3.27, the iso-momentum lines are plotted. Similar results are obtained as within the mass transfer plots. Momentum is transferred from the outer layer into the blending layer. The transfer of momentum into the blending layer continues throughout the 5.4m data collection distance, while the majority of the

transfer is completed within a distance of 2.6m, or 52h, down-stream from the canopy. After this region, the momentum seems to be constant, therefore the effects of the canopy are small.

Combining figures 3.24, 3.25 and 3.27, the momentum and shear forces within the system can be shown in Figure 3.28. The values for which the shear is zero lies near the region of peak momentum. The maximum shear line occurs near the inflection points of each iso-momentum line.

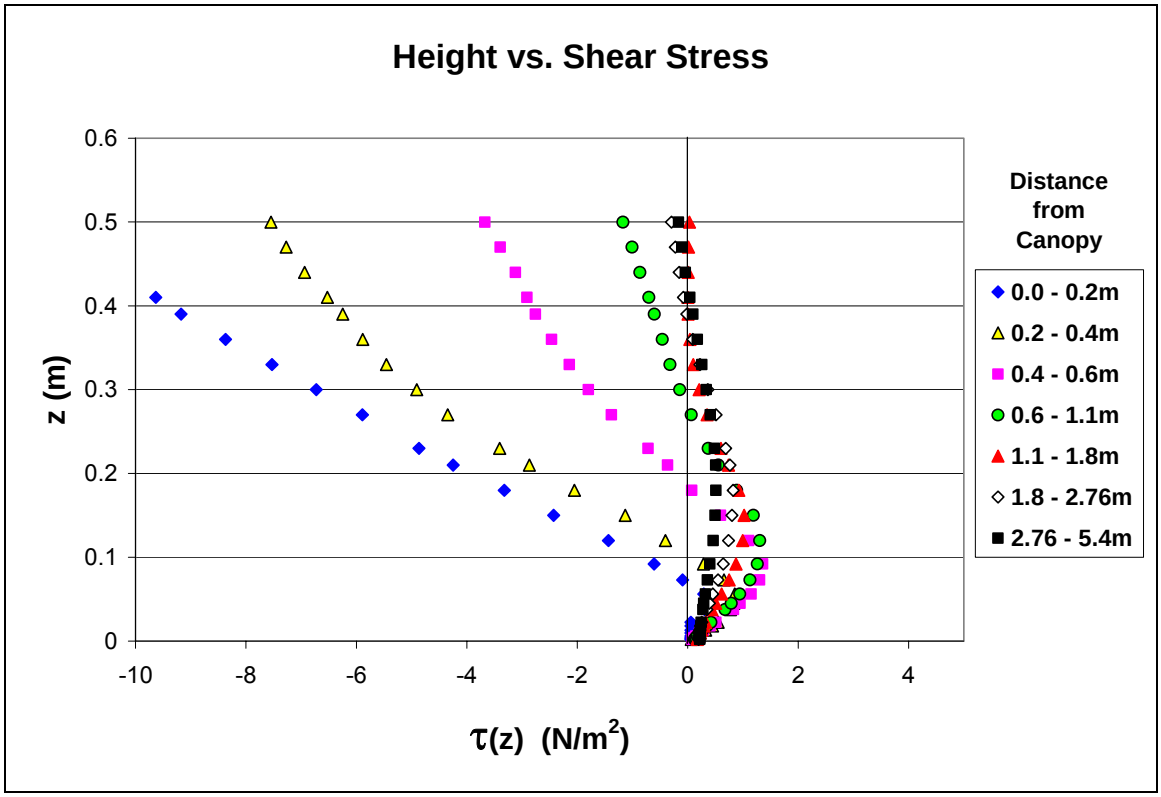

Figure 3.24 Shear stress throughout the wind field

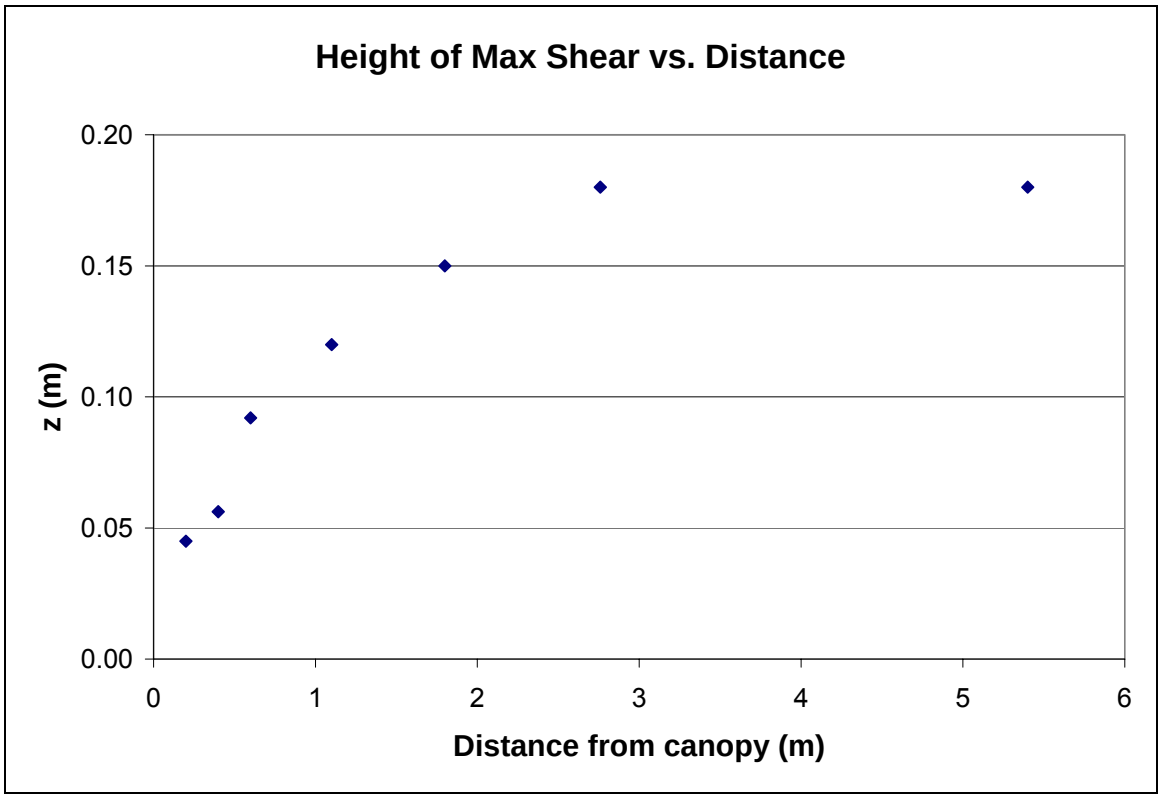

Figure 3.25 Height of maximum shear stress vs. distance downwind of canopy

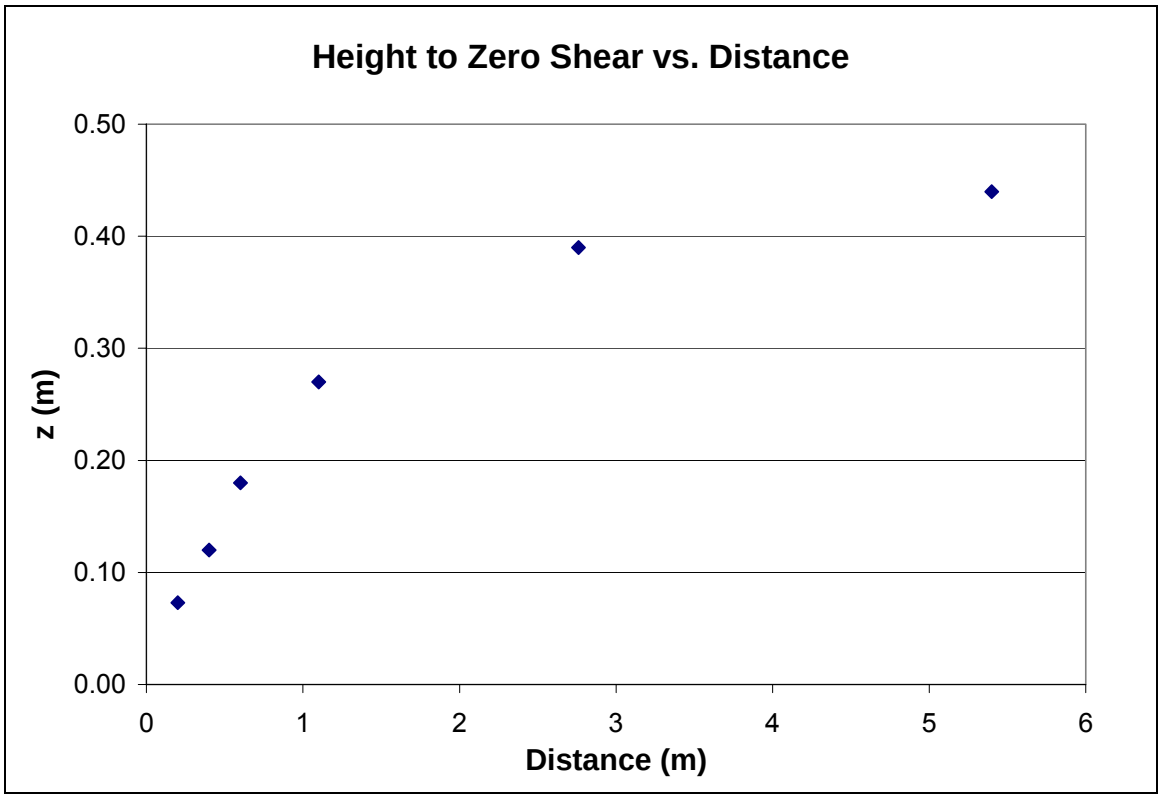

Figure 3.26 Height to zero shear stress vs. distance downwind of canopy

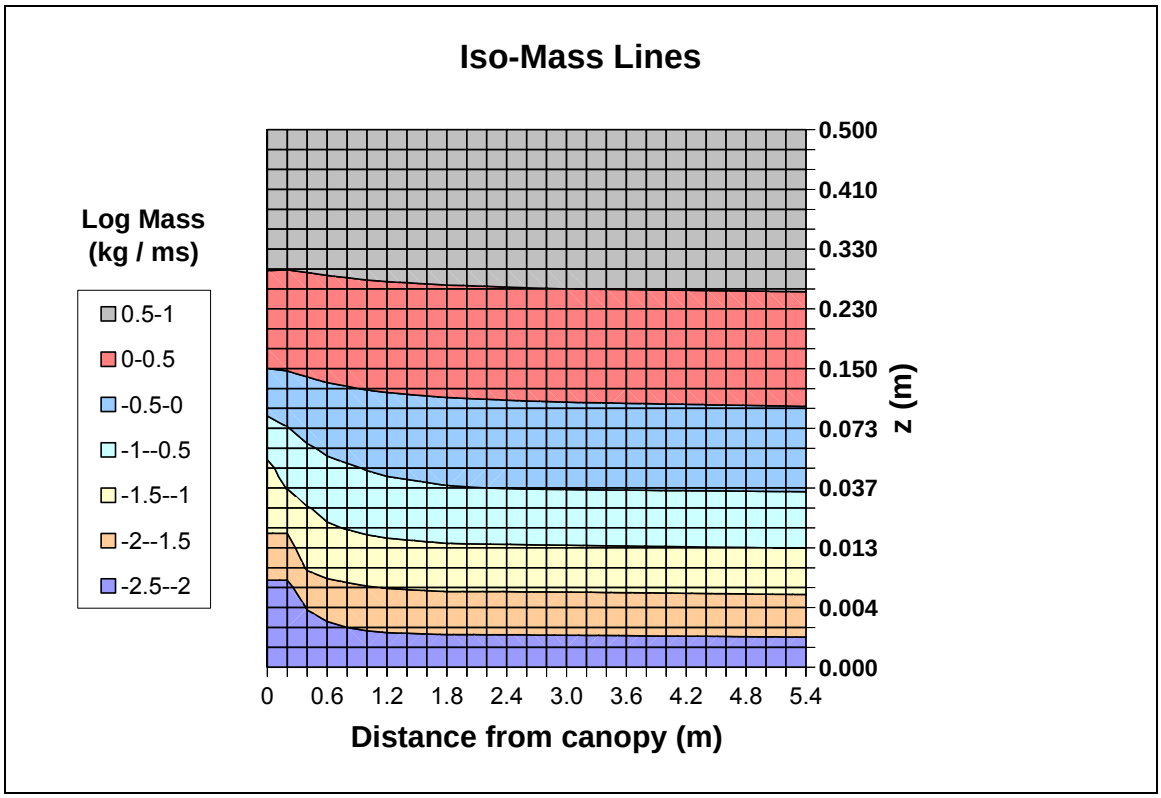

Figure 3.27 Iso-mass flow lines downwind from the canopy.

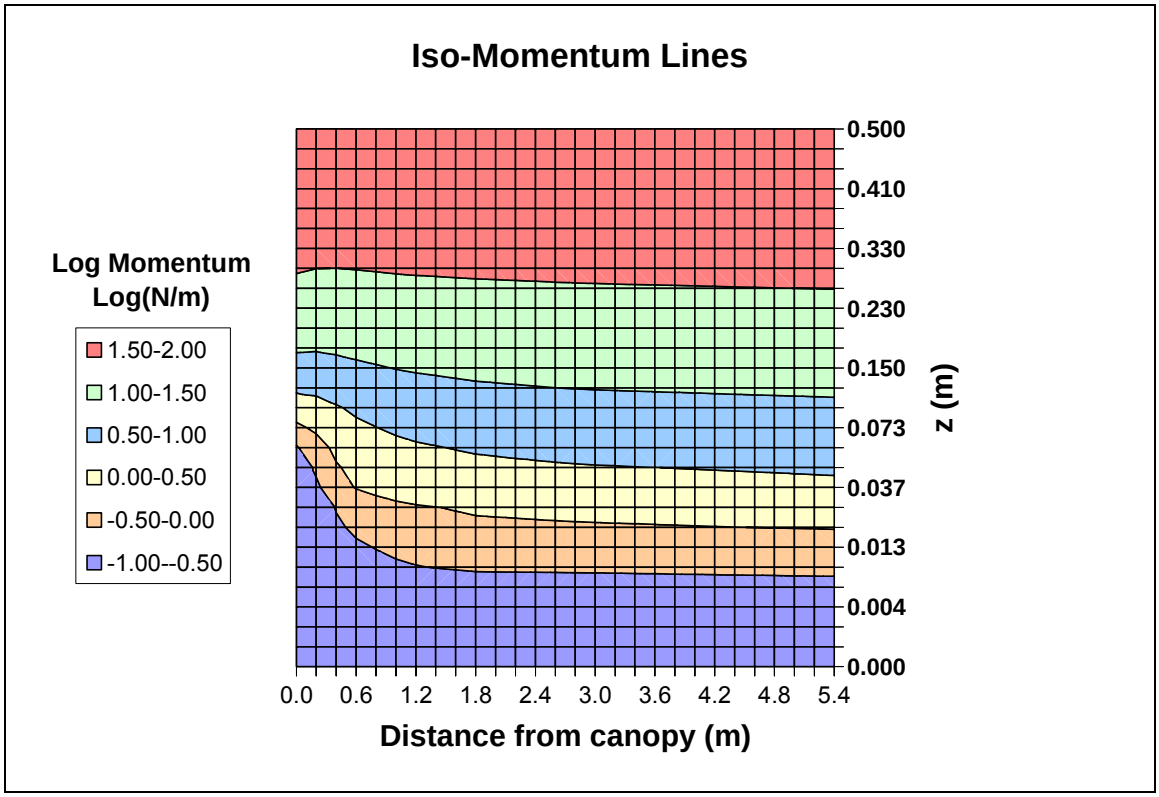

Figure 3.28 Iso-momentum flow lines downwind from the canopy

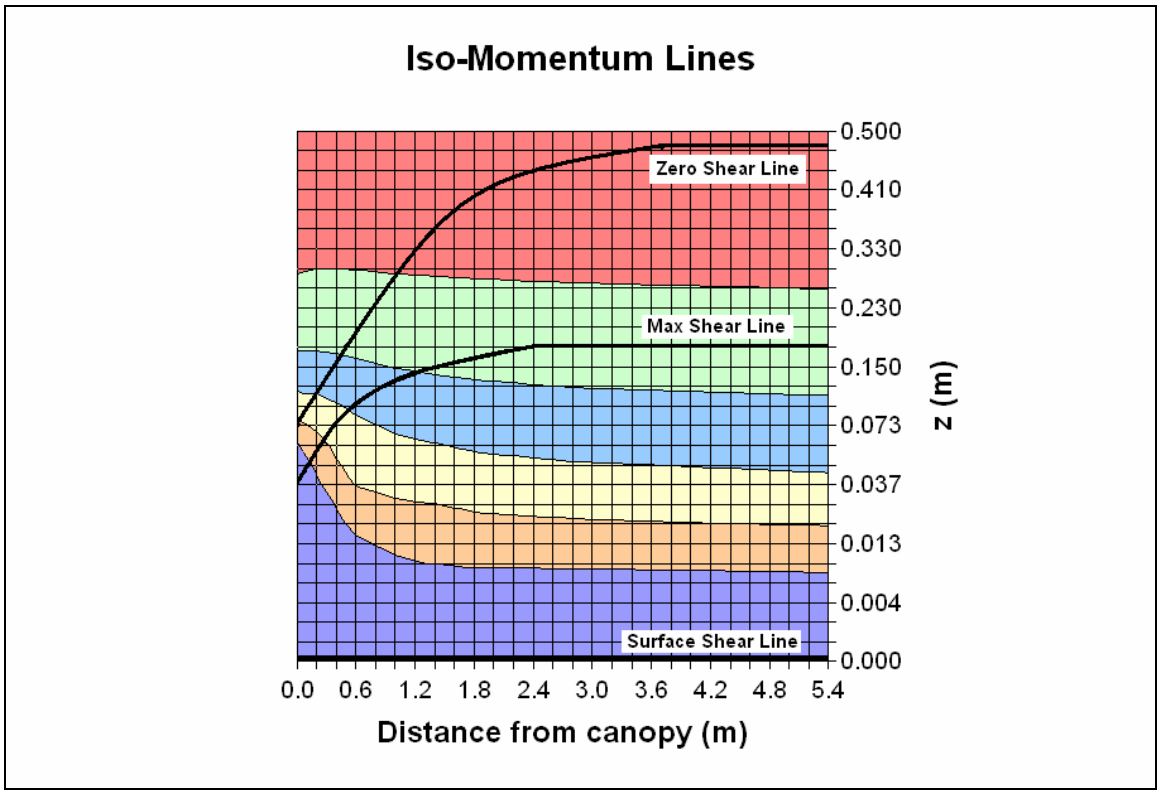

Figure 3.29 Iso- momentum flow lines and shear forces.

4. Discussion

4.1 Aerodynamic characterization of the canopy by roughness and displacement height

The aerodynamic characterization of the canopy is essential to our efforts. The top of the canopy is not a solid wall. The wind therefore penetrates some distance into the canopy. A description of this process was given by Finnegan (2000), and some information can also be found in Stull (1988) and Garratt (1992). The velocity profile above a canopy can be fitted to the equation

$$\frac{U}{U_*} = \frac{1}{\kappa} \ln\left(\frac{z-d}{z_0}\right) \qquad (4.1)$$

Equation 4.1 contains the canopy roughness (z_{0i}) and a displacement distance (d) as parameters. Both can be estimated by using the classical semi-log plot of measured velocity data.. We have used the velocity profile measured at the edge of the canopy (x=0) to do that. The displacement distance was determined by an iterative process. A plot of velocity (u) vs. (z-d) on a semi-log graph was made for different values of d. If the selected d was too small, the plot began to curve upwards, and if the d was too large, the plot began to curve downwards. Iterations were completed until the data plot showed no curvature (see Fig. 9.8 in Boundary Layer Meteorology by Stull, 1988). The displacement distance d was found to be 0.023 m. This displacement distance is less than half the canopy height or 0.5h. An estimate of d = 2/3h is often used,. Once d was determined, the canopy roughness (z_{0i}) could be obtained by extrapolation of the linear fitted plot of u vs, ln(z-d) to zero velocity u = 0 (Fig. 4.1)..The canopy roughness was determined to be approximately 0.013 m. This roughness is similar to uncut grass in the real world (see Fig 9.6 in Boundary Layer Meteorology). In Figure 4.1 the shear velocity (U*) is proportional to the slope of the line. U* was computed using Equation 4.2. The shear velocity was found to be 1.73 m/s. Referring to Figure 3.4, this value is appropriate.

$$U_* = \frac{U}{\kappa} \ln\left(\frac{z-d}{z_0}\right) \tag{4.2}$$

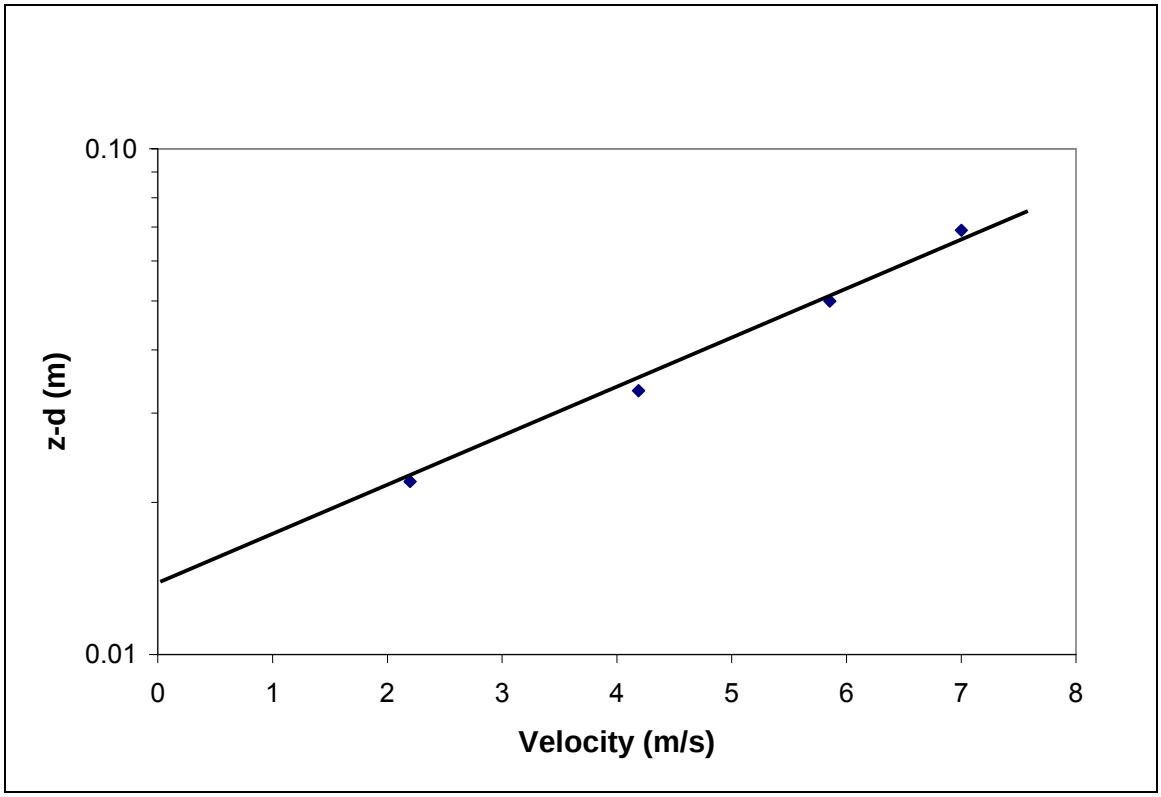

Figure 4.1 Determination of canopy roughness (z_{0c})

4.2 Comparison of experimental and other flow fields

The transition of the atmospheric boundary layer from land covered by tall vegetation (trees, shrubs, cattails) to water is a “hybrid” flow. It has elements of the following more fundamental flow fields: (1) flow over a backward facing step, (2) flow through a porous medium, (3) boundary layer growth over a flat plate, (4) roughness transition over a flat plate, (5) blending layer between a fast and a slow jet.

(1) Flow over a backward facing step is representative of wind blowing over a bluff or over buildings onto a lake. The flow lines will separate from the ground or the top of buildings, and reach (reattach to) the lake at the end of a flow separation region (wake). The wake region behind the step will be filled with low-momentum fluid. After reattachment, there will be momentum infusion from the high velocity region above the wake into the low velocity region above the lake. While this momentum transfer from above progresses downwind from the (stagnation) point onwards towards the lake, the shear stress exerted at the lake surface will cause the development of an internal boundary layer of growing thickness. The reattachment point is thought to occur at a horizontal distance of 6 to 8 building/bluff heights.

(2) If a lake is surrounded by plants (trees, brush, crops on farm fields or cattails) instead of buildings or bluffs, flow separation is less likely to occur because these plants are permeable to wind, There will still be a low momentum region in the wake of the plants, and there will still be momentum infusion from above into this wake. With the absence of flow separation and reattachment, the internal boundary layer above the lake may begin at the shoreline.

If a flow reattachment point exists on the lake surface its distance (L) from the shoreline is most likely a function of building/bluff height (h), and the permeability (K) and porosity (ε) of the plant field. L = f(h,K,ε).

(3) The growth of the internal boundary layer over the water surface is different from the classical flat plate boundary layer because the free stream velocity above the lake is increasing due to the infusion of momentum from above. The shear stress at the reattachment point of the wind (which can be the shoreline) is not infinite and diminishing with distance. Instead, it is small and growing in downwind direction over the lake.

(4) The transition from land to water is also a roughness transition. The roughness of the land upwind from the lake determines the wind velocity profile and hence the initial momentum deficit at the boundary with the lake. The momentum thickness of this initial wind profile including the height of the vegetation or buildings over which the wind is blowing may be a controlling parameter of potential flow separation and reattachment. Therefore an earlier statement for the reattachment point should be amended to include land roughness (k). L = f(h,K,ε,k).

(5) The momentum transfer through a mixing (blending) layer between two parallel fluid streams of different but uniform velocity can be taken as a simplified model of the momentum transfer from the fast moving wind above the height of the plants or buildings into the region above the lake surface.

The velocity profiles in Figures 3.1 and 3.2 change considerably with distance from the canopy. There is strong evidence that only elements (2), (3) and (5) of the five elements listed above are present. Elements (1) and (4) are absent. There is no separated flow region (Element 1) because the experimental canopy is highly permeable, and the flow coming through it has a nearly linear profile over the canopy height. This may not be totally representative of real canopies

with a lower permeability. There is also not much evidence of a roughness transition (Element 4) although the canopy and the wind tunnel floor have a huge difference in absolute roughness (1.3cm and 0.001cm<respectively); the flow coming out of the canopy resembles a Couette flow and makes a transition to a smooth boundary layer flow.

The velocity profiles in Figures 3.1 and 3.2 also show some similarity to the velocity profiles measured in a wind tunnel downwind from a dune crest (Walker and Nickling, 2003), but they are also significantly different. Figure 4.2 gives a conceptual model of the velocity profiles and flow regions observed on the lee-side region of a dune. We shall compare this figure with the five elements listed above and our data.

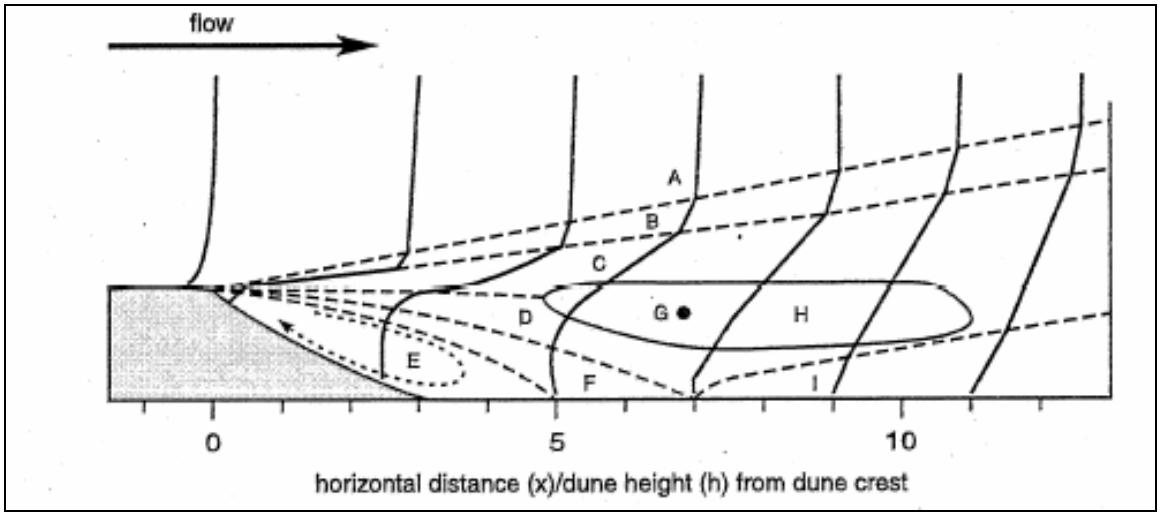

Figure 4.2. Conceptual model of lee-side flow regions over a transverse aeolian dune. Labeled regions represent: A, outer flows; B, overflow; C, upper wake; D, lower wake; E, separation cells; F, turbulent shear layer; G, turbulent stress maximum: H, turbulent shear zone; I, internal boundary layer (reproduced from Walker and Nickling, 2002)

Figure 4.2 identifies eight flow regions (A through I). In our analysis we have only used three. We gave combined A and B into the “outer layer”; C,D,G and H

constitute the “Mixing/transition/blending layer”; and I is the “surface/boundary layer”. Flow regions E and F are absent in our data because the canopy is permeable; there is no evidence of a separated flow region in our experimental results.

5. Normalization of wind tunnel data

With reference values for velocity and height, the results in Figures 3.1, 3.2, 3.5, 3.6 have been normalized and replotted. The reference velocity (U_{ref}) is the velocity at x=0 and z=6h above the wind tunnel floor; the reference height is the canopy height h=5.0cm. Normalized velocity profiles are given in Figures 5.1 and 5.2. Shear stresses on the wind tunnel floor (τ/τ_r) are given in Figures 5.3 and 5.4, respectively. The normalized shear stress is of particular interest because it characterizes the reduction in momentum applied to a lake surface in response to wind sheltering. It can be seen in Figure 5.4 that wind sheltering extends over a distance of about 100 canopy heights, i.e. the wind shear stress is reduced over this distance. Normalized shear stress starts at a value of about 0.2 (not zero) at the foot of the canopy and looses its memory of the sheltering effect after roughly 100 canopy heights. For trees of 10m height that would represent a distance of about 1000m. If the wind fetch of a lake is smaller than 100h wind sheltering will be very significant, if it larger than 1000h, wind sheltering will be small.

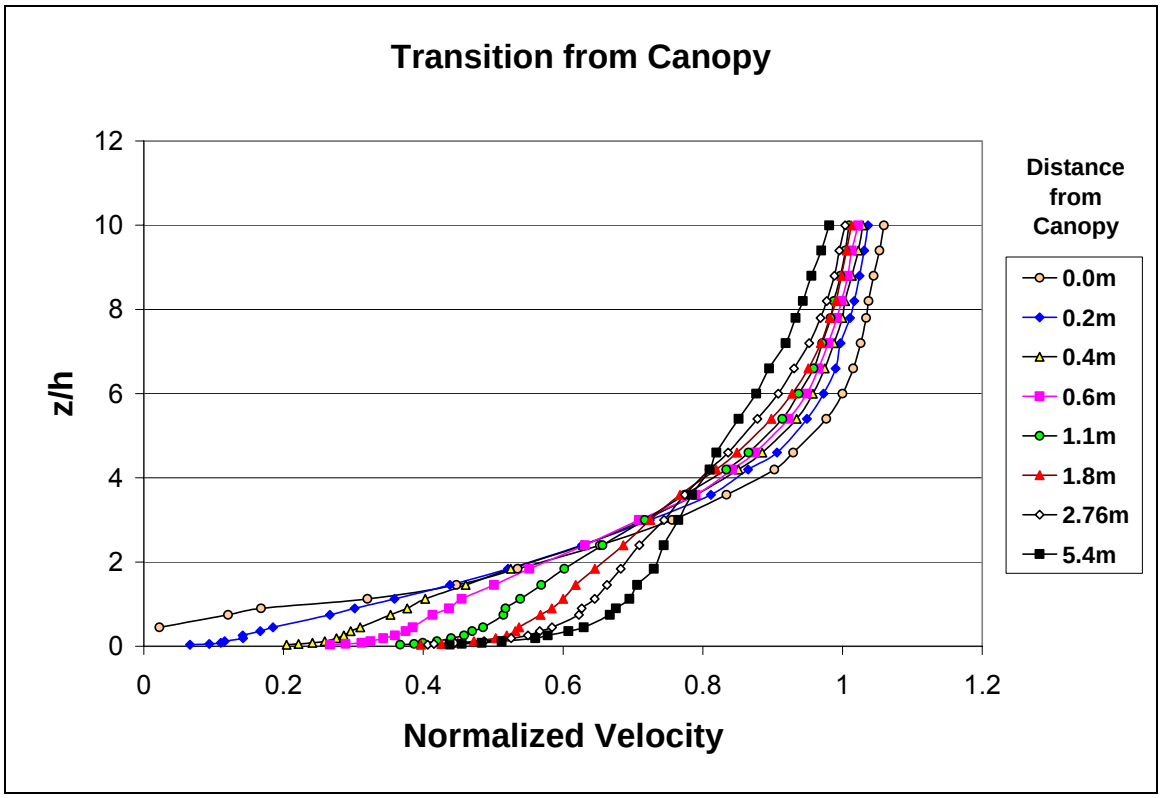

Figure 5.1 Normalized velocity profiles in Cartesian coordinates

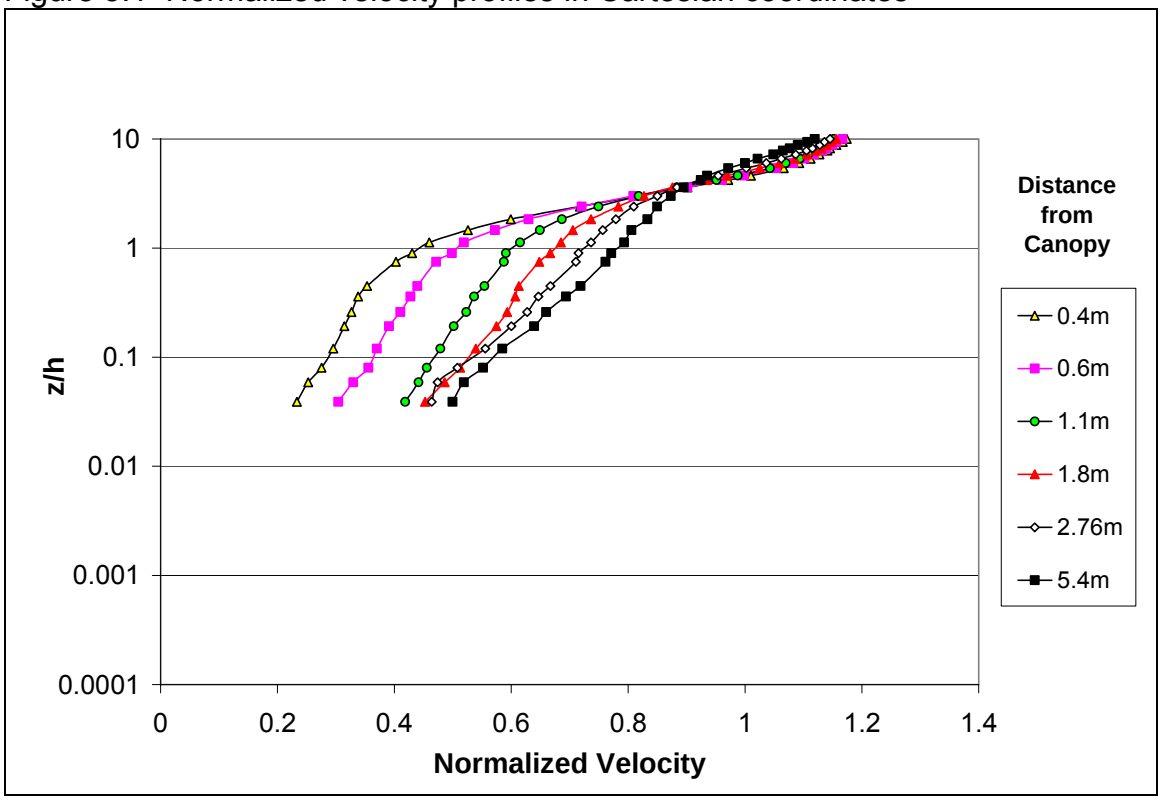

Figure 5.2 Normalized log-velocity profile

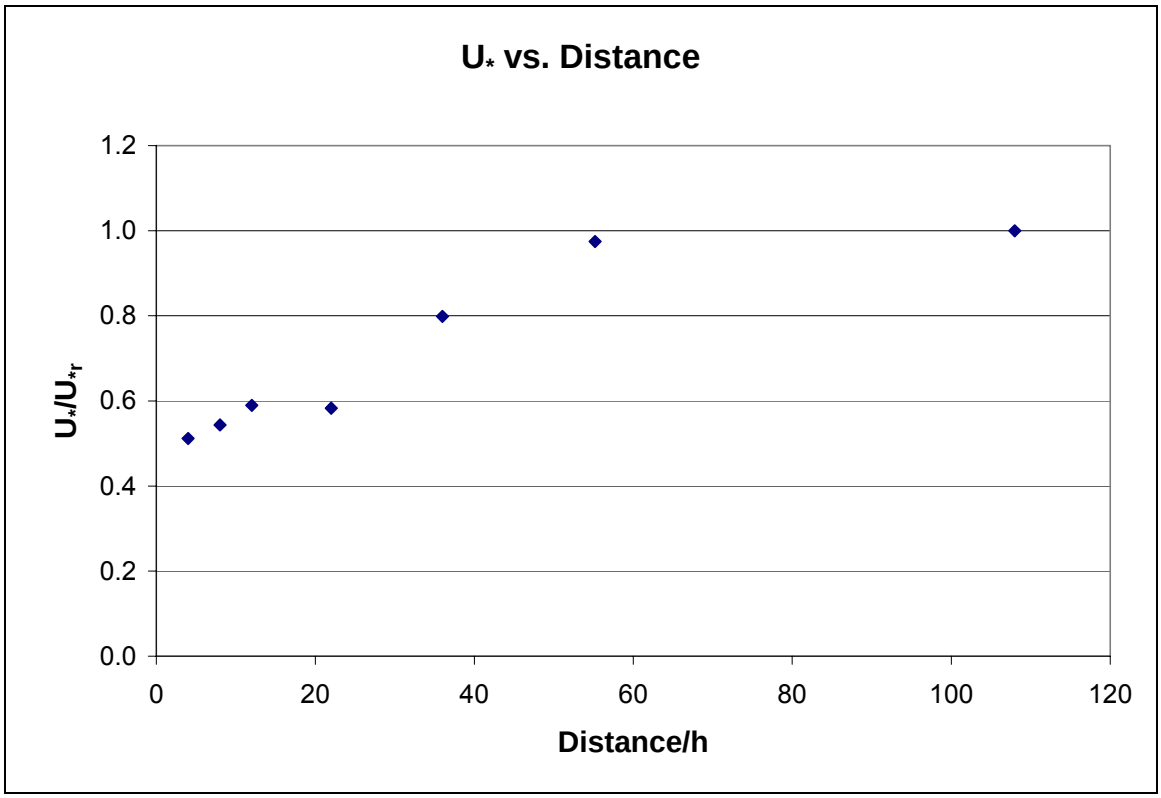

Figure 5.3 Normalized shear velocity (U_*/U_r)

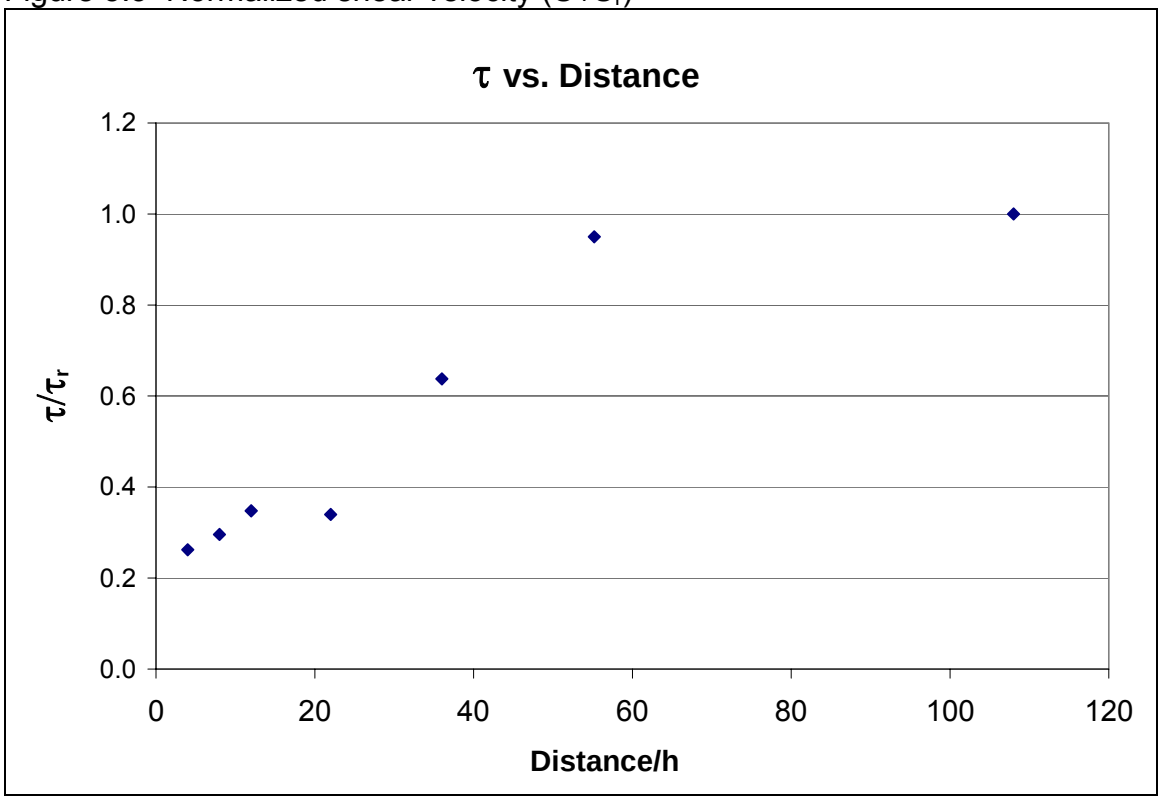

Figure 5.4 Normalized surface shear stress (τ/τ_r)

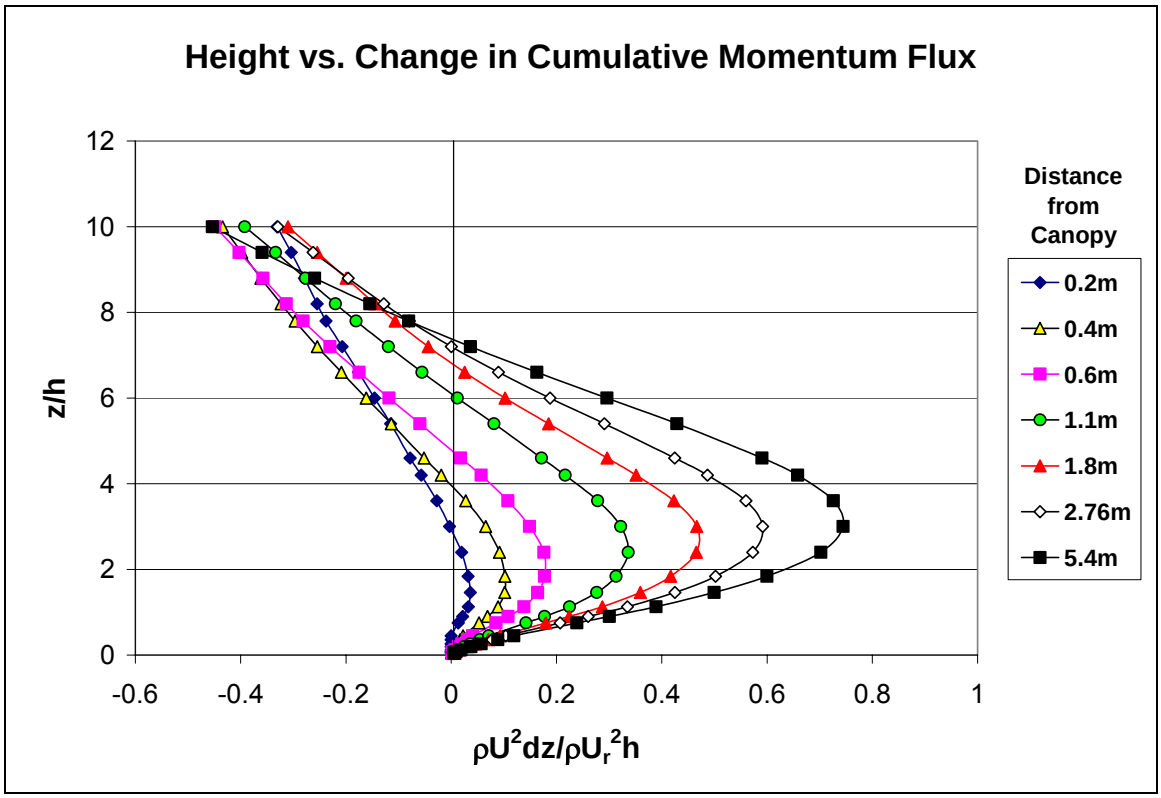

Figure 5.5 Normalized height vs. change in cumulative momentum flow

6. Application of experimental results to field situations

Water quality (computer) models can simulate vertical mixing and heat transfer in small lakes. Mixing processes are driven by heat and momentum transfer at the lake surface, which in turn are linked to wind speed, air temperature, solar radiation and relative humidity. In many model applications the weather data come from a land-based station some distance away from a lake. Wind stresses on the lake surface are calculated from measured wind velocities using empirical drag coefficients (Wuest and Lorke, 2003) that may account for wind fetch and the state of the water surface in terms of wave characteristics. Wind sheltering by the terrain and vegetation covers surrounding the lake is accounted for by a ”wind sheltering coefficient” that can be determined only by model calibration.

The results of the experimental study described herein may provide a means to overcome this deficiency.

The chicken wire canopy used in the wind tunnel simulates to some degree of realism a vegetation cover (trees, bushes, reeds, crops) on the land surrounding a small lake. The shear stress distribution measured downstream from the canopy includes the wind sheltering effect of the canopy on a flat and smooth surface downwind. We assume that this solid surface in the experiment represents a lake surface. Although the roughness of the two surfaces may not scale correctly, we believe that this potential deficiency does not affect the results seriously. The height, the roughness and the porosity of the canopy exert the most important control over the wind velocity field downstream from the canopy. The canopy roughness was determined from the velocity profile to be 1.3cm. The relative roughness of the canopy is 1.3/5.0 = 0.26.

To apply the wind sheltering effect observed downstream of the experimental canopy to a real lake setting, we need to normalize the velocity and shear stress data as shown in Section 5. We selected the experimental canopy height (h) as the logical reference length for distances and elevations. As a reference velocity we selected the measured wind speed at x=0 and z=6h. For lake model applications wind velocity usually comes from a weather stations where wind velocities are measured and recorded 10 m above ground level. To select a reference shear stress we have several options, but not all are practical. Because our wind tunnel experiments cover only a limited distance downwind from the canopy we select the shear stress at the furthest down-wind point x/h = 5.4/0.05 = 108 from the canopy as the reference shear stress.

A kinematic feature is the shape of the velocity profile over the canopy in the experiment compared to the prototype. It depends on the roughness of the canopy. Rough canopies have velocity profiles with smaller vertical gradients than smooth canopies (Figure 6.1). When the two profiles are overlayed, it is apparent that the rough boundary velocity profile has a larger velocity deficit to fill downstream from the canopy.

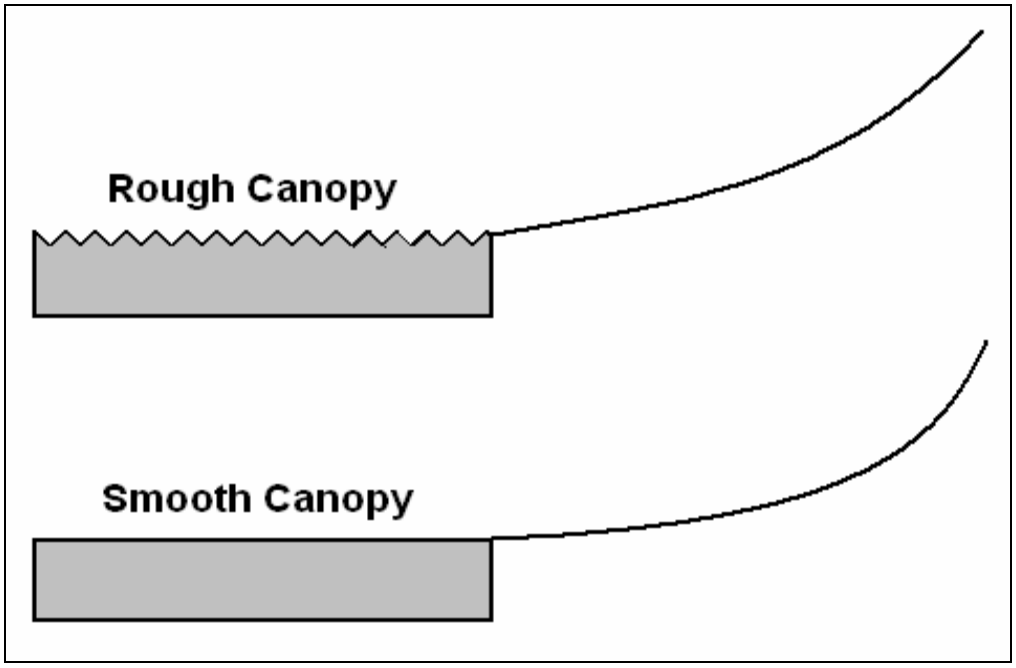

Figure 6.1: Wind velocity profile over a rough and a smooth canopy

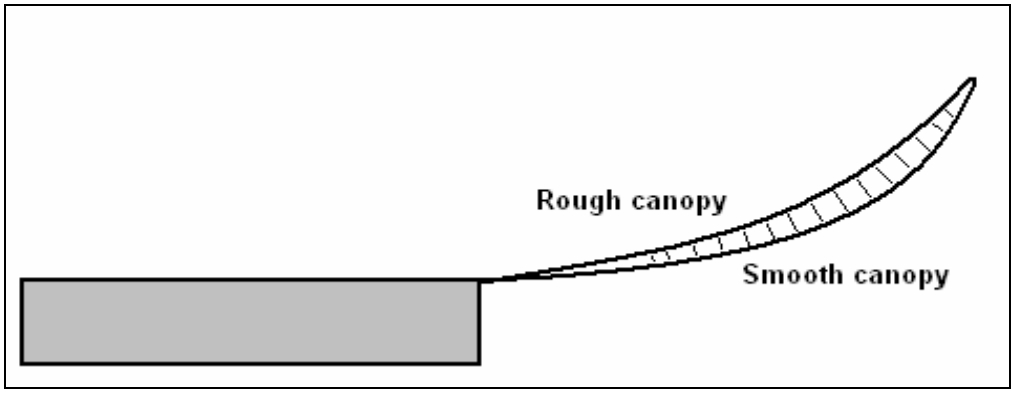

Figure 6.2: Overlay of the rough and smooth canopy wind velocity profiles

It is also of interest to consider the wind velocity profile in the wind tunnel without a canopy. This profile was measured and is plotted in Figure 6.3. Far downwind

from the canopy the wind velocity profile would be expected to assume this shape, because the memory of the canopy has been lost.

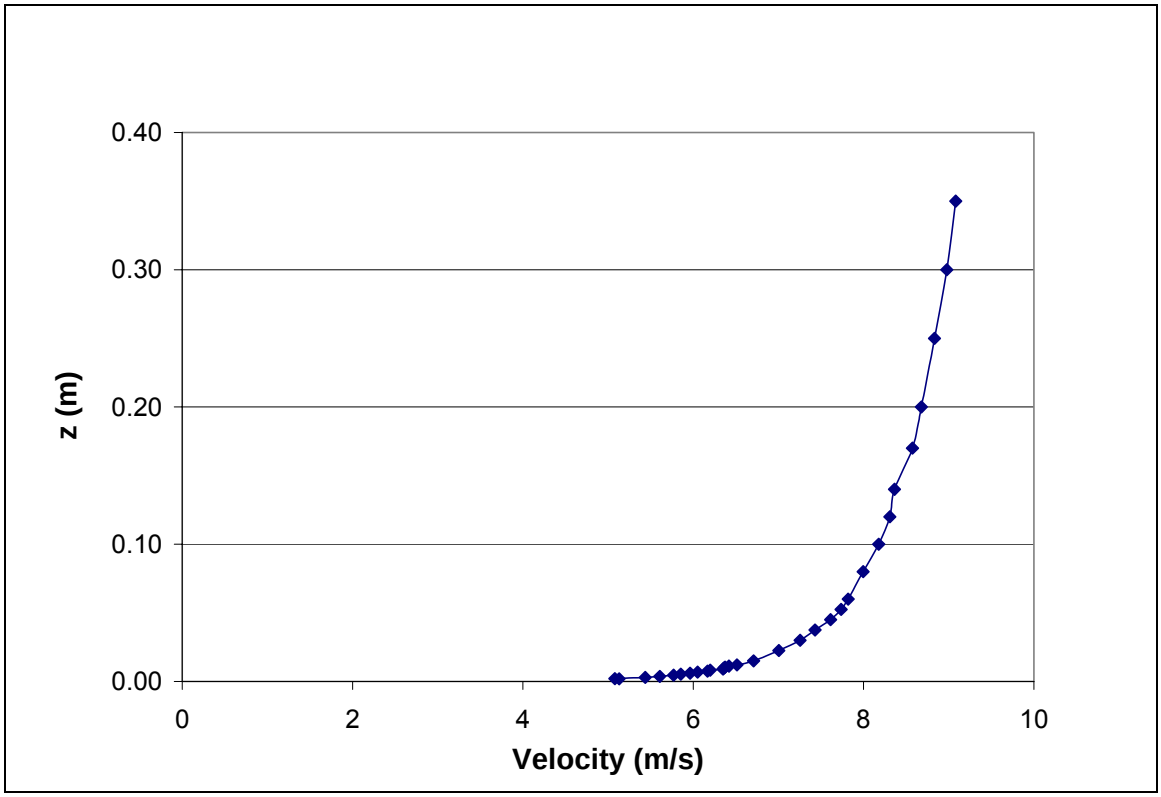

Figure 6.3: Velocity profile in the wind tunnel with no canopy (undisturbed wind velocity profile). Data were from the data set in Part B. The wind tunnel speed was set to 10 m/s.

The approximate power input from the wind to a lake surface (2-D) is the integral $\int \tau U^* dx$ over the entire wind fetch (F). That power input produces among other things vertical mixing in a lake, and is needed in lake stratification models. The reduction in power input due to wind sheltering depends on the wind fetch F. The above integral is for 2-D flow along the wind direction. It has to be applied to different wind fetches according to the shape of a lake surface in order to obtain the wind power input over an entire lake surface.

7. References

Anderson RY, Dean WE. 1988. Lacustrine varve formation through time. *Palaeogrogr. Palaeoclimat. Palaeoecol. 62: 215-235*

Anis A, Moum JN. 1995. Surface wave-turbulence interactions – scaling $\varepsilon(z)$ near the sea-surface. *J. Phys. Oceanogr. 25: 2025-45*

Banner ML, Peregrine DH. 1993. Wave breaking in deep water. *Annu. Rev. Fluid Mech. 25: 373-97*

Banner ML, Phillips OM. 1974. On the incipient breaking of small scale waves. *J. Fluid. Mech. 65: 647- 56*

Bäuerle E. 2001. Three-dimensional wind-induced baroclinic circulation in rectangular basins. *Adv. Water Res. 24: 11-27*

Bear J. 1988. Dynamics of fluids in porous media. *Dover Pubns. 784 pp.*

Belcher SE, Hunt JCR. 1998. Turbulent flow over hills and waves. *Annu. Rev. Fluid Mech. 30: 507-38*

Bicudo JR. 1988. The measurement of reaeration in streams. *PhD Dissertation. University of Newcastle upon Tyne. 383 pp.*

Bicudo JR, Giorgetti MF. 1990. The effect of strip bed roughness on the reaeration rate coefficient. *Proceedings of the 15th Biennial International Conference of the IAWPRC. Kyoto, Japan.*

Bradley E, Coppin P, Godfrey J. 1991.Measurements of sensible and latent heat flux in the western equatorial Pacific Ocean. *J. Geophys. Res. 96:3375-89*

Burchard H. 2001. Simulating the wave-enhanced layer under breaking surface waves with two equation turbulence models. *J. Phys. Oceanogr. 31: 3133-45*

Charnock H, 1955. Wind stress on a water surface. *Q. J.R. Meteorol. Soc. 350:639-40*

Condie SA, Webster IT. 2001. Estimating stratification in shallow water bodies from mean meteorological conditions. *J. Hydraulic Eng. 127(4): 286-92*

Dake JMK, Harleman DRF. 1969. Thermal stratification in lakes: analytical and laboratory studies. *Water Res. Res. 5(2): 484-495*

Danckwerts PV. 1951. Significance of liquid-film coefficients in gas-absorption. Introduction of the surface renewal concept. *Ind. Eng. Chem.* 43(6): 1460-1467

Dorman CE, Mollo-Christensen E. 1973. Observation of the structure of moving gust patterns over a water surface. *J. Phys. Oceanogr. 3: 120-32*

Edinger JE. 2001. Waterbody hydrodynamic and water quality modeling: An introductory workbook and CD-ROM on three-dimensional waterbody modeling. *ASCE Press. 215 pp.*

Fairall CW, Bradley EF, Rogers DP, Edson JB, and Young GS. 1996. Bulk parameterization of the air-sea fluxes for Tropical Ocean-Global Atmosphere Response Experiment. *J. Geophys. Res. 101: 3747-64*

Farell C, Iyengar AKS. 1999. Experiments on the wind tunnel simulation of atmospheric boundary layers. *J. of Wind Engin. 79: 11-35*

Finnegan J. 2000. Turbulence in plant canopies. *Annu. Rev. Fluid Mech. 32: 519-571*

Garrett JR, 1992. *The atmospheric boundary layer*. Cambridge University Press, Cambridge UK, 316 pp.

Geernaert GL, Davidson K, Larsen S, Mikkelsen T. 1988. Wind stress measurements during the tower ocean wave and radar dependence experiment. *J. Geophys.Res. 93: 13913-23*

Guan D, Zhang Y, Zhu T. 2003. A wind-tunnel study of windbreak drag. *Agric. For. Meteorol. 118: 75-84*

Haidvogel DB, Wilkin JL, Young R. 1991. A semi-spectral primitive equation ocean circulation model using vertical sigma and orthogonal curvilinear horizontal coordinates. *J. Comp. Phys. 94: 151-*

Higbie R. 1935 Penetration theory leads to use of the contact time in the calculation of the mass transfer coefficients in the two film theory. *Trans. Am. Inst. Chem. Engrs 31: 365*

Hocking GC, Patterson JC. 1994. Modelling tracer dispersal and residence time in a reservoir. *Ecol. Model. 74(1-2): 63-75*

Hondzo M, Stefan HG. 1993. lake water temperature simulation model. *J. Hydraulic Eng. ASCE 119(11):1251-1273*

Jähne B and Hauβecker H. 1998, Air-water gas exchange. *Annu. Rev. Fluid Mech. 30: 443-68*

Jessup AT, Zappa CJ, Yeh H. 1997. Defining and quantifying microscale wave breaking with infrared imagery. *J. Geophys. Res. 102(C10): 23,145-53*

Kenney WA. 1987. A method for estimating windbreak porosity using digitized photographic silhouettes. *Agric. For. Meteorol. 39: 91-94*

Kolb BH, Heineman MC. 1995. Controlling mechanisms of sediment-driven dissolved oxygen dynamics in New Bedford Outer Harbor. *Marine Freshwater Res. 46(1): 69-79*

Lawrence I, Breen P. 1998. Design guidelines: stormwater pollution control ponds and wetlands. *CRCFE Rep.* Cooperative Research Centre for Freshwater Ecology, Canberra, Australia

Mastenbroek K. 1998. High-resolution wind fields from ERS SAR. *Earth Obs. Quart. 59: 20-22*

Melville WK. 1996. The role of surface-wave breaking in air-sea interaction. *Annu. Rev. Fluid Mech. 28: 279-321*

Mourad PD, Walter BA. 1996. Viewing a cold air outbreak using satellite-based synthetic aperture radar and advanced very high resolution radiometer imagery. *J. Geophys. Res. 101(C7): 16,391-400*

Mourad PD, Thompson DR, Vandemark DC. 2000. Extracting fine-scale wind fields from synthetic aperture radar images of the ocean surface. *Johns Hopkins APL Tech. Dig. 21(1): 108-115*

Porté-Agel F, Meneveau C, Parlange MB. 2000. A scale dependent dynamic model for large-eddy simulation: application to a neutral atmospheric boundary layer. *J. Fluid Mech. 415:261-84*

Porté-Agel F, Parlange MB, Meneveau C, Eichinger W. 2001. A priori field study of the subgrid-scale heat flux and dissipation in the atmospheric surface layer. *J. Atmos. Sci. 58: 2673-98*

Porté-Agel F, Pahlow M, Meneveau C, Parlange MB. 2001. Atmospheric stability effect on subgrid-scale physics for large-eddy simulation. *Adv. Water Res. 24(9-10):1085-102*

Portielje R, Lijklema L. 1995. The effect of reaeration and benthic algae on the oxygen balance of an artificial ditch. *Ecol. Model. 79(1): 35-48*

Schlichting H, Gersten K. 2000. *Boundary layer theory. 8th revised and enlarged edition.* Springer. 799 pp.

Schulz HE. 1990. Investigation of the flowing water reoxygenation mechanism and its correlation with the turbulence level near the surface – II. *PhD Dissertation. University of São Paulo, Brazil (In Portugese)*

Schulz HE, Bicudo JR, Barbosa AR, Giorgetti MF. 1990. Turbulent water aeration: analytical approach and experimental data. In *Air Water Mass Transfer. Eds. Wilhelms SC, Gulliver JS. ASCE Press. 142-155*

Scully NM, Leavitt PR, Carpenter SR. 2000. Century-long effects of forest harvest on the physical structure and autotrophic community of a small temperate lake. *Can. J. Fish. Aquat. Sci. 57(Suppl. 2): 50-59*

Sikora TD, Thompson DR, Bleidorn, JC. 2000. Testing the diagnosis of marine atmospheric boundary layer structure from synthetic aperture radar. *Johns Hopkins APL Tech. Dig. 21(1): 94-99*

Simon A, Kocsis O, Stips A, Wüest A. 2002. Momentum and turbulent kinetic energy balance in the surface boundary layer of developing waves. *J. Geophys. Res. (no pub date yet)*

Smagorinsky JS. 1963. General circulation experiments with the primitive equations: 1. the basic experiment.*Mon. Weather Rev. 91: 99-164*

Smits, AJ. 2000. A physical introduction to fluid mechanics. *John Wiley & Sons. 527 pp.*

Steedman RJ, Kushneriuk RS. 2000. Effects of experimental clearcut logging on thermal stratification, dissolved oxygen, and lake trout (*Salvelinus namaycush*) habitat volume in three small boreal forest lakes. *Can. J. Fish. Aquat. Sci. 57(Suppl. 2): 82-91*

Stoffelen A, Anderson DLT. 1993. Wind retrieval and ERS-1 scatterometer radar backscatter measurements. *Adv. Space. Res. 13: 53-60*

Stull RB. 1988. An introduction to boundary layer meteorology. *Kluwer Acad. Publ. 670 pp.*

Terray EA, Donelan MA, Agrawal YC, Drennan WL, Kahma KK, et al. 1996. Estimates of kinetic energy dissipation under breaking waves. *J. Phys. Oceanogr.26: 792-807*

Thitimajshima P, Rangsanseri Y, and Rakprathanporn P. 1998. A simple SAR speckle reduction by wavelet thresholding. *Proc. 19th Asian Conference on Remote Sensing (ACRS).*

Thompson DR, Beal RC. 2000. Mapping high-resolution wind fields using synthetic aperture radar. *Johns Hopkins APL Tech. Dig. 21(1): 58-67*

Thorpe SA. 1995. Dynamical processes of transfer at the sea surface. *Prog. Oceanogr. 35: 315-52*

Upstill-Goddard RC, Watson AJ, Liss PS, Liddicoat, MI. 1990. Gas transfer in lakes measured with SF_6. *Tellus B.*: 42(4): 364-377

Van Dorn W. 1953. Wind stress on an artificial pond. *J. Marine Res. 12: 249-276*

Vicjers D, Mahrt L. 1997. Quality control and flux sampling problems for tower and aircraft data. *J. Atm. Oc. Tech.* 14: 512-526
Walker, I.J. and W.G. Nickling. 2002. Dynamics of secondary airflow and sediment transport over and in the lee of transverse dunes. *Progress in Physical Geography* 26: 47-75.

Walker, I.J. and W.G. Nickling. 2003. Simulation and measurement of surface shear stress over isolated and closely spaced transverse dunes in a wind tunnel. *Earth Surf. Process. Landforms* 28: 1111-1124.

Wang H, Takle ES, Shen J. 2001. Shelterbelts and windbreaks: mathematical modeling and computer simulations of turbulent flows. *Annu. Rev. Fluid Mech. 33: 549-86*

Wang Y, Hutter K. 1998. A semi-implicit semispectral primitive equation model for lake circulation dynamics and its stability performance. *J. Comp. Phys. 139: 209-41*

Wang Y, Hutter K, Bäuerle E. 2001. Three-dimensional wind-induced baroclinic circulation in rectangular basins. *Adv. Water Res. 24: 11-27*

*W*ang Y. 2003. Importance of subgrid-scale parameterization in numerical simulations of lake circulation. *Adv. Water Res. 26: 277-94*

Wanninkhof R, Ledwell J, Crusius J. 1990. Gas transfer velocities on lakes measured with sulfur hexafluoride. In: *Air Water Mass Transfer*. Eds.

Wanninkhof R, McGillis WR. 1999. A cubic relationship between air-sea CO_2 exchange and wind speed. *Geophys. Res. Lett. 26 (13): 1889-92*

Wilhelms, S.C. and Gulliver J.S., American Society of Civil Engineers. 441-458

Wismann V. 1992. A C-band scatterometer model derived from the data obtained during the ERS-1 calibration/validation campaign. *Proc. First ERS-1 Symp., Cannes, France. 55-59*

Wu J. 1969. Wind stress and surface roughness. *J. Geophys. Res.74: 444-455*

Wu J. 1970. Wind-wave interactions. *Phys. Fluids. 13: 1926-1930*

Wüest A and Lorke A. 2003. Small-scale hydrodynamics in lakes. *Annu. Rev. Fluid Mech. 35: 373-412*

Yelland MJ, Taylor PK. 1996. Wind stress measurements from the open ocean. *J. Phys. Oceanogr. 26: 541-58*

Part B Pipe cleaner experiments

Summary of independent experimental variables for data set #2 (pipe cleaners)

Height of canopy (pipe cleaners): h=0.075m or 7.5cm
Velocity setting in wind tunnel: 10 m/s
Velocity profiles measured at: x = 0.0m, 0.2m, 0.4m, 0.6m, 1.1m, 2.0m, 3.25m, 4.07m, 5.94m, 6.68m

Reference velocity at x=0m and z=6h: U_{ref} = 9.46 m/s
Reference height: h = 0.075m or 7.5cm

Computed canopy porosity: ε = 78%
Computed canopy roughness: z_{0c} = 0.005 m
Computed canopy displacement height: d = 0.066 m
Computed canopy shear velocity: U* =1.0 m/s

Computed surface roughness downstream from canopy: z_{0s} = 0.00001 m

1. Introduction – similar to Part A

2. Wind tunnel experiment

The experiment in the wind tunnel of the Saint Anthony Falls Laboratory (Figure 2.1) at the University of Minnesota described in Part A was repeated except that the canopy was changed. A model canopy was created from pipe cleaners. Pipe cleaners were inserted into a foam board of 2.5cm thickness, and the board was placed on the wind tunnel floor. It covered the total width of the wind tunnel and extended over a length of 2m in flow direction. Foam board without pipe cleaners was installed on the wind tunnel floor downstream from the canopy and represented an aerodynamically smooth surface (Figures 2.2 to 2.4). The wind tunnel velocity setting was 10 m/s.

The canopy made of pipe cleaners had a height of approximately 7.5 cm and a porosity of about 78%. The experiment was run at an air temperature of 28°C. The Reynolds number based on the model canopy height of 0.075 m was approximately Re = 50 000. Based on the wind tunnel height of H = 1.6 m it would have been Re = 1 070 000.

Wind velocity profiles were measured at the end of the canopy (x=0) and at nine positions downwind of the canopy (x = 0.2 m, 0.4 m, 0.6 m, 1.1 m, 2.0 m, 3.25 m, 4.07 m, 5.94 m and 6.68 m).

Figure 2.1 Test section of the St. Anthony Falls Laboratory wind tunnel

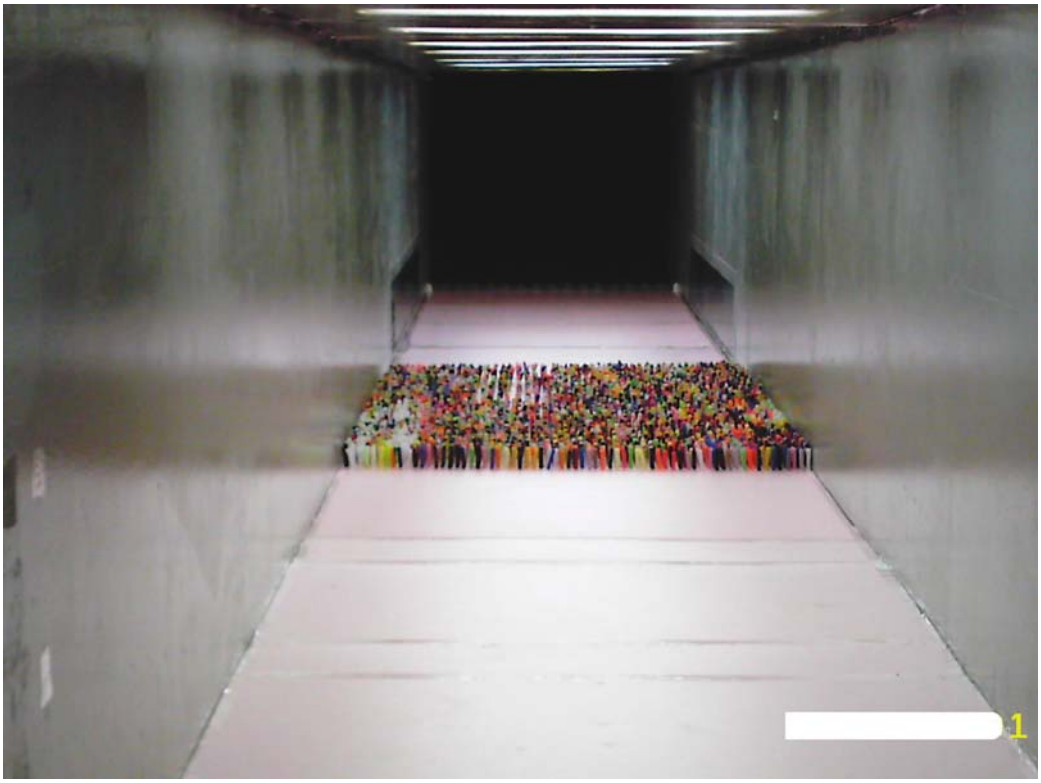

Figure 2.2 Wind tunnel test section with canopy made of pipe cleaners

Figure 2.3 Wind tunnel test section with canopy made of pipe cleaners

Figure 2.4: Close-up view of canopy made of pipe cleaners

3. Data analysis and results

3.1 Velocity data

Figures 3.1 and 3.2 show the measured velocity profiles plotted against distance from the wind tunnel floor using both linear and semi-logarithmic scales.

The reference velocity determined from the x=0m distance profile was found to be 9.46 m/s. We selected the surface shear stress at the furthest downwind measurement point as the reference shear stress. The reference surface shear stress is 0.16 N/m^2.

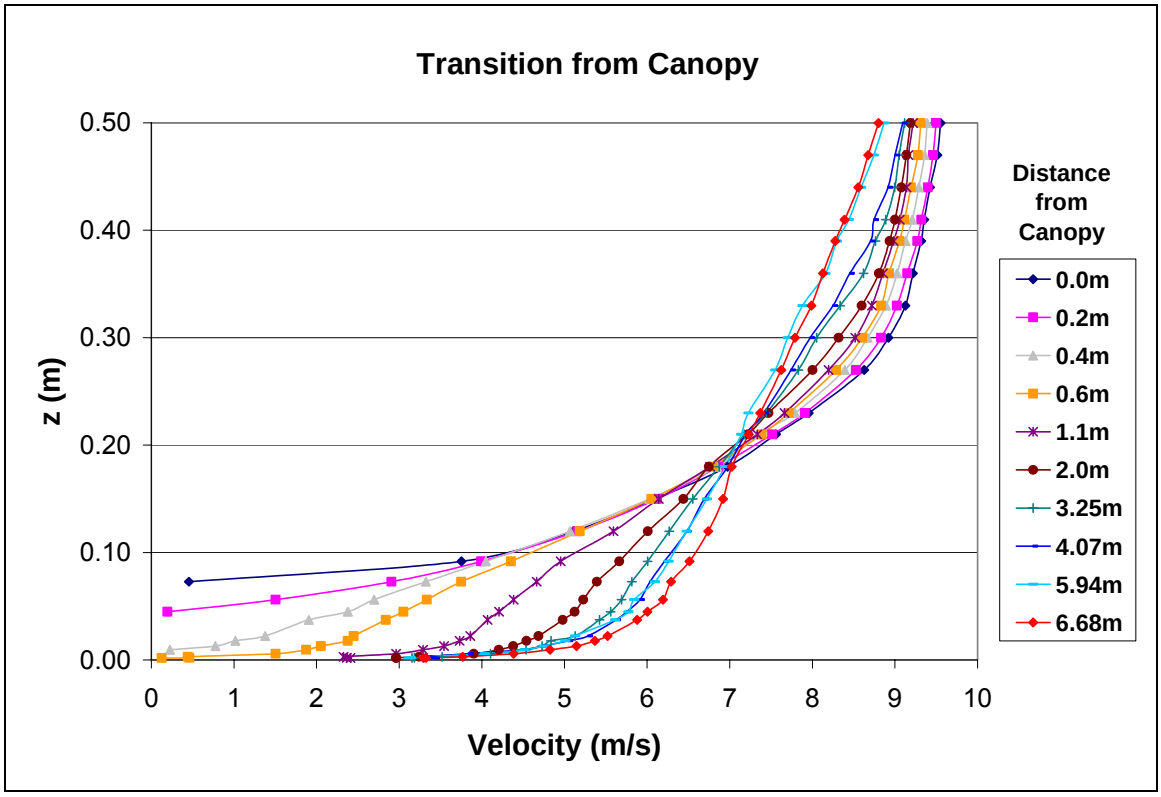

Figure 3.1 Velocity profiles in Cartesian coordinates

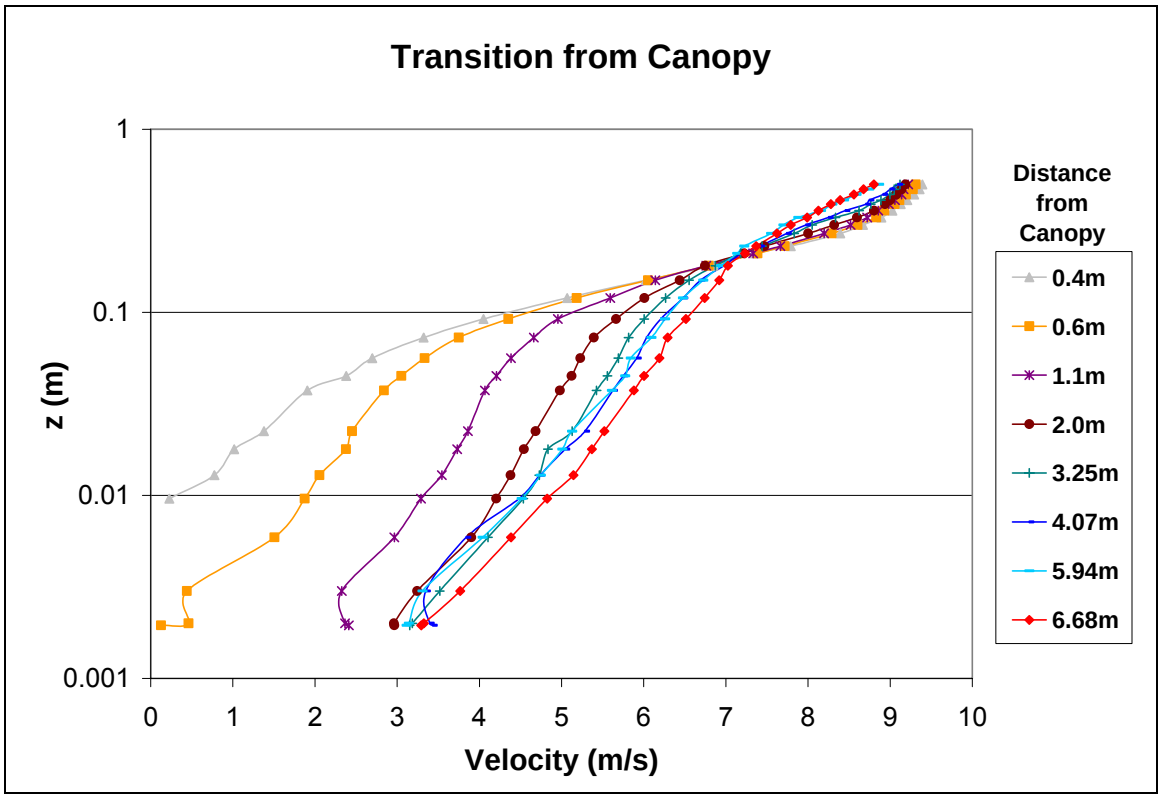

Figure 3.2 Semi-logarithmic plot of velocity profiles.

3.2 Surface (boundary) layer: surface roughness, surface shear stress, surface layer thickness downwind from the canopy

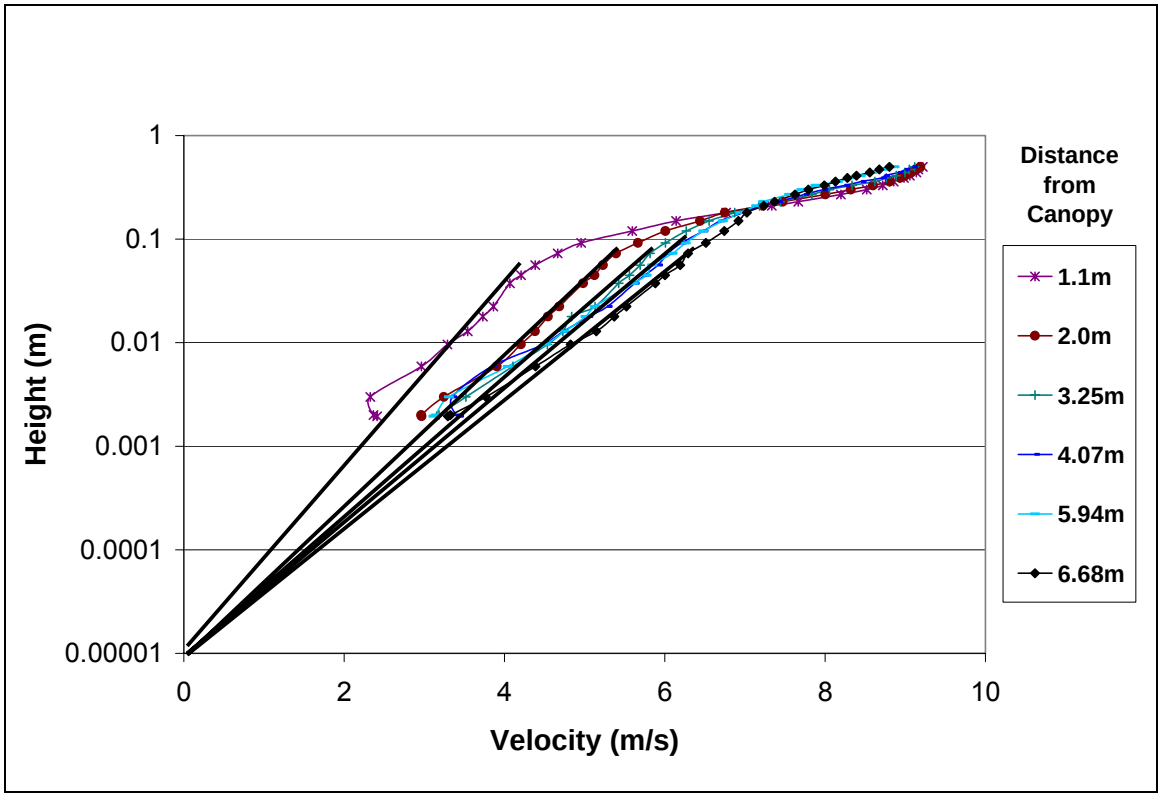

Figure 3.3 Determination of surface roughness (z_{os}) downstream from canopy

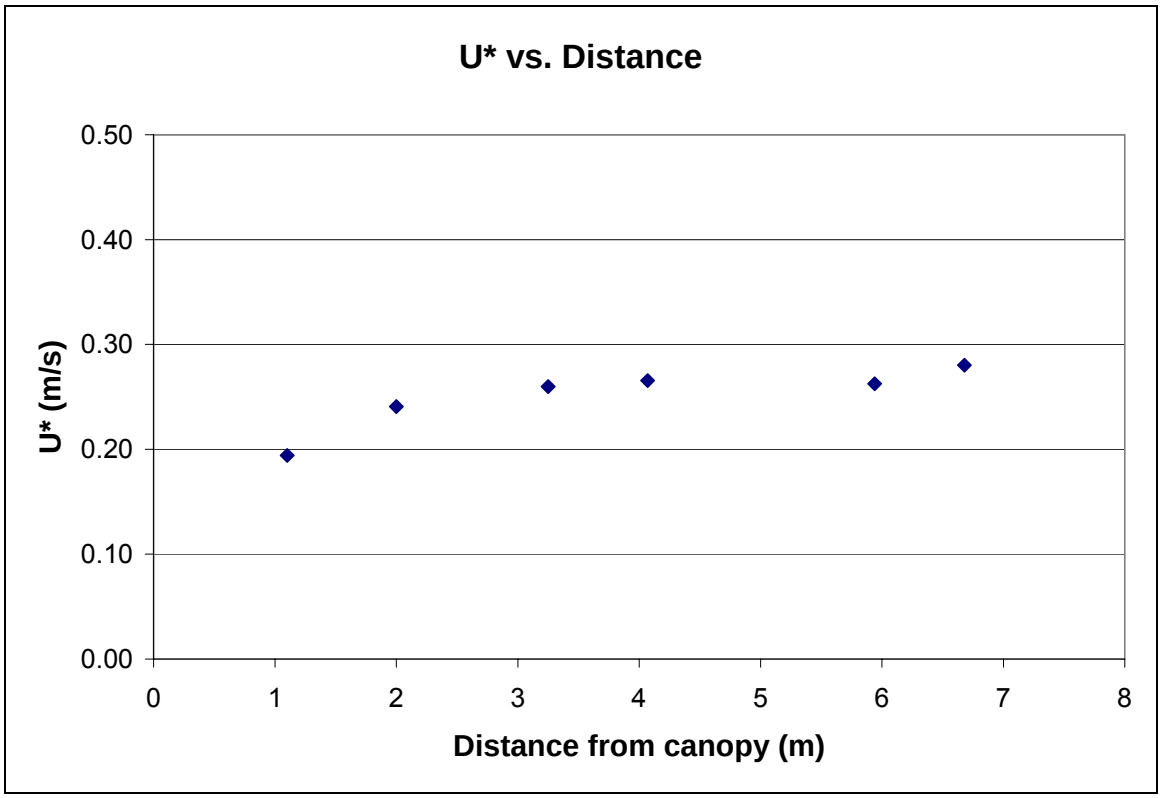

Figure 3.4 Shear velocity (U*) vs. distance from canopy

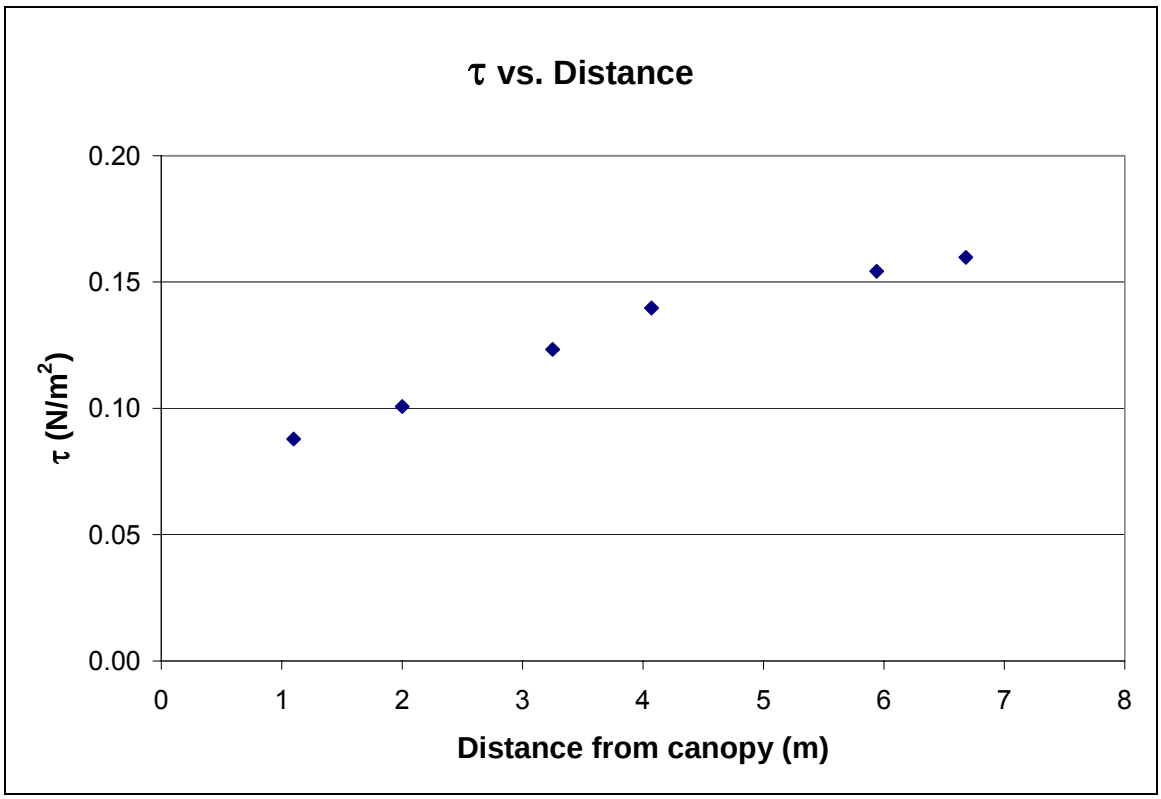

Figure 3.5 Surface shear stress (τ) vs. distance from canopy

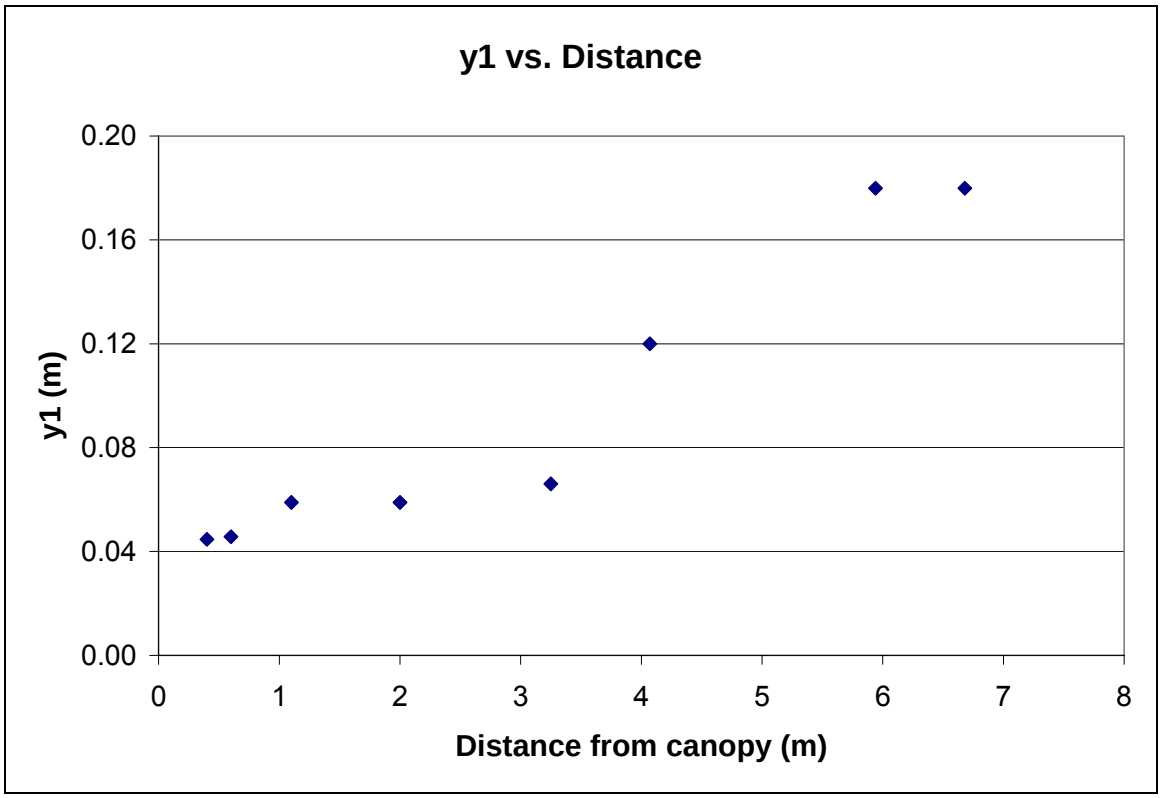

Figure 3.6 Upper end of surface layer (y1) vs. distance from canopy

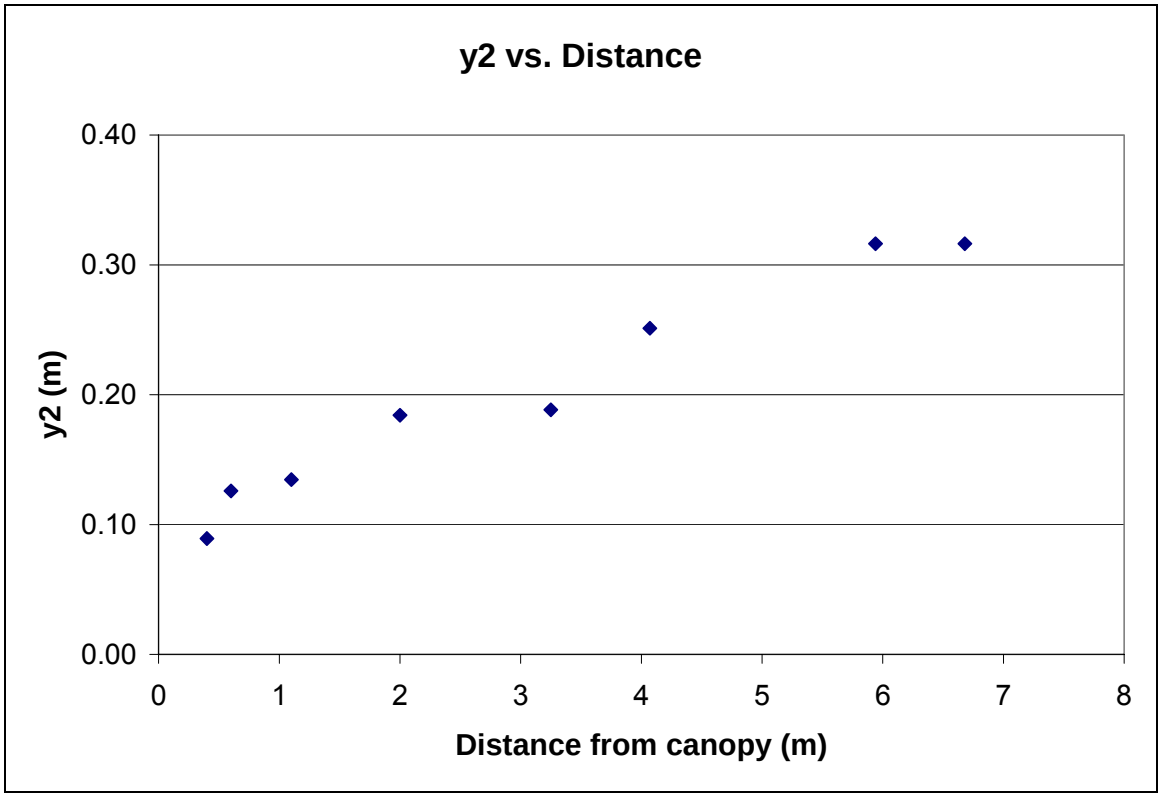

Figure 3.7 Lower end of blending layer (y2) vs. distance from canopy

3.3 Mixing (transition/blending) layer: surface roughness, surface shear stress, and surface layer thickness downwind from canopy

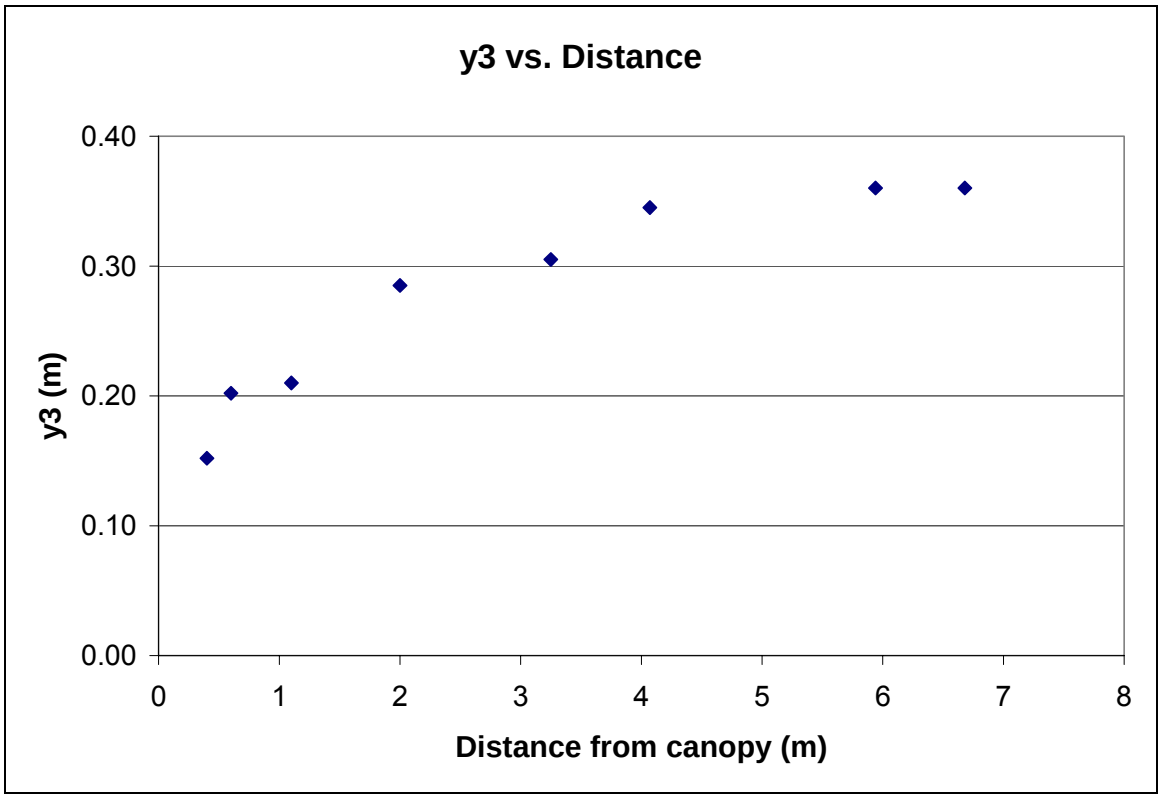

Figure 3.9 Upper end of the blending layer (y3) vs. distance from canopy

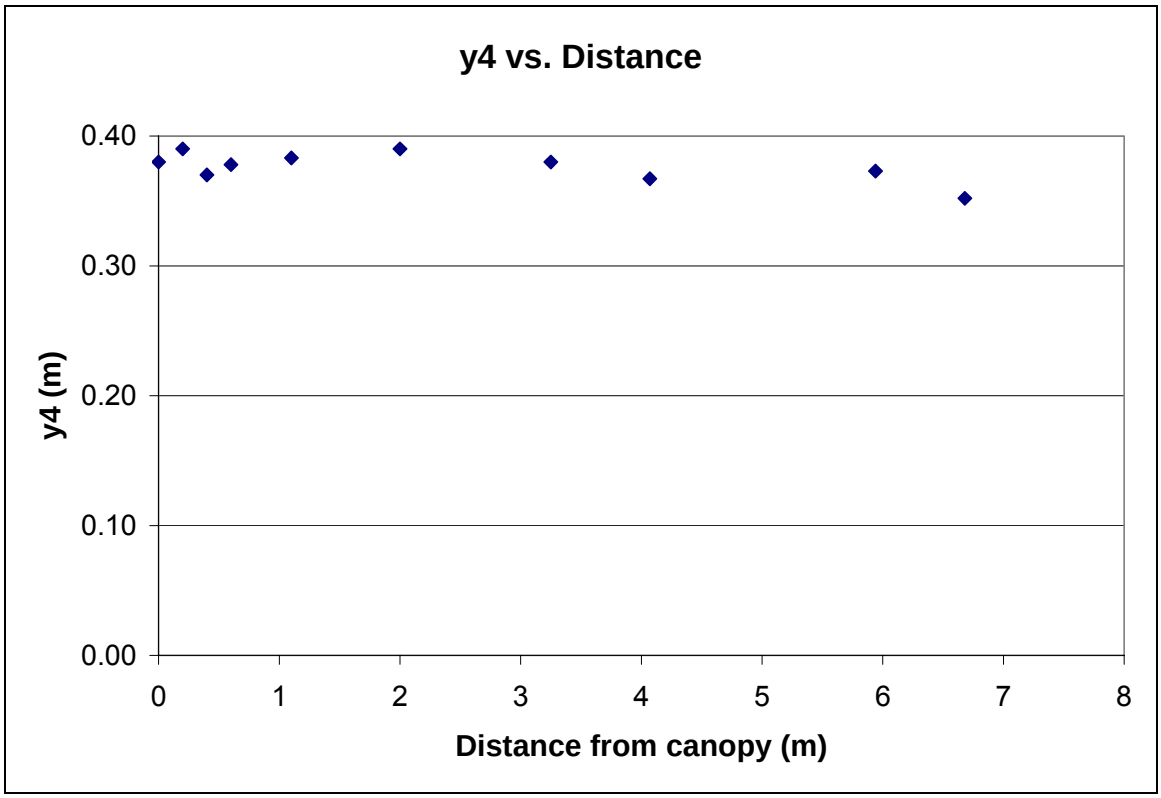

Figure 3.10 Lower end of outer layer (y4) vs. distance from canopy

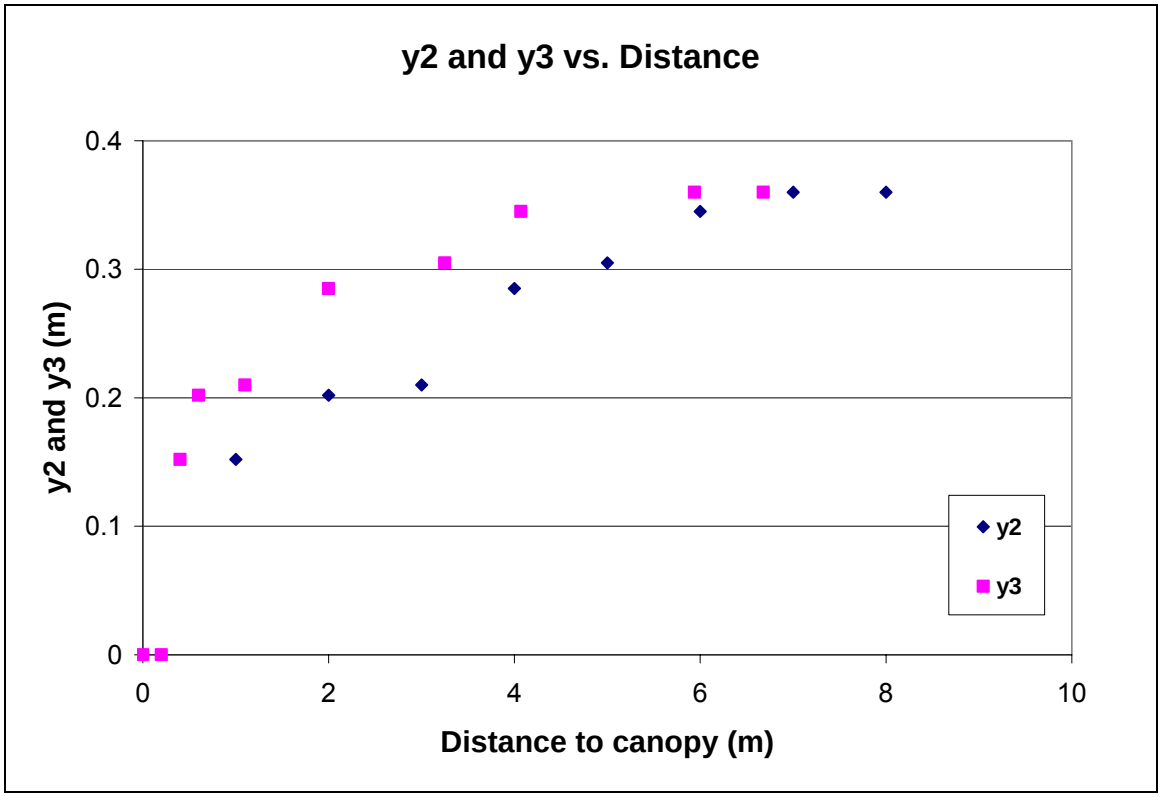

Figure 3.12 Upper (y3) and lower (y2) end of the mixing/blending layer vs. distance from the canopy. The distance between y2 and y3 is the **thickness of the mixing/blending layer**

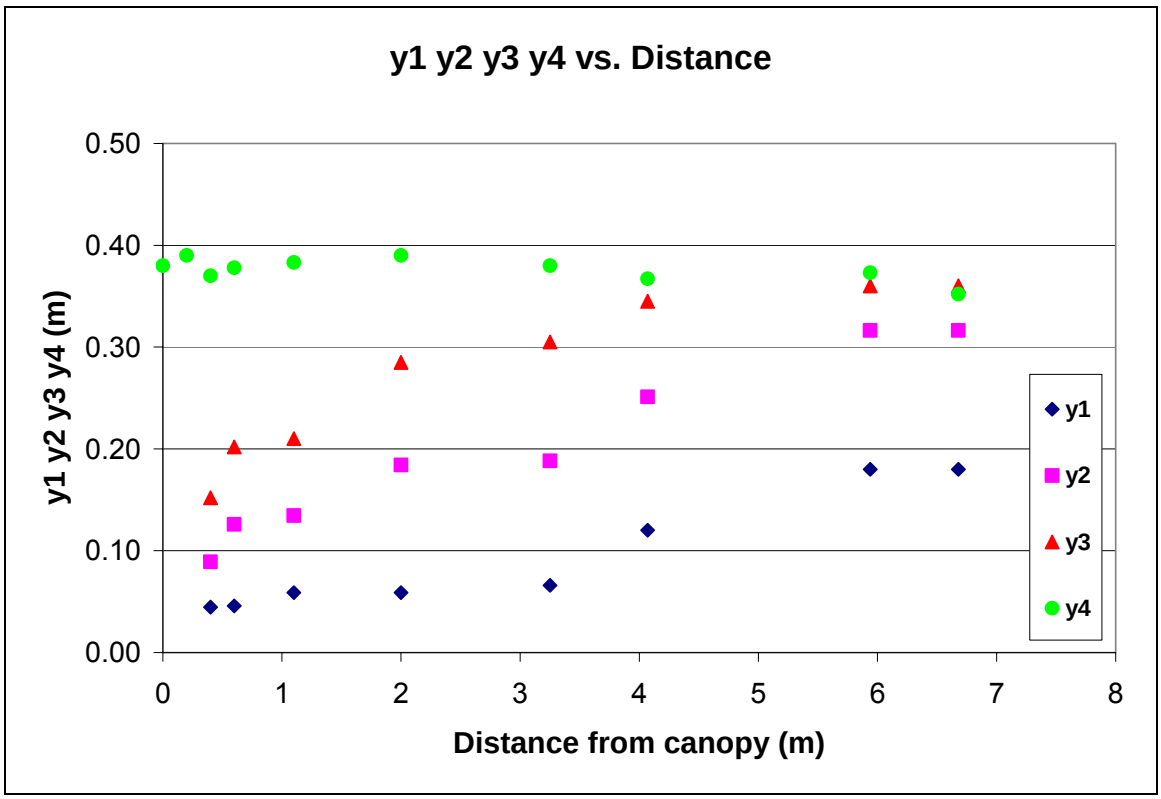

Figure 3.14 Upper and lower boundaries of the surface layer, the mixing layer and the outer layer

3.4 Outer (free stream) layer

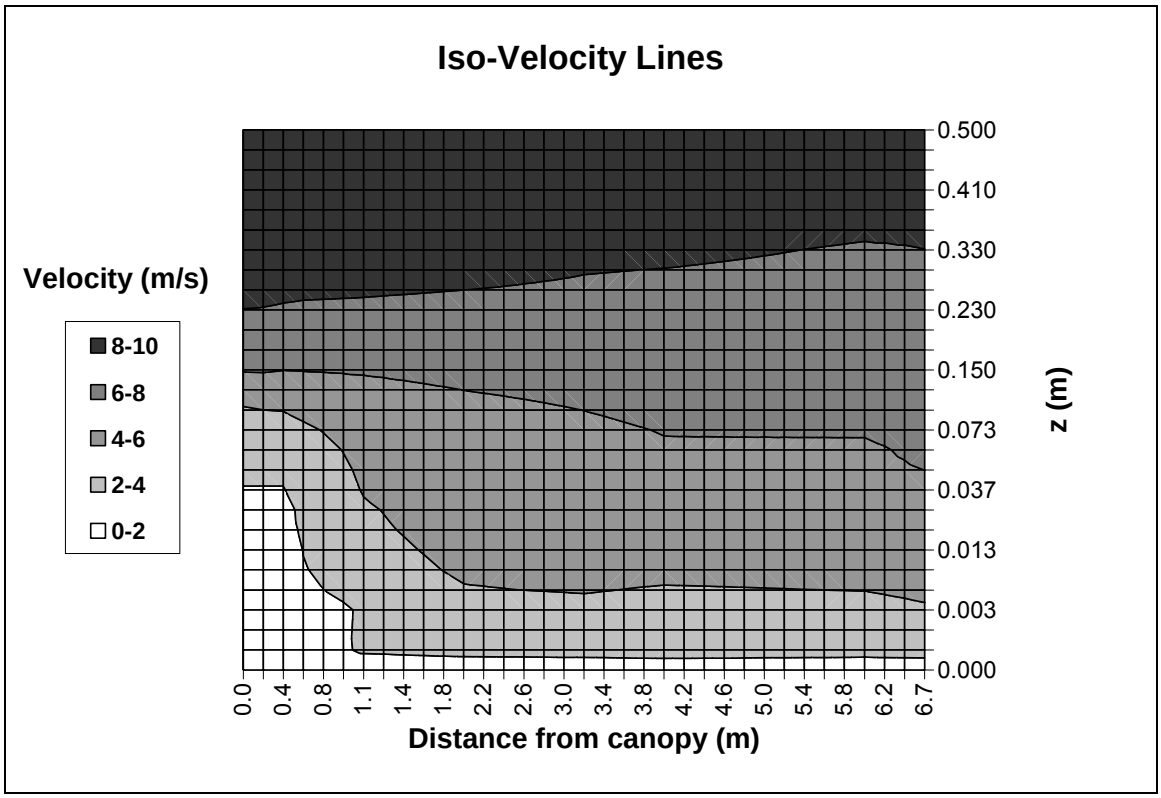

Figure 3.15 Iso-velocity lines plotted at 2 m/s intervals

3.5 Mass and momentum flow downwind from the canopy

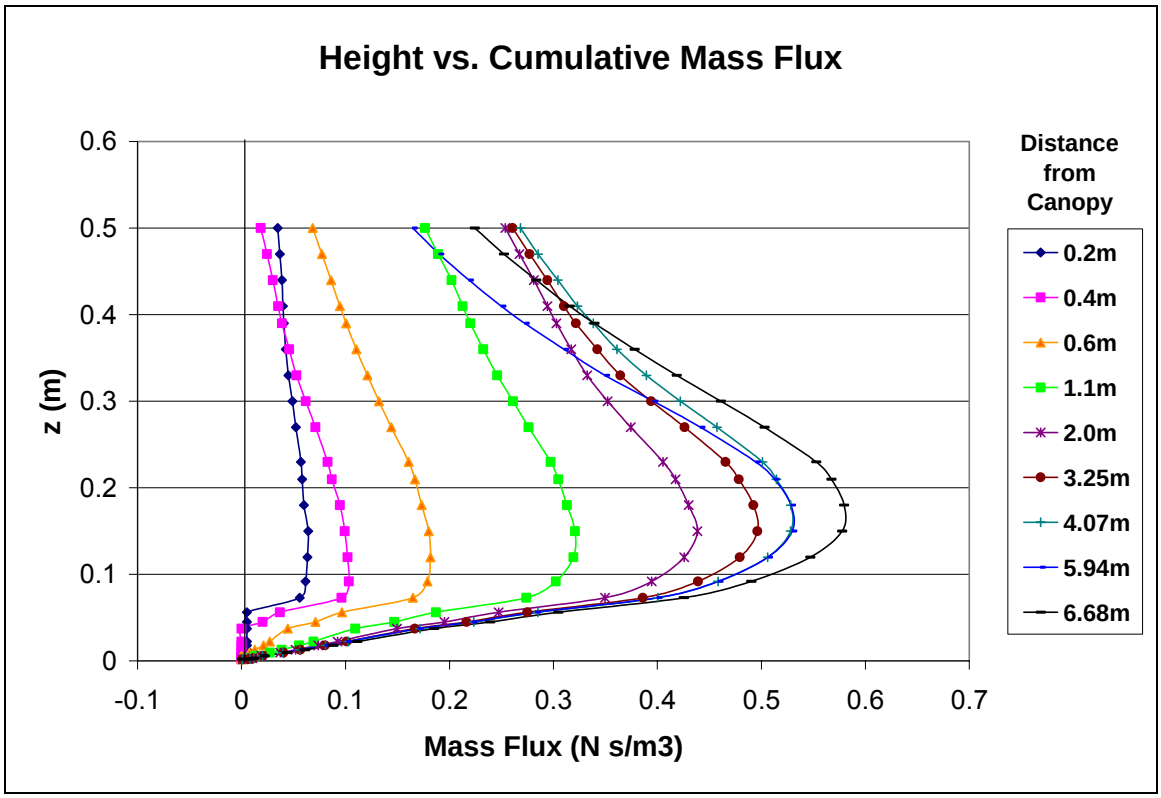

Figure 3.16 Cumulative mass flow downwind from the canopy

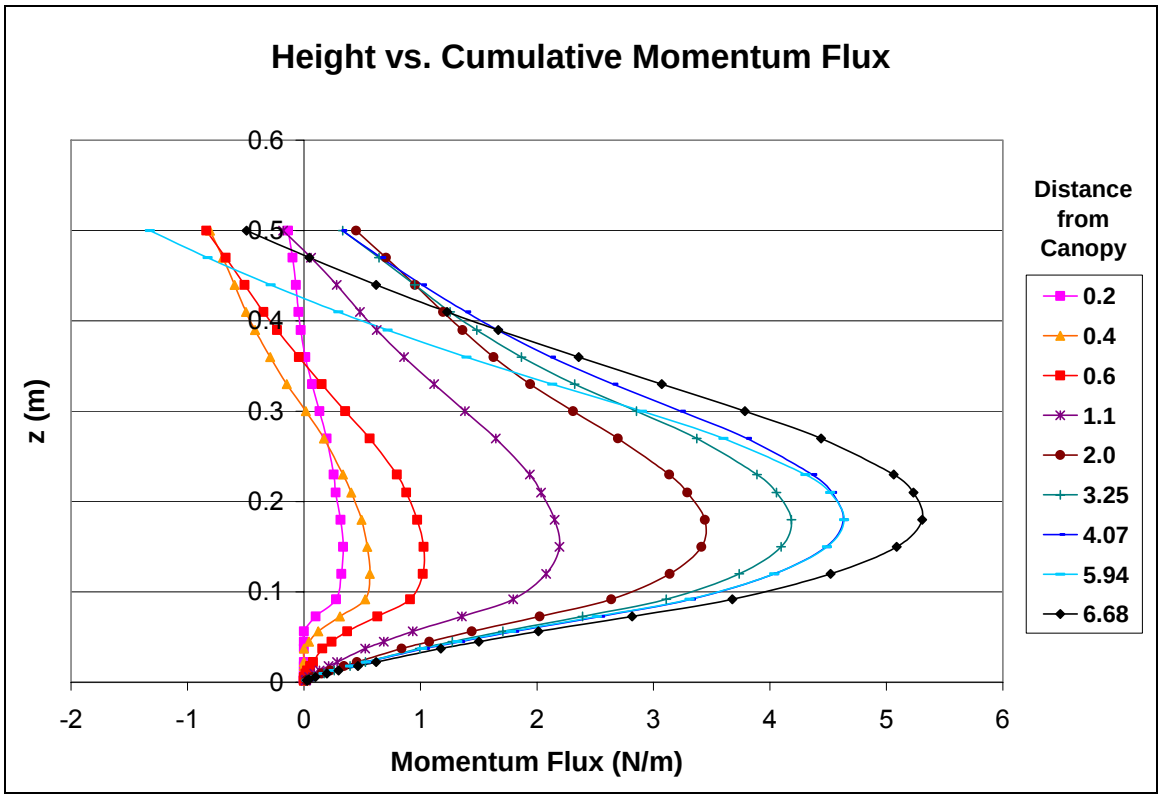

Figure 3.17 Cumulative momentum flow downwind from the canopy.

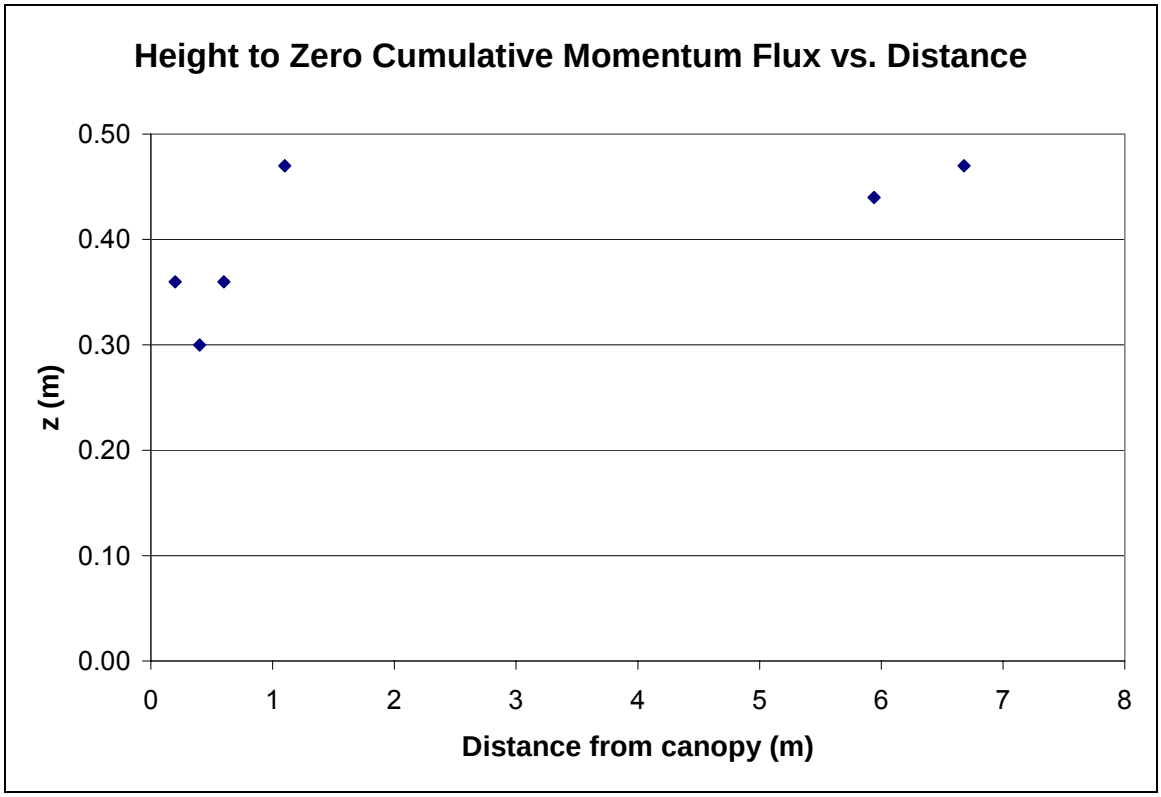

Figure 3.22 Height of no change of cumulative flow of momentum between x=0 and a distance (x) downwind from the canopy

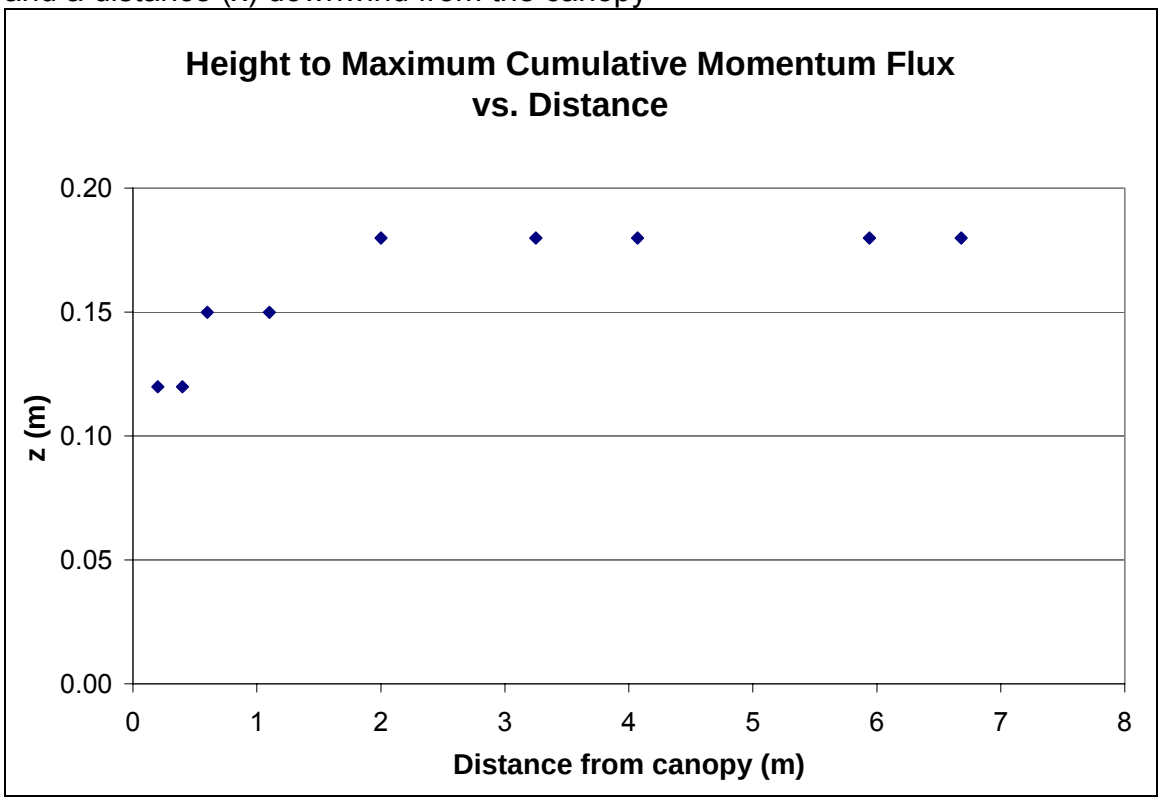

Figure 3.23 Height of maximum change in cumulative flow of momentum

3.6 Shear stress distribution in the wind field downwind from the canopy

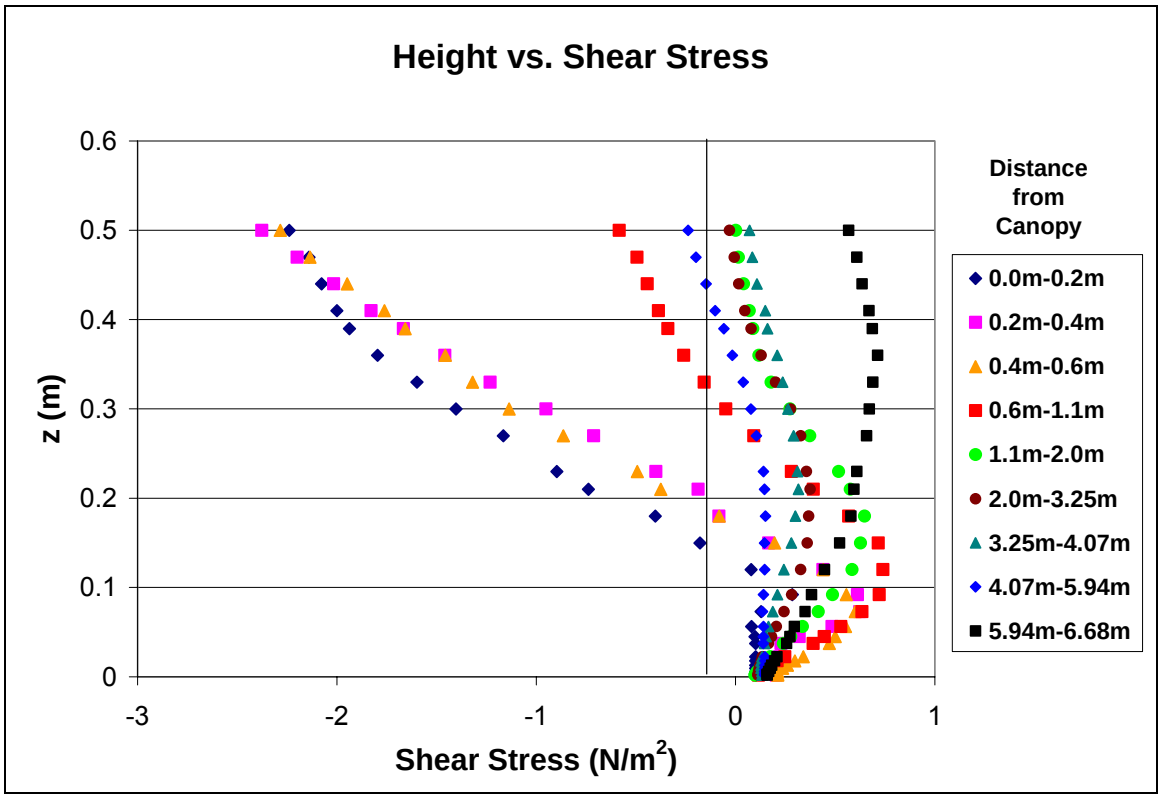

Figure 3.24 Shear stress throughout the wind field

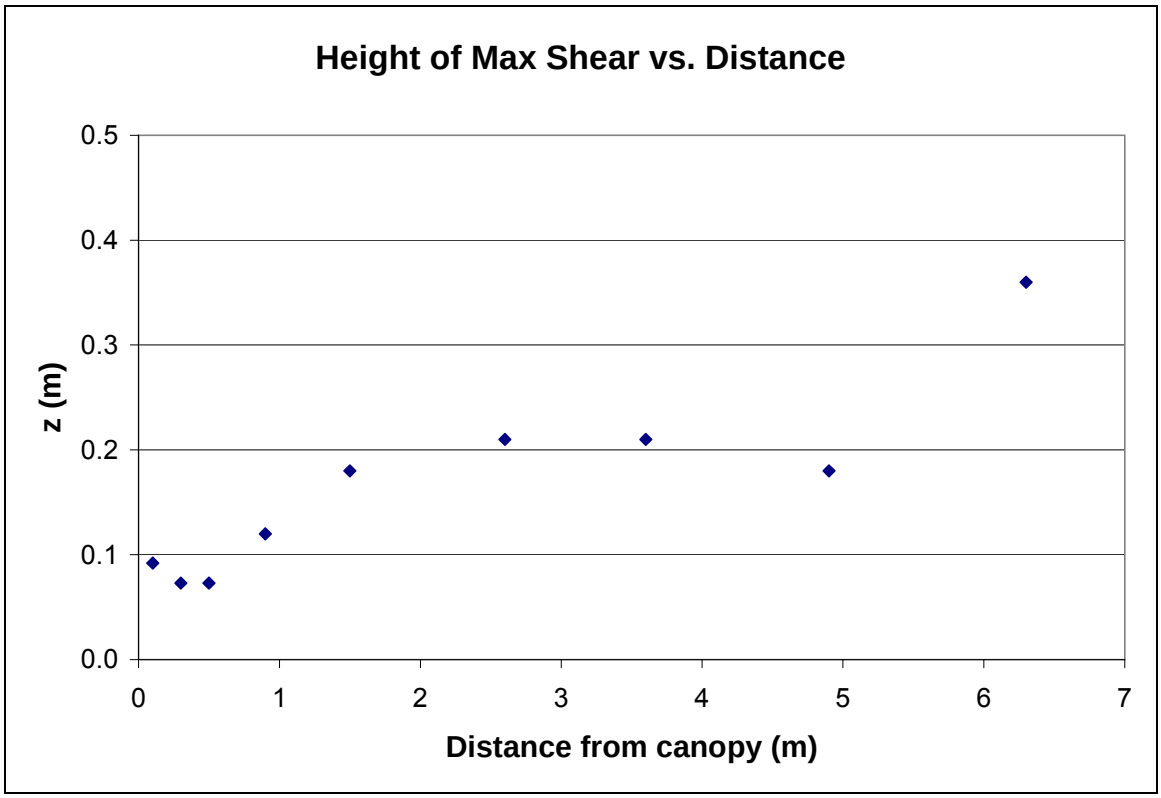

Figure 3.25 Height of maximum shear stress vs. distance downwind of canopy

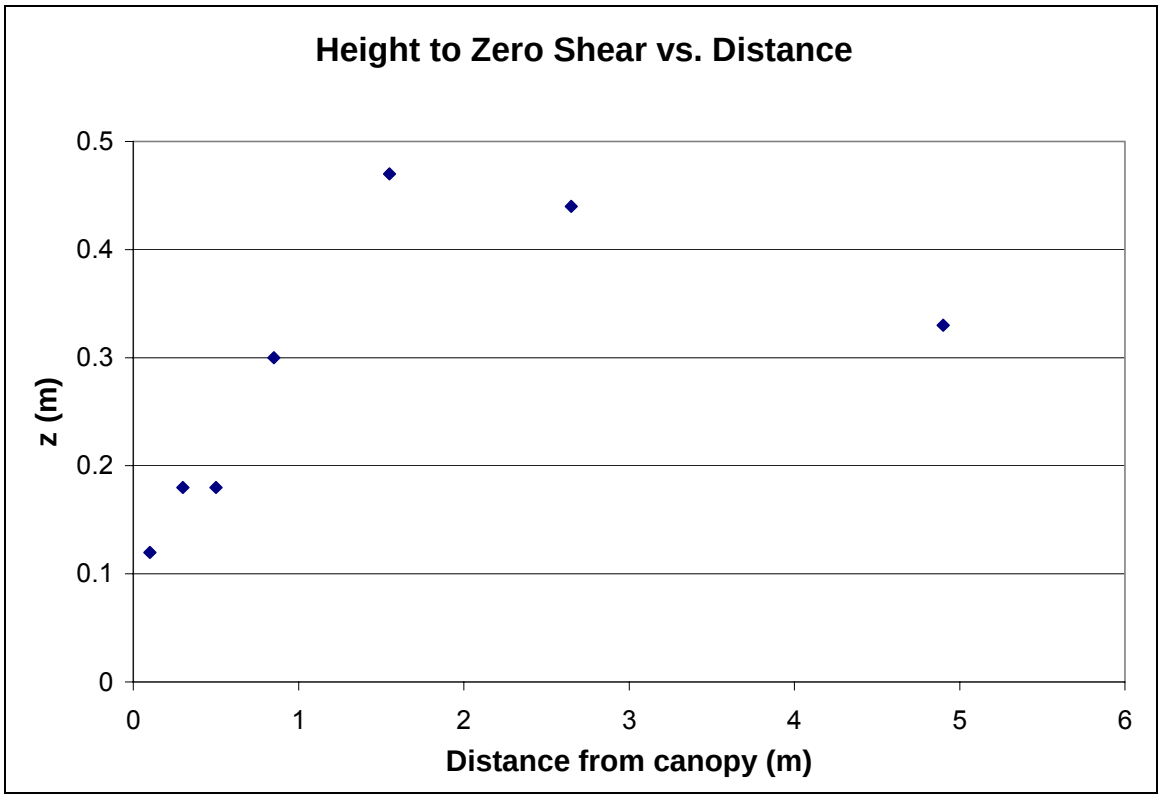

Figure 3.26 Height to zero shear stress vs. distance downwind from the canopy

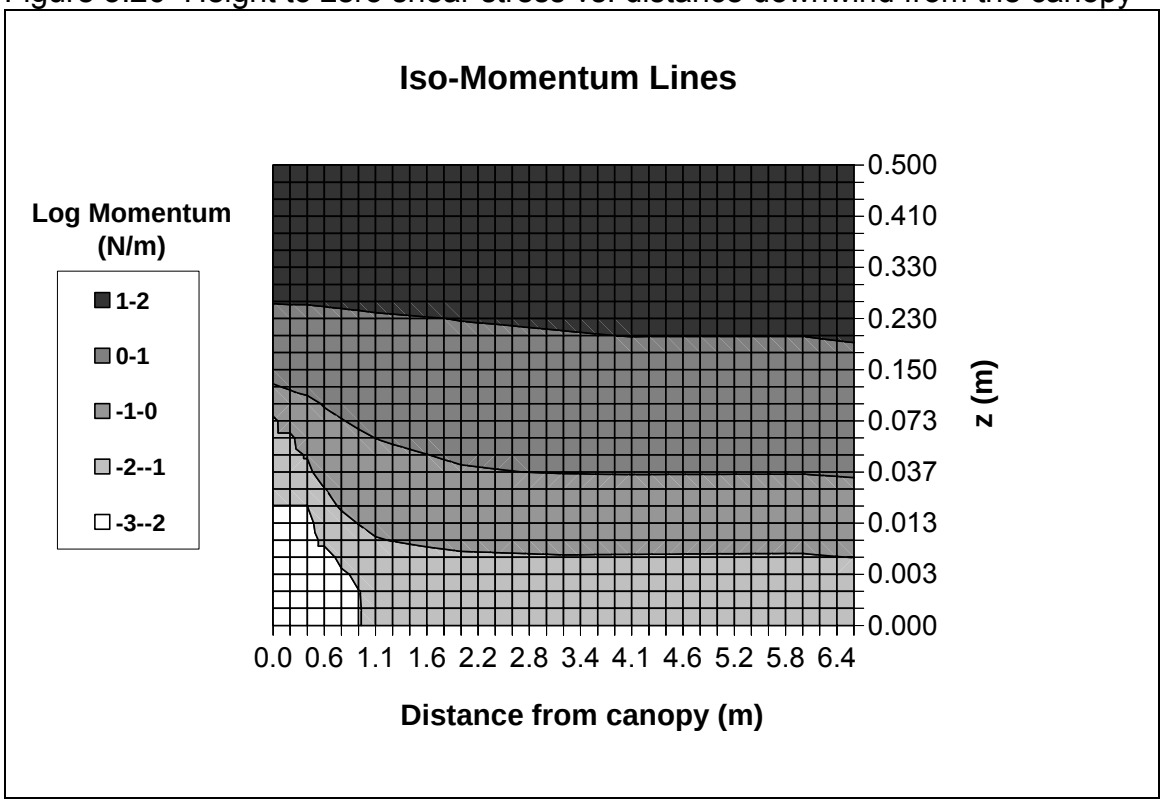

Figure 3.28 Iso-momentum flow lines downwind from the canopy.

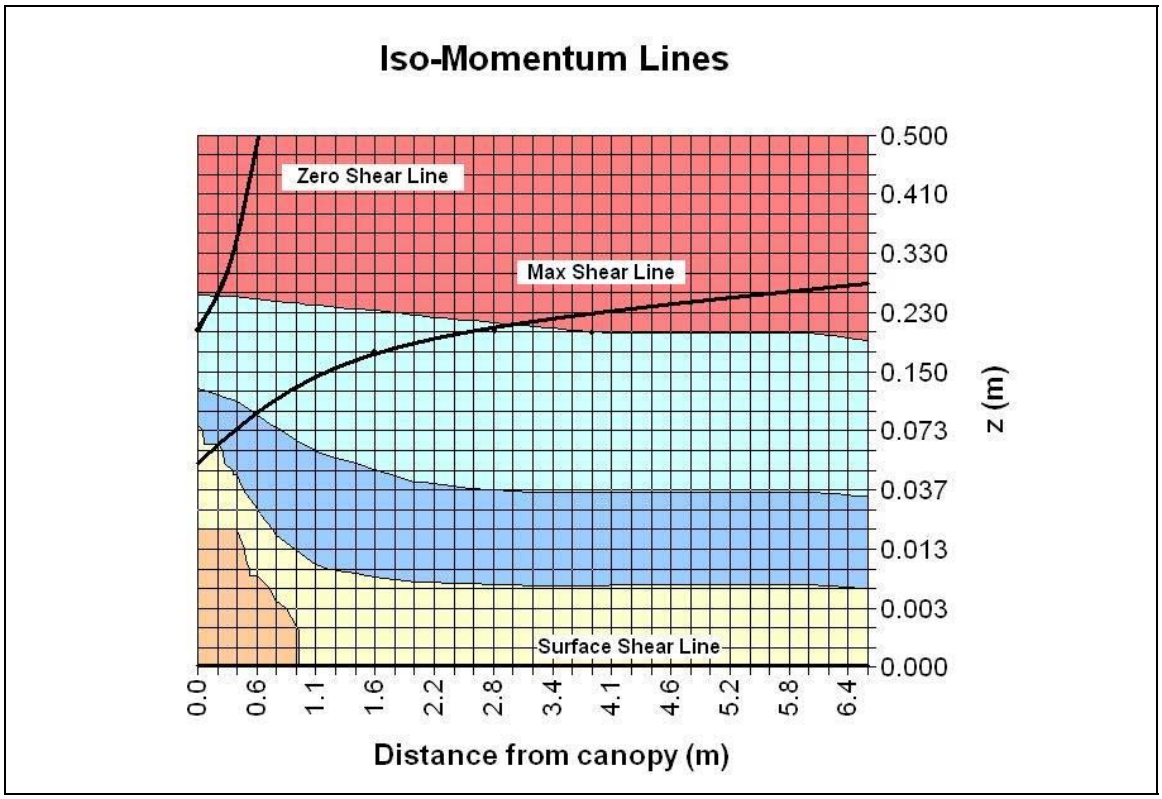

Figure 3.29 Iso-momentum flow lines and shear stress lines

4. Discussion

4.1 Aerodynamic characterization of the canopy by roughness and displacement height

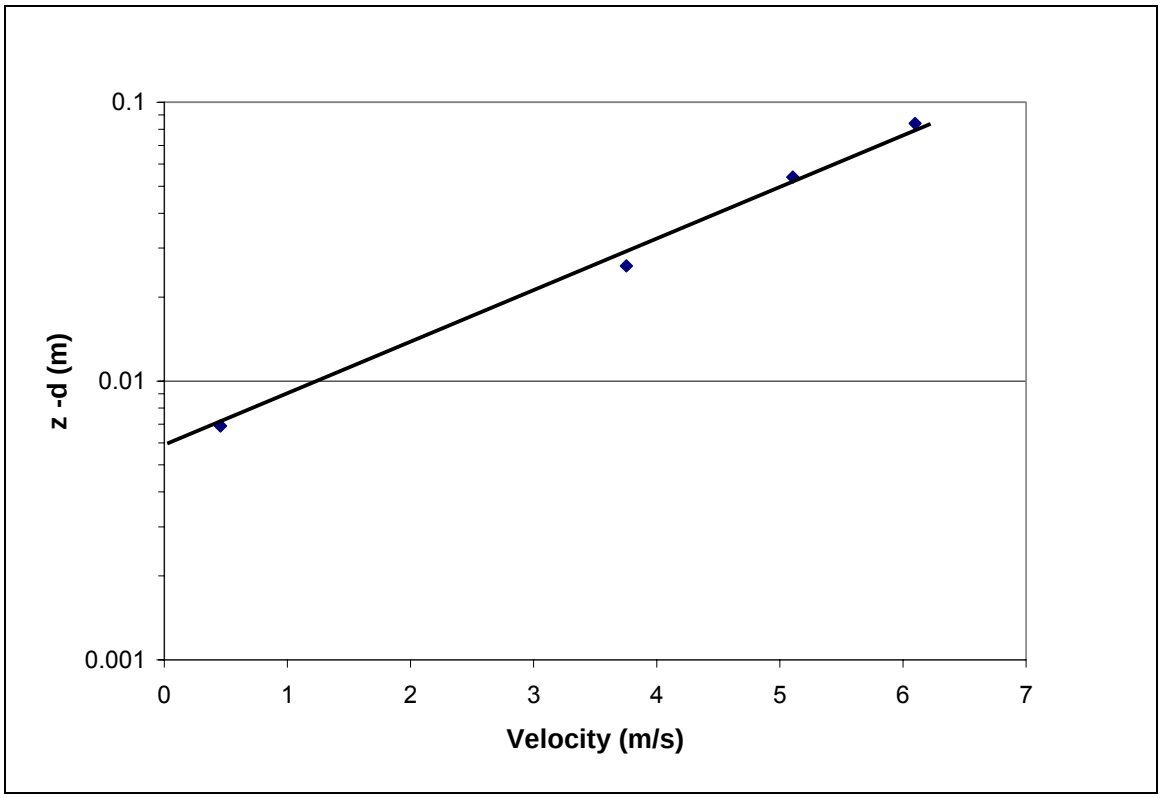

Figure 4.1 Determination of canopy roughness (z_{0c}).

Part C. Solid step experiment

Summary of independent experimental variables for data set #3 (solid step)

Height of canopy (step): h=0.050m or 5.0cm
Velocity setting in wind tunnel: 10 m/s
Velocity profiles measured at: x = 0.0m, 0.2m, 0.4m, 0.6m, 1.1m, 2.0m, 2.76m, 4.07m, 5.94m, 6.68m

Reference velocity at x=0m and z=6h: U_{ref} = 8.95 m/s
Reference height: h = 0.075m or 7.5cm

Computed canopy porosity: ε = 0%
Computed canopy roughness: z_{0c}= 0.00001 m
Computed canopy displacement height: d = 0.0508 m
Computed canopy shear velocity: U* = 0.48 m/s

Computed surface roughness downstream from canopy: z_{0s} = 0.00001 m

1. Introduction – similar to Part A

2. Wind tunnel experiment

The experiment in the wind tunnel of the Saint Anthony Falls Laboratory (Figure 2.1) at the University of Minnesota described in Part A was repeated except that the canopy was changed. A model canopy was created from styrofoam boards. It covered the total width of the wind tunnel and extended over a length of 2m in flow direction. Foam board was installed on the wind tunnel floor downstream from the canopy and represented an aerodynamically smooth surface (Figures 2.2 to 2.4). The wind tunnel velocity setting was 10 m/s.

The solid step canopy made of styrofoam boards had a height of approximately 5.0 cm and a 0.0% porosity. The experiment was run at an air temperature of 28°C. The Reynolds number based on the model canopy height of 0.050 m was approximately Re = 34 000. Based on the wind tunnel height of H = 1.6 m it would have been Re = 1 070 000.

Wind velocity profiles were measured at the end of the canopy (x=0) and at nine positions downwind of the canopy (x = 0.2 m, 0.4 m, 0.6 m, 1.1 m, 2.0 m, 2.76 m, 4.07 m, 5.94 m and 6.68 m).

Figure 2.1. Test section of the St. Anthony Falls Laboratory wind tunnel

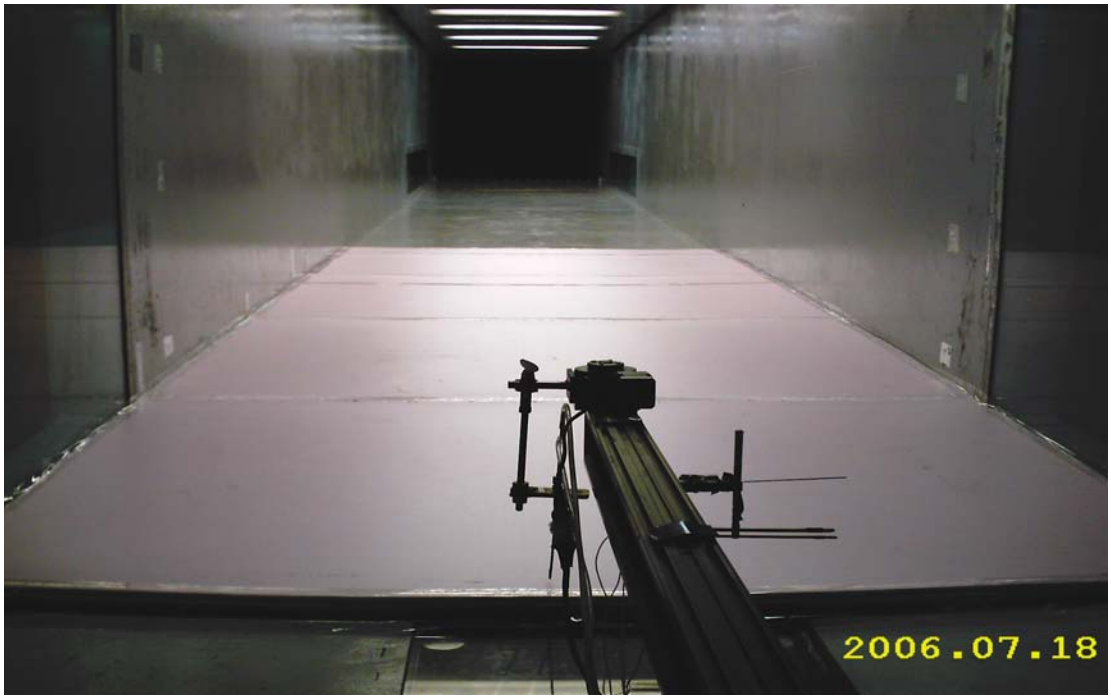

Figure 2.2: Setting up the foam board model in the tunnel

Figure 2.3: Test section with the foam boards looking downstream.

3. Data analysis and results

3.1 Velocity data

Figures 3.1 and 3.2 show the measured velocity profiles plotted against distance from the wind tunnel floor using both linear and semi-logarithmic scales.

The reference velocity determined from the x=0m distance profile was found to be 8.95 m/s. We selected the surface shear stress at the furthest downwind measurement point as the reference shear stress. The reference surface shear stress is 0.16 N/m^2.

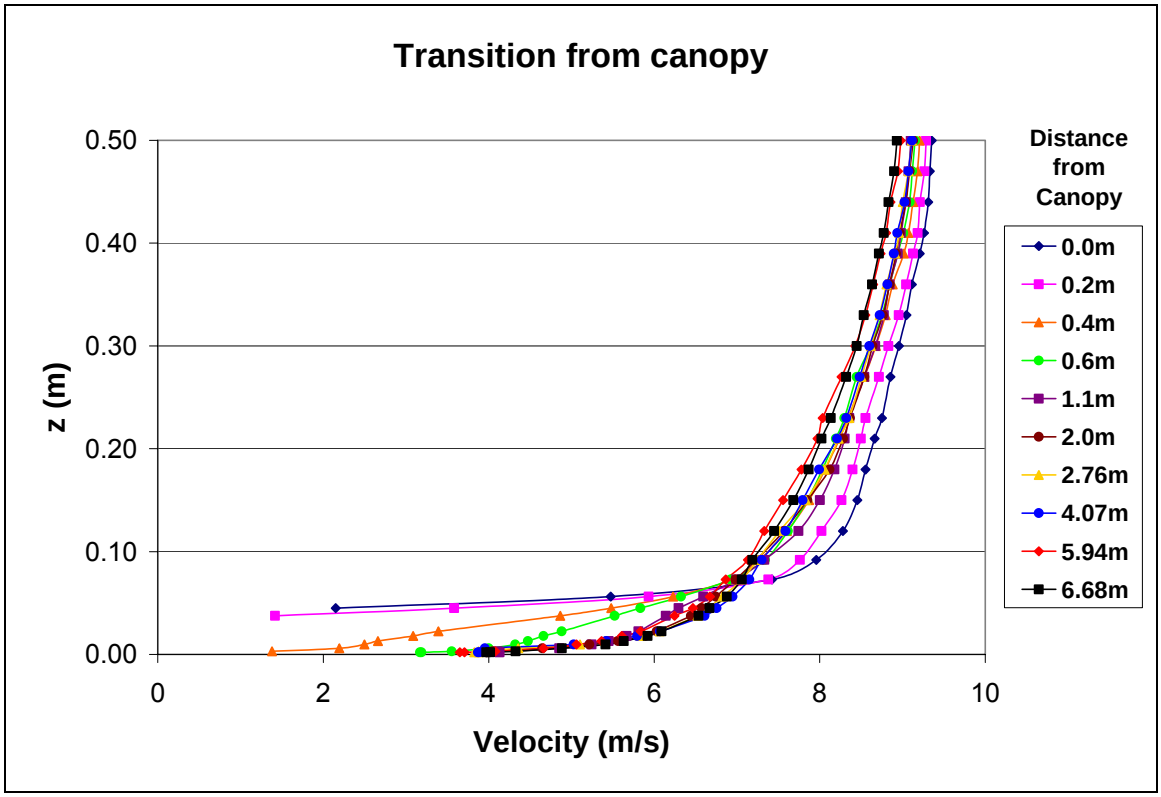

Figure 3.1: Velocity profiles in Cartesian coordinates.

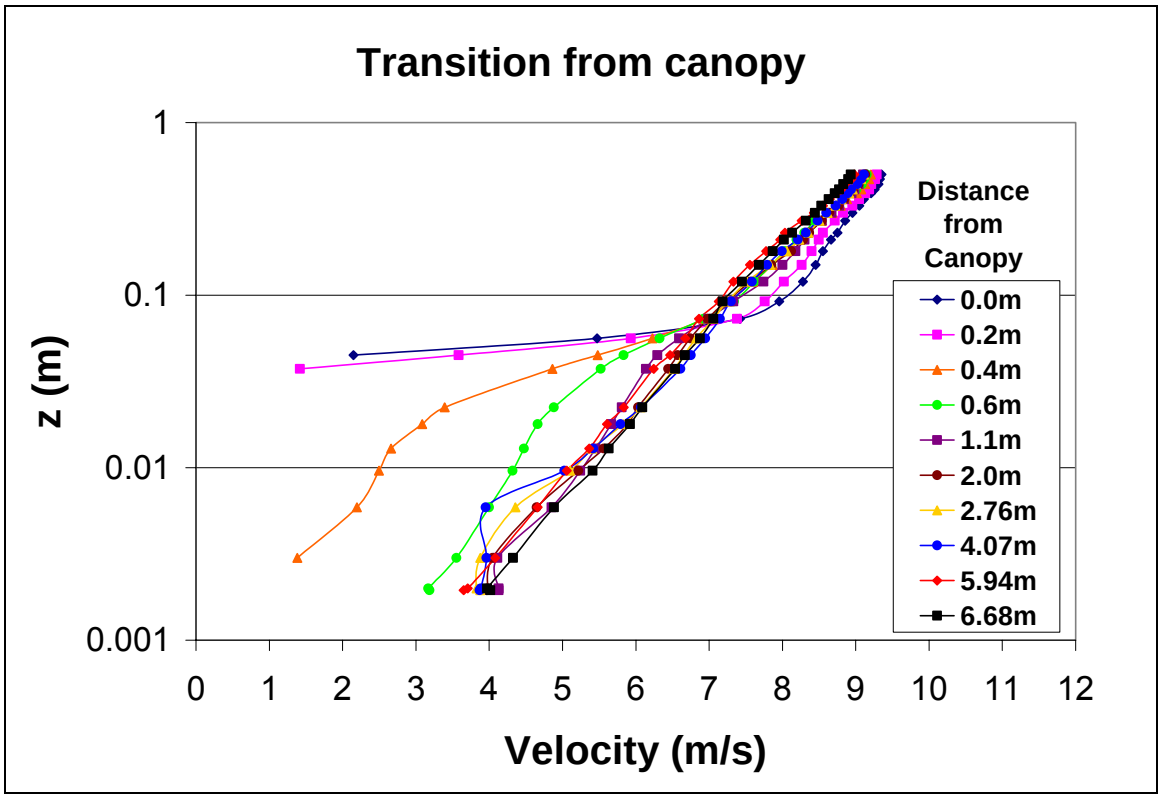

Figure 3.2: Semi-logarithmic plot of velocity profiles.

3.2 Surface (boundary) layer: surface roughness, surface shear stress, surface layer thickness downwind from the canopy

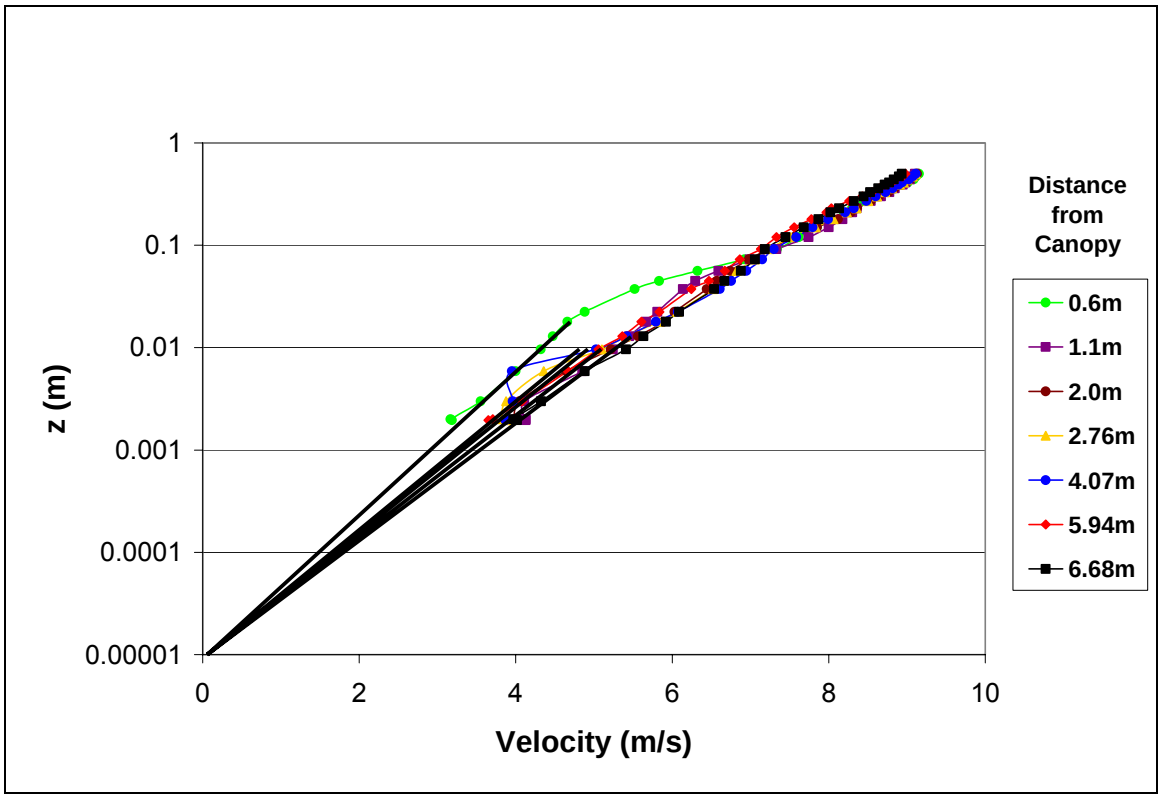

Figure 3.3 Determination of surface roughness (z_{os}) downstream from canopy

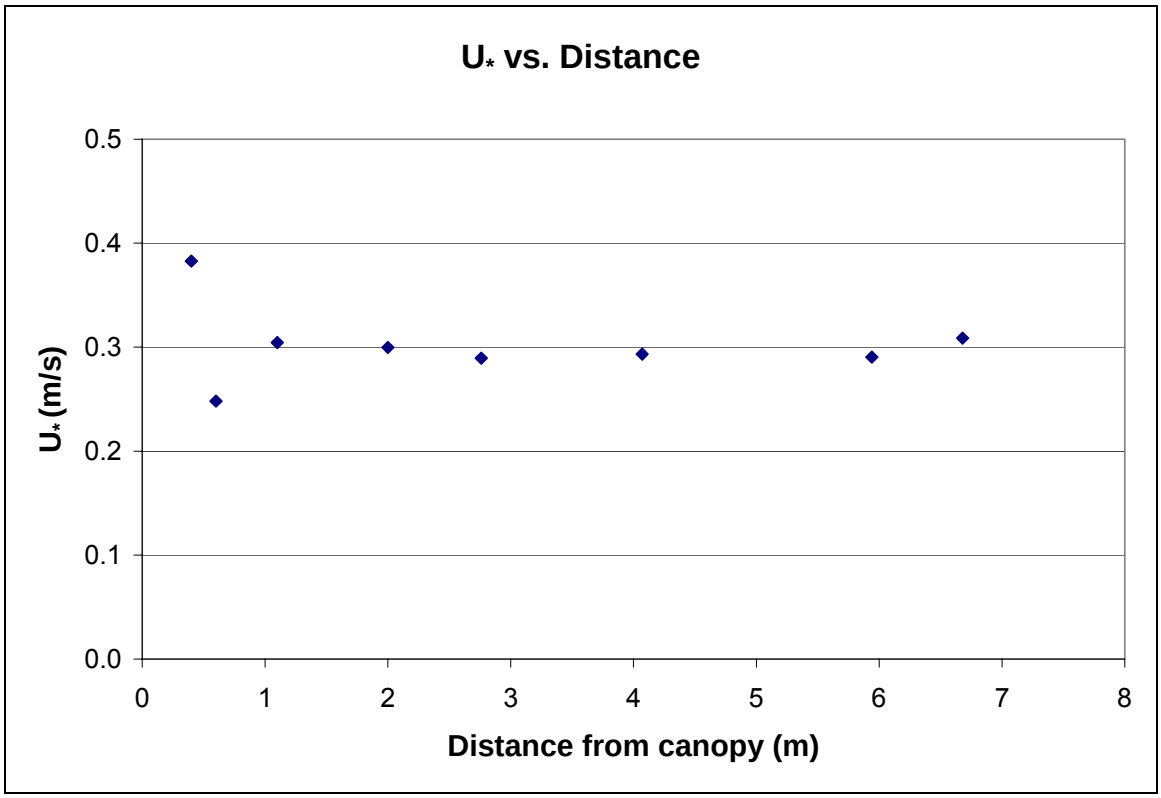

Figure 3.4 Shear velocity (U*) vs. distance from canopy

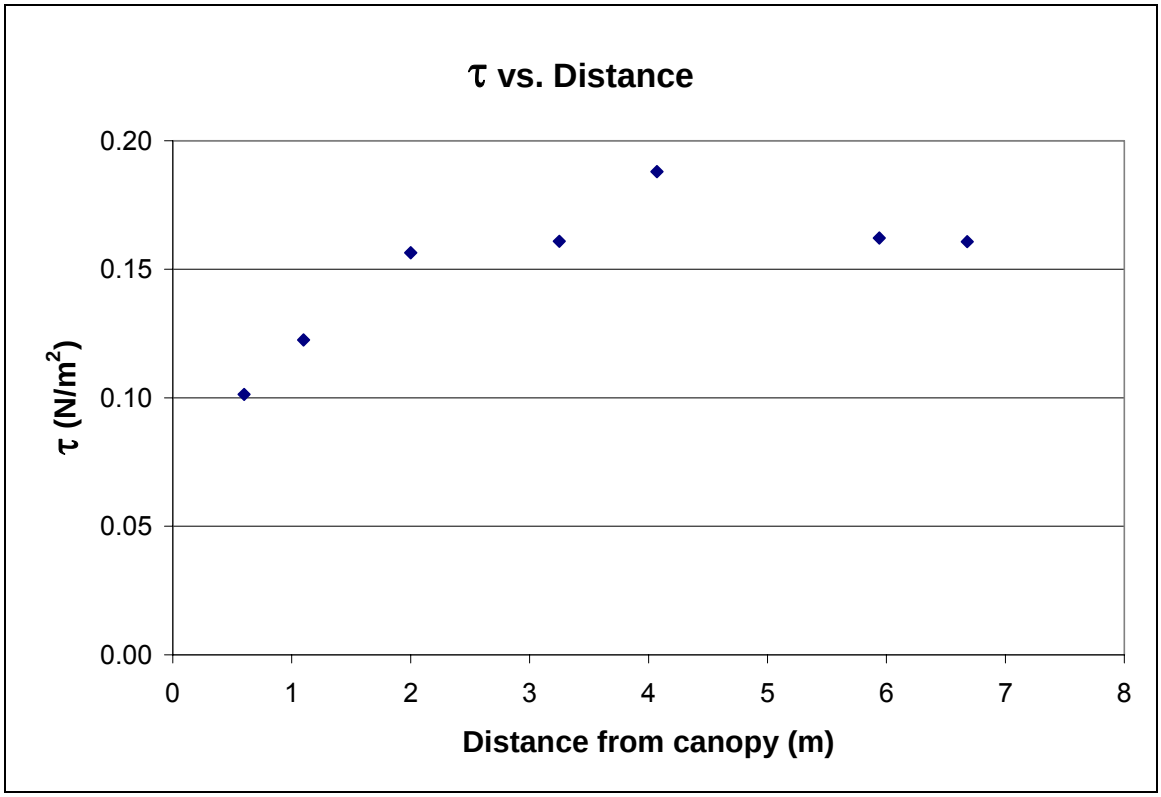

Figure 3.5 Surface shear stress (τ) vs. distance from canopy

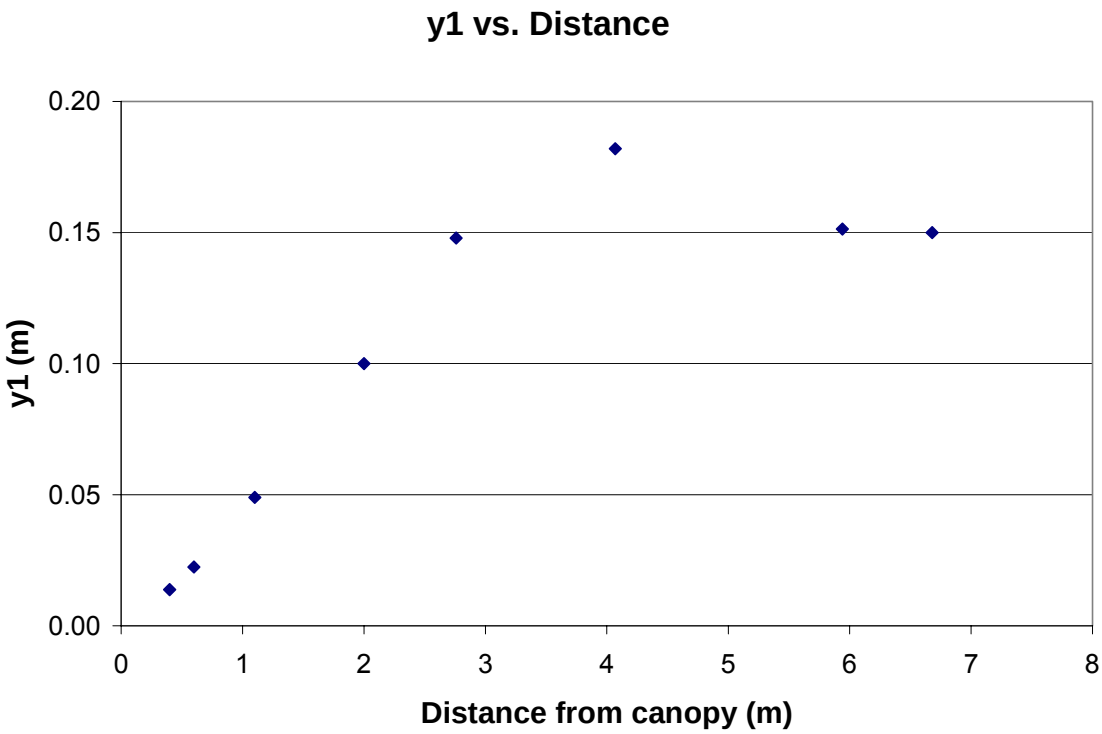

Figure 3.6 Upper end of surface layer (y1) vs. distance from canopy

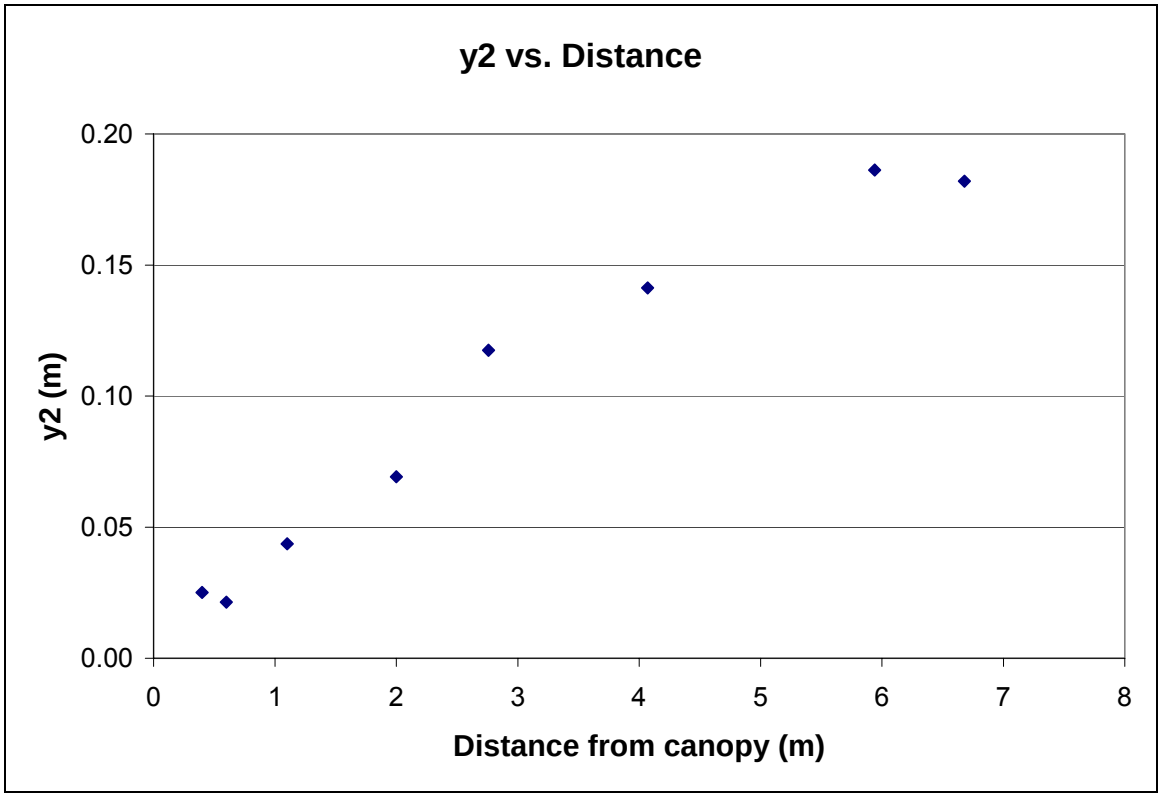

Figure 3.7 Lower end of blending layer (y2) vs. distance from canopy

3.3 Mixing (transition/blending) layer: surface roughness, surface shear stress, and surface layer thickness downwind from canopy

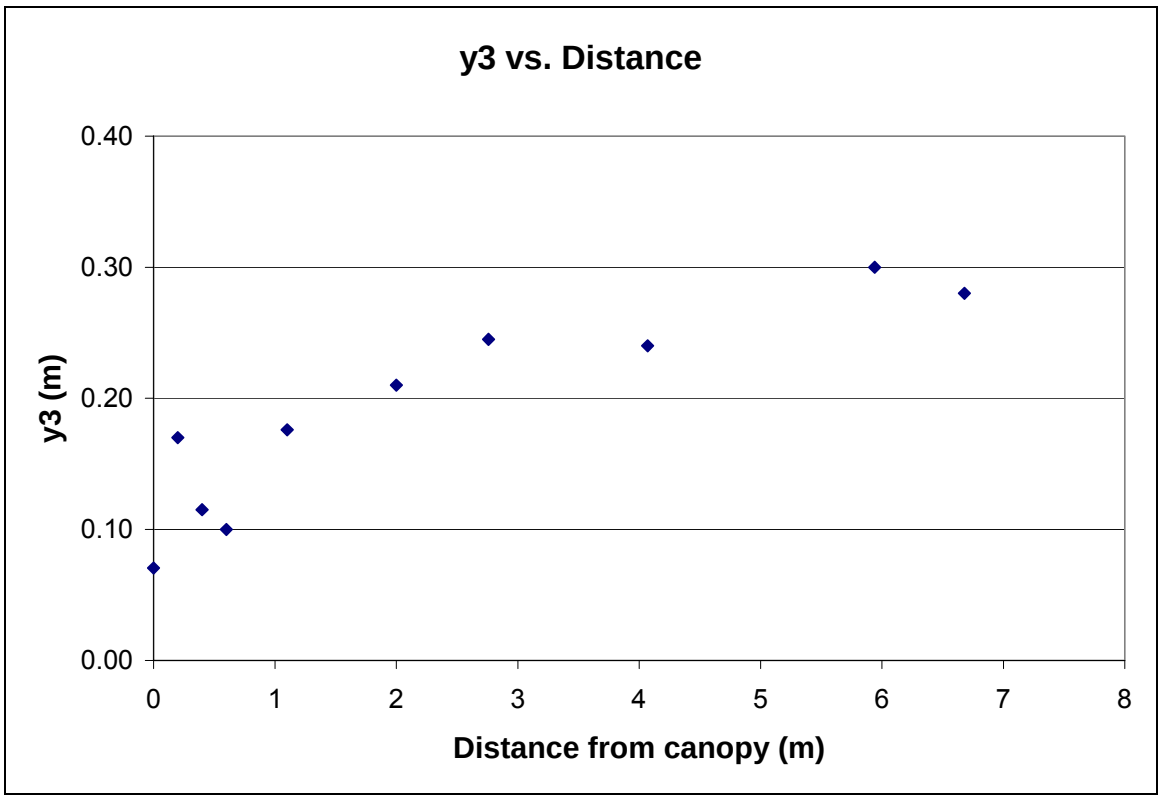

Figure 3.9 Upper end of the blending layer (y3) vs. distance from canopy

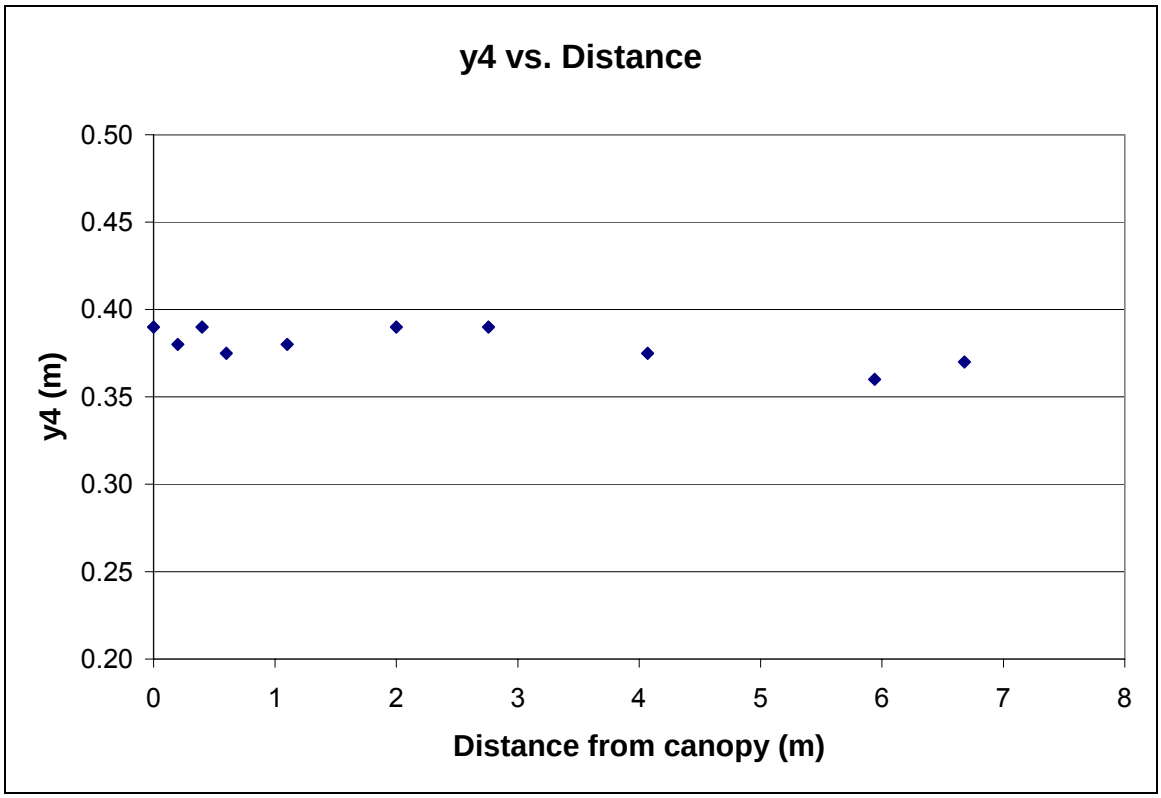

Figure 3.10 Lower end of outer layer (y4) vs. distance from canopy

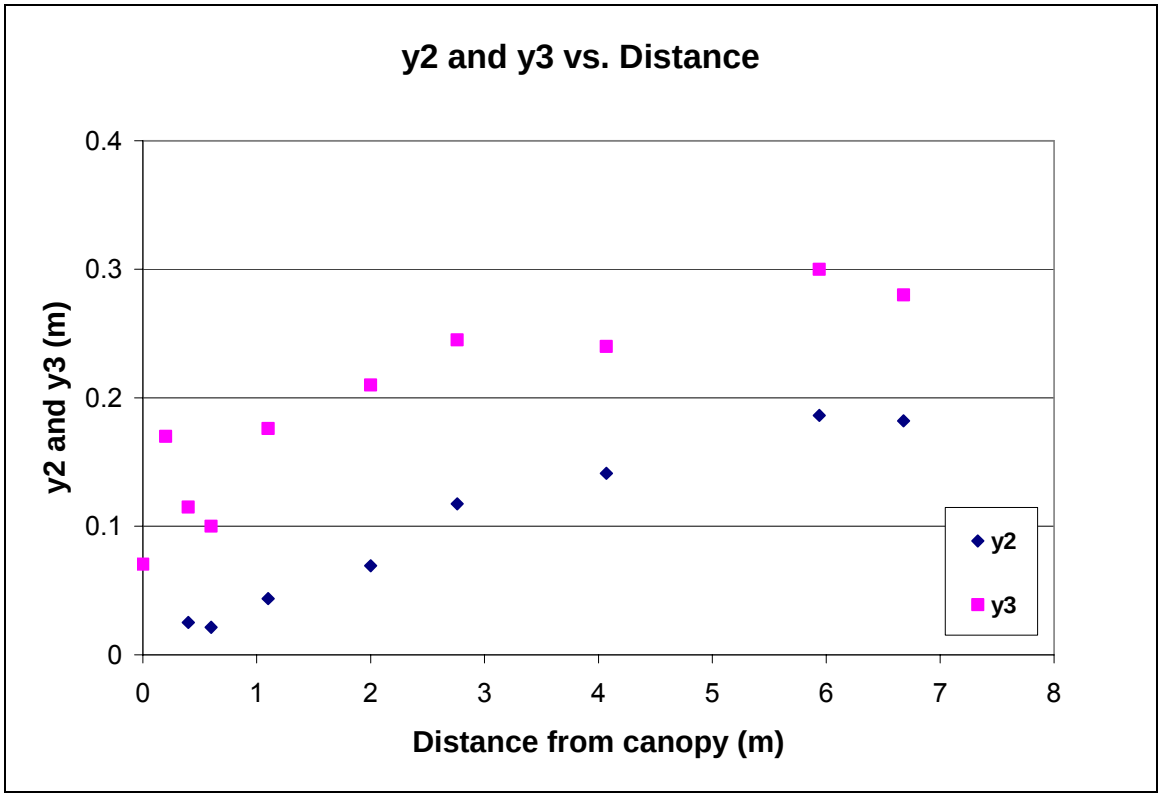

Figure 3.12 Upper (y3) and lower (y2) end of the mixing/blending layer vs. distance from the canopy. The distance between y2 and y3 is the **thickness of the mixing/blending layer**

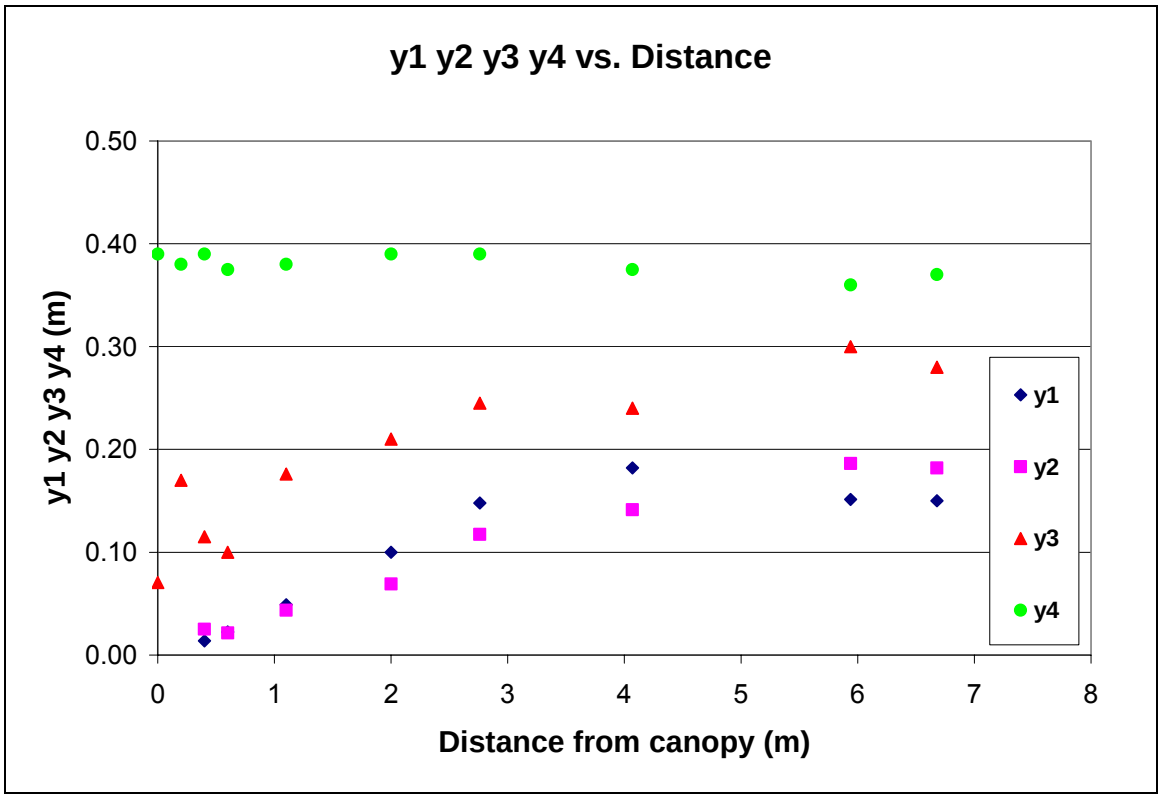

Figure 3.14 Upper and lower boundaries of the surface layer, the mixing layer and the outer layer

3.4 Outer (freee stream) layer

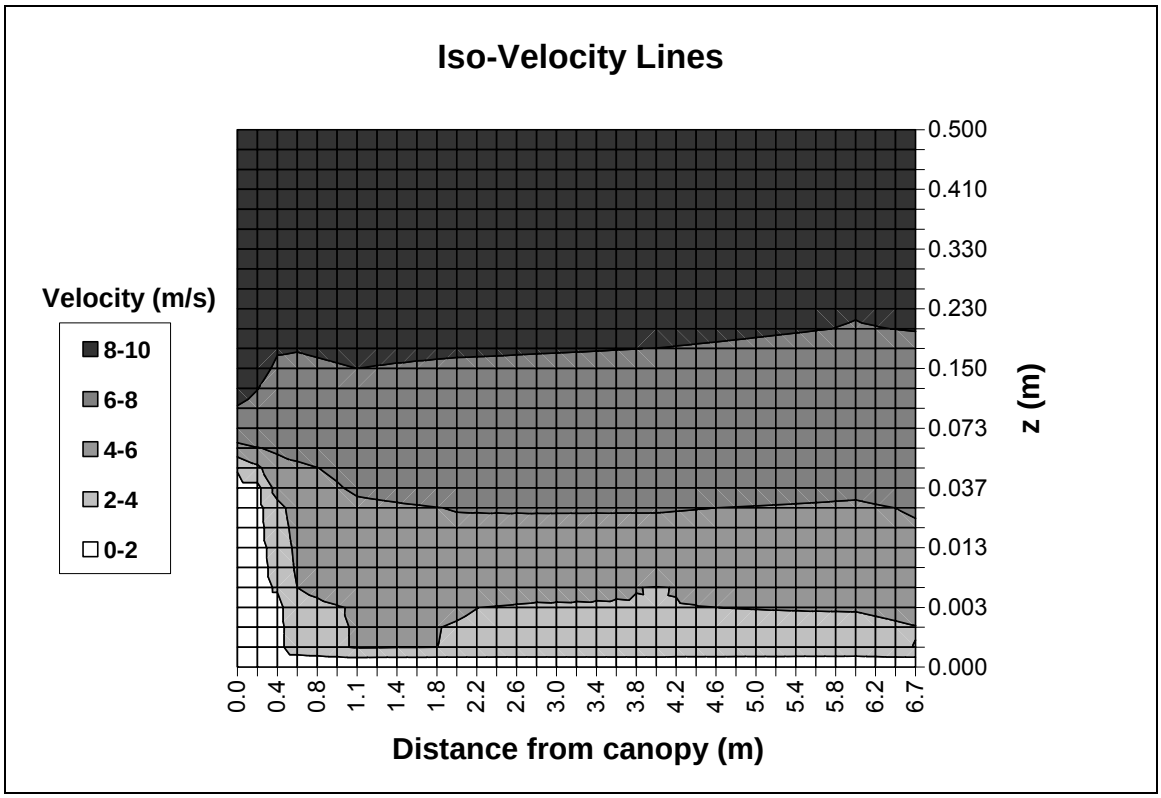

Figure 3.15: Iso-velocity lines plotted with 2 m/s intervals.

3.5 Mass and momentum flow downwind from the canopy

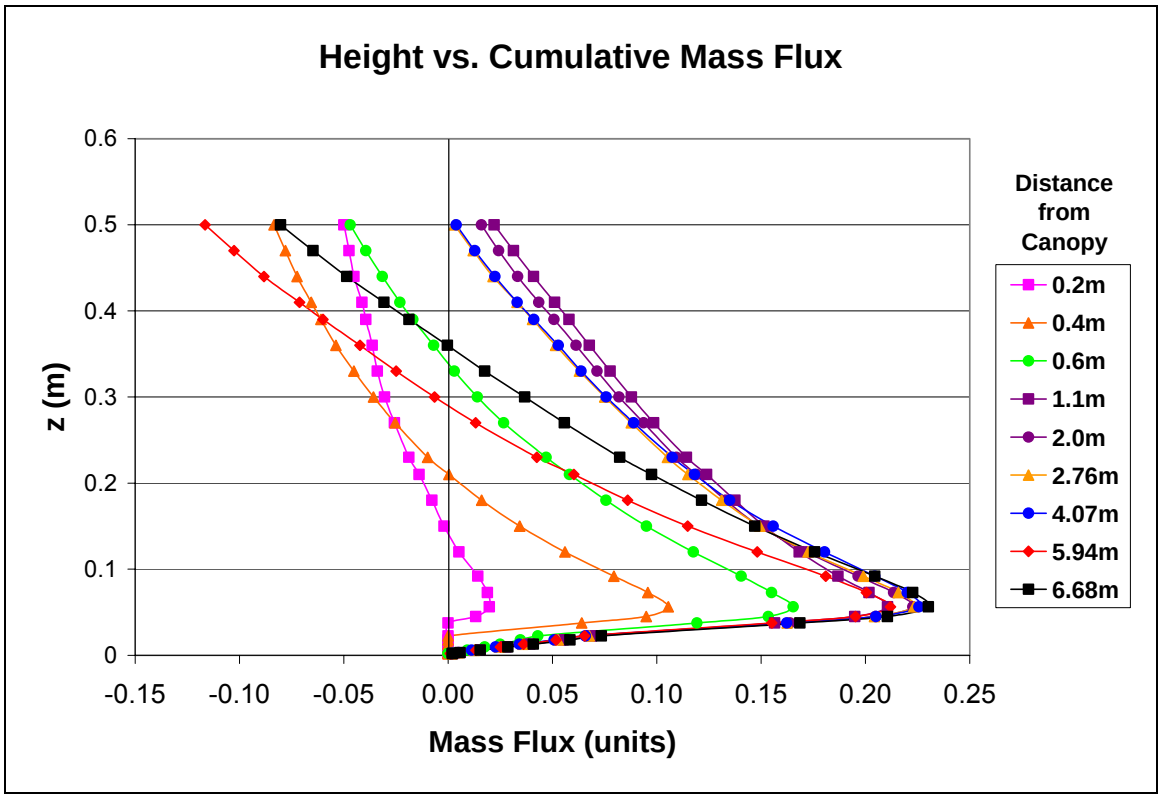

Figure 3.16 Cumulative mass flow downwind from the canopy

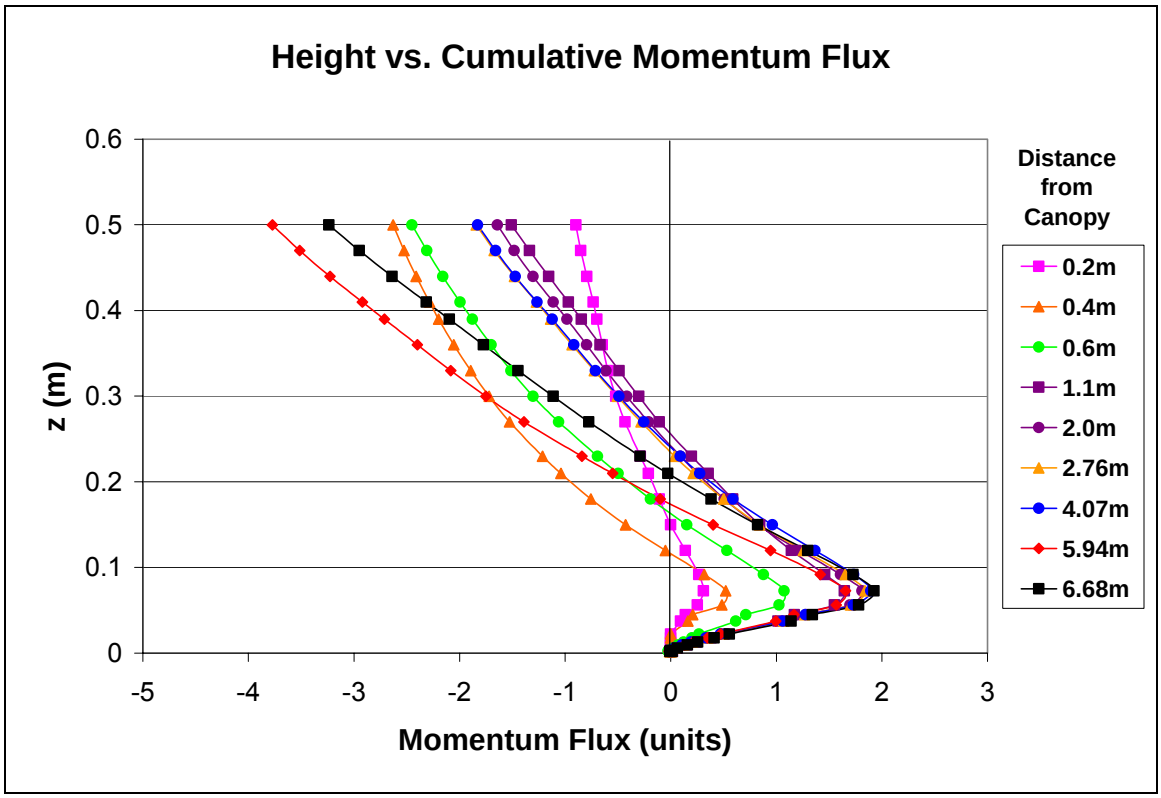

Figure 3.17 Cumulative momentum flow downwind from the canopy.

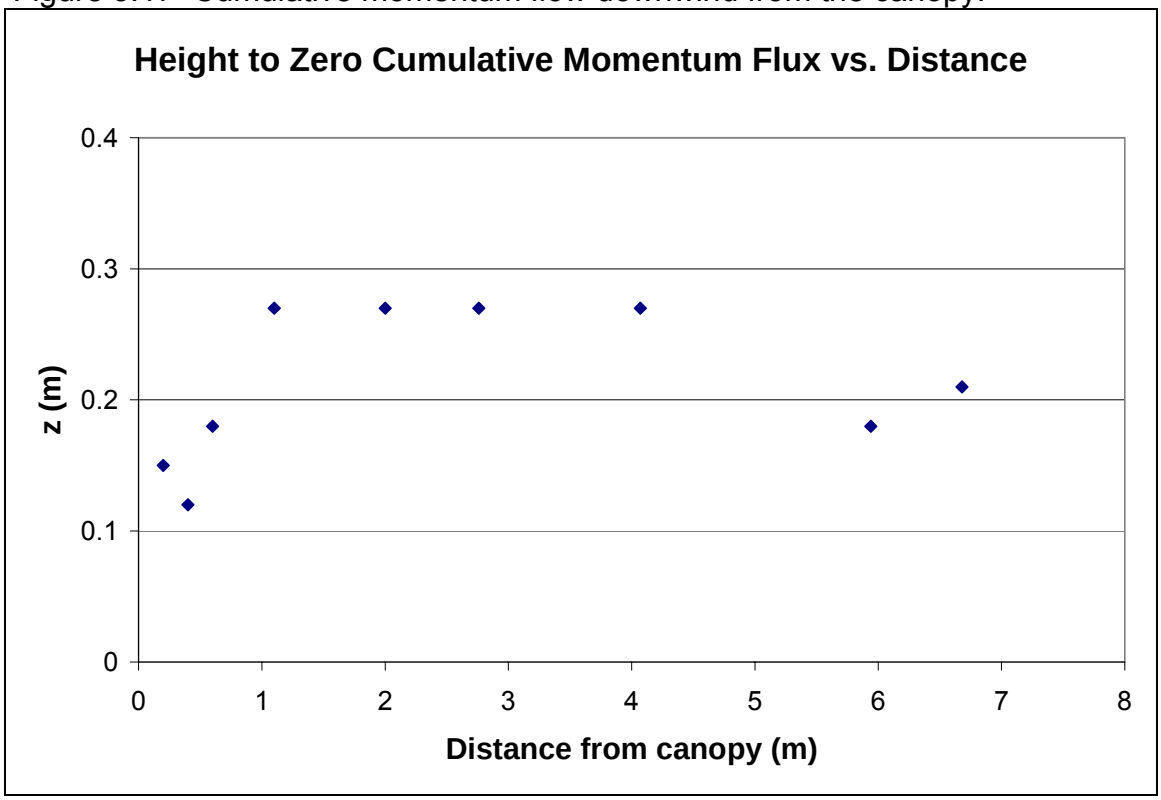

Figure 3.22 Height of no change of cumulative flow of momentum between x=0 and a distance (x) downwind from the canopy

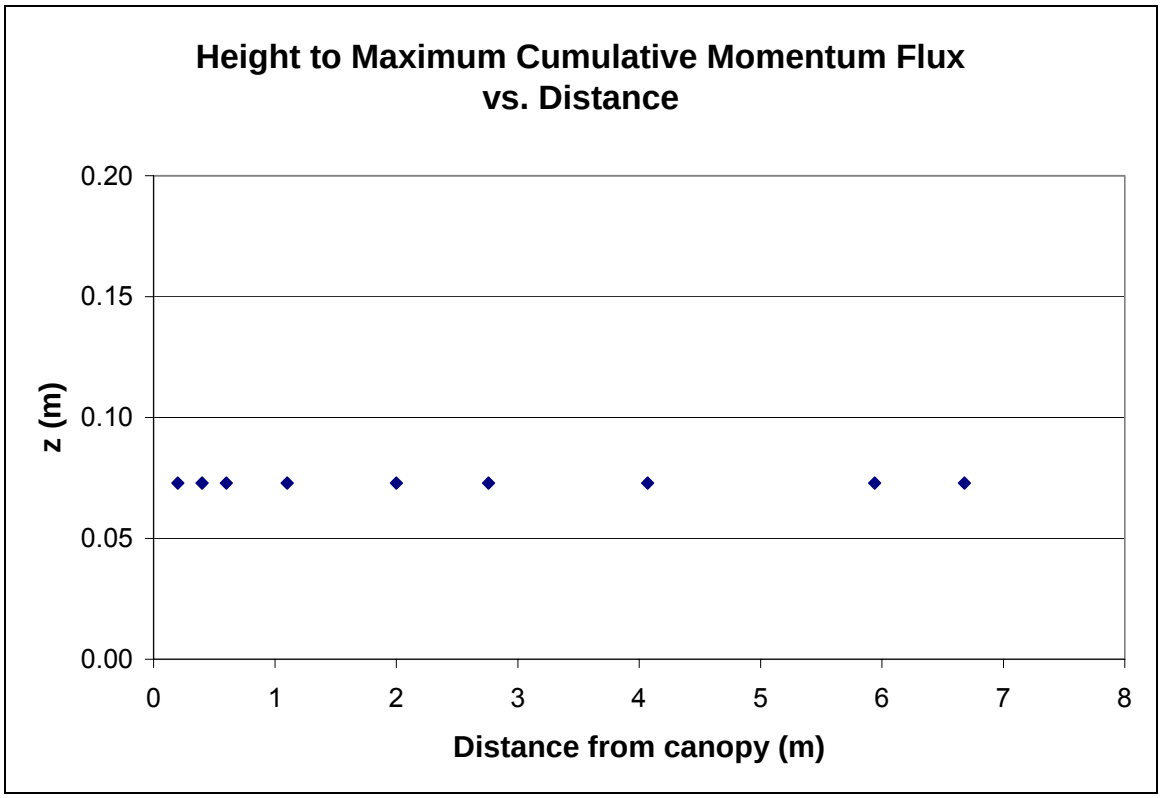

Figure 3.23 Height of maximum change in cumulative flow of momentum

3.6 Shear stress distribution in the wind field downwind from the canopy

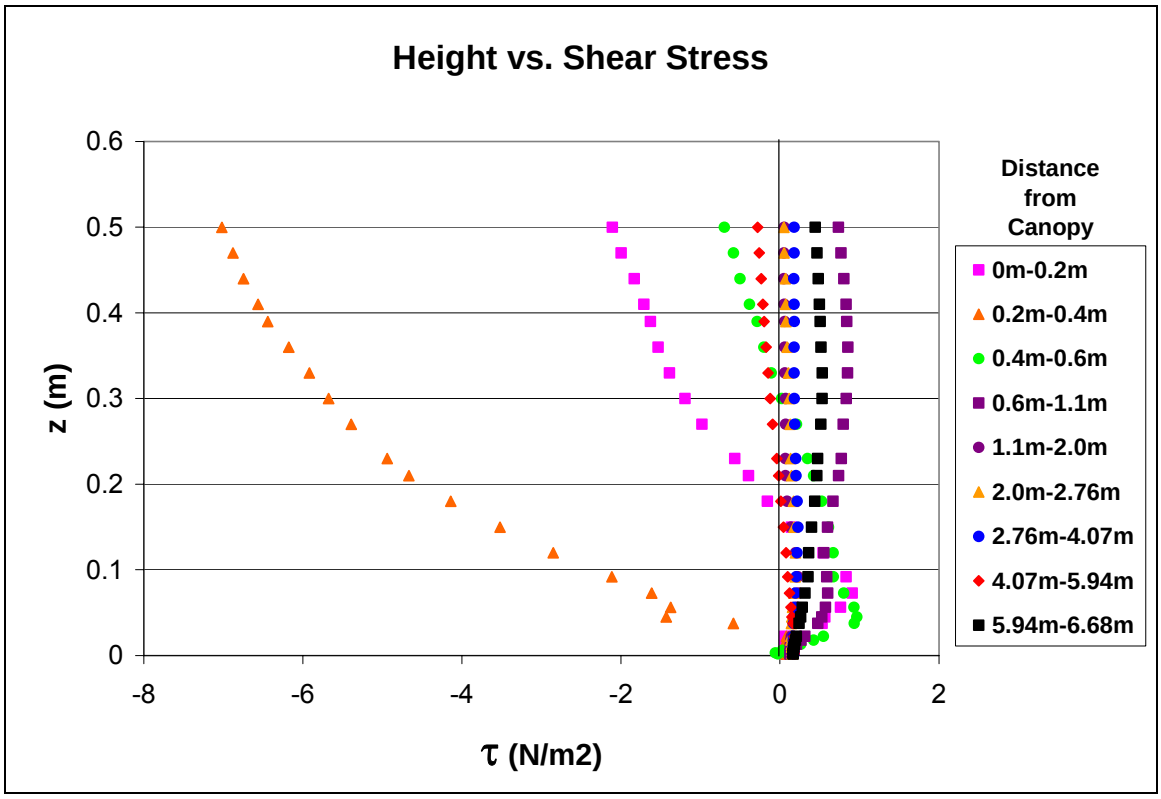

Figure 3.24 Shear stress throughout the wind field

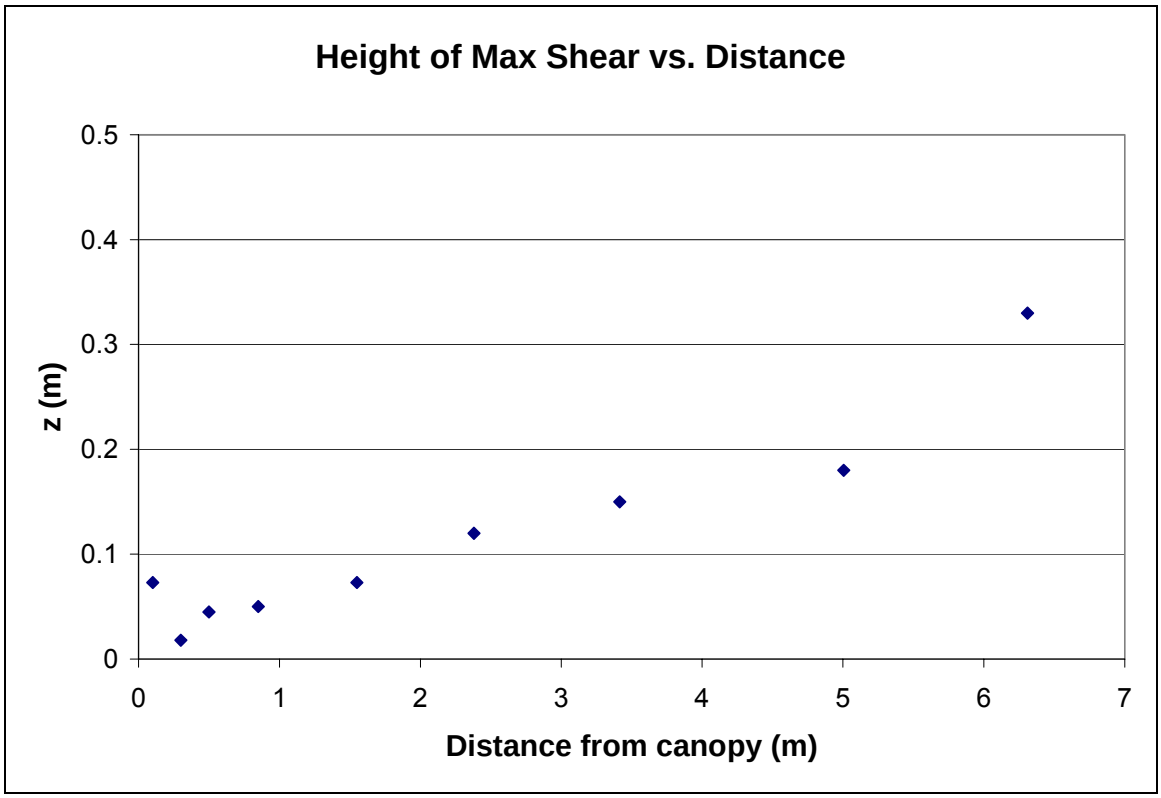

Figure 3.25 Height of maximum shear stress vs. distance downwind of canopy

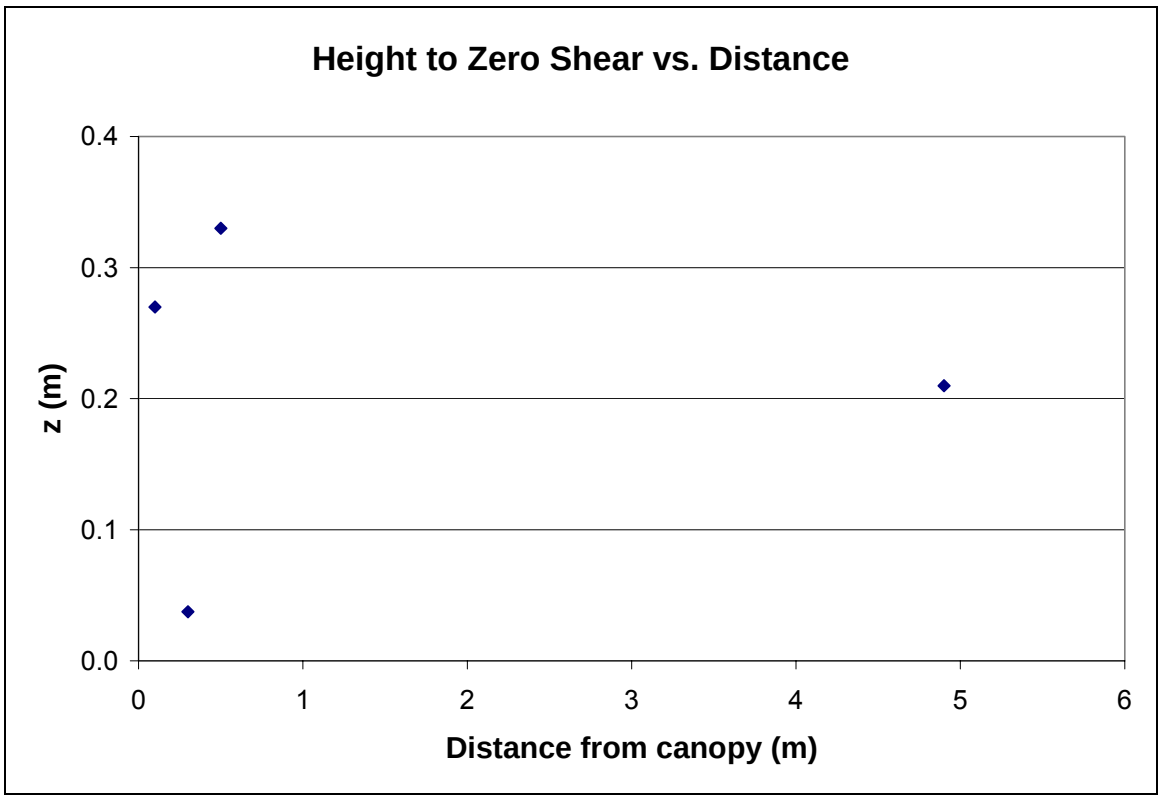

Figure 3.26 Height to zero shear stress vs. distance downwind from the canopy

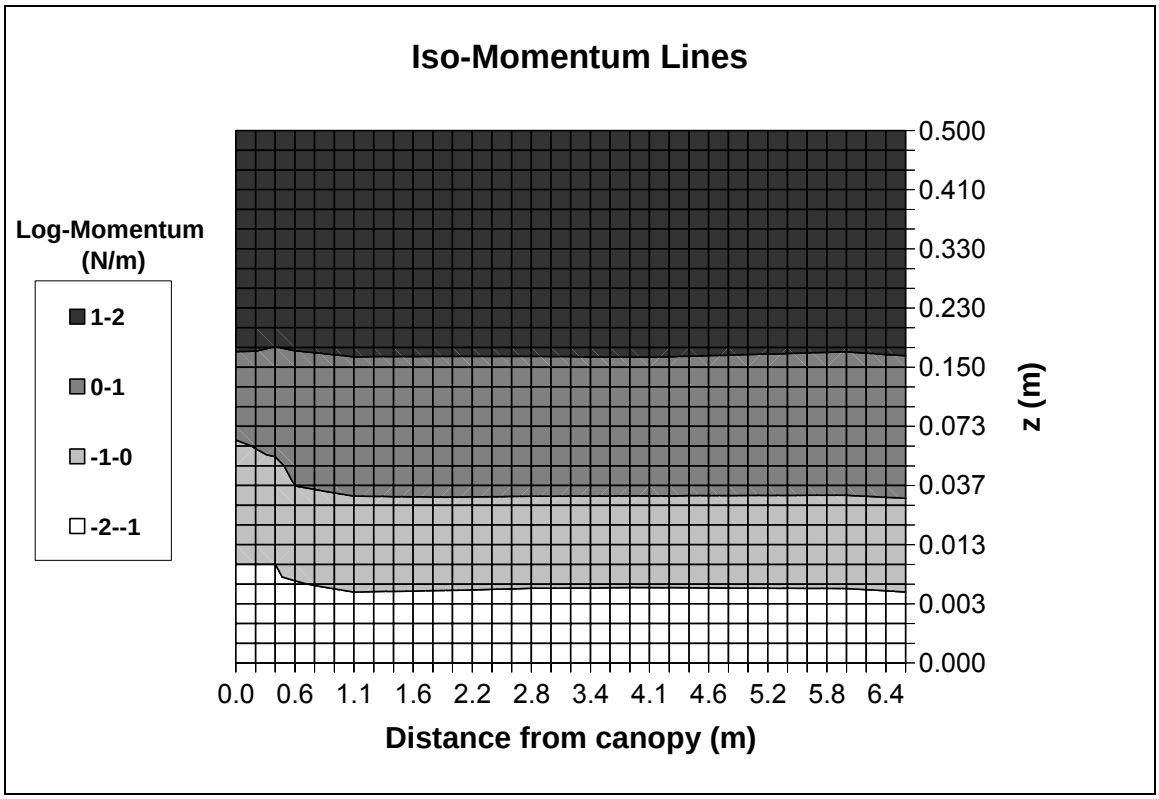

Figure 3.28 Iso-momentum flow lines downwind from the canopy.

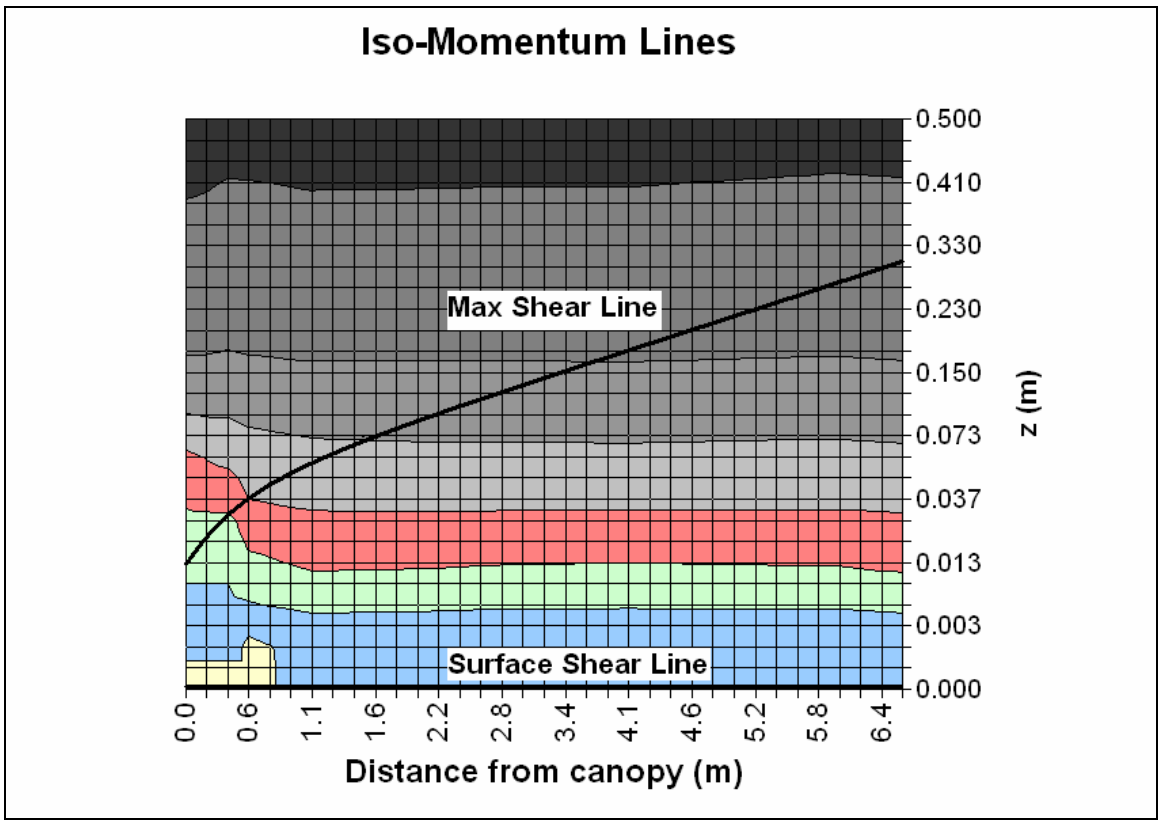

Figure 3.29 Iso-momentum flow lines and shear stress lines

4. Discussion

4.1 Aerodynamic characterization of the canopy by roughness and displacement height

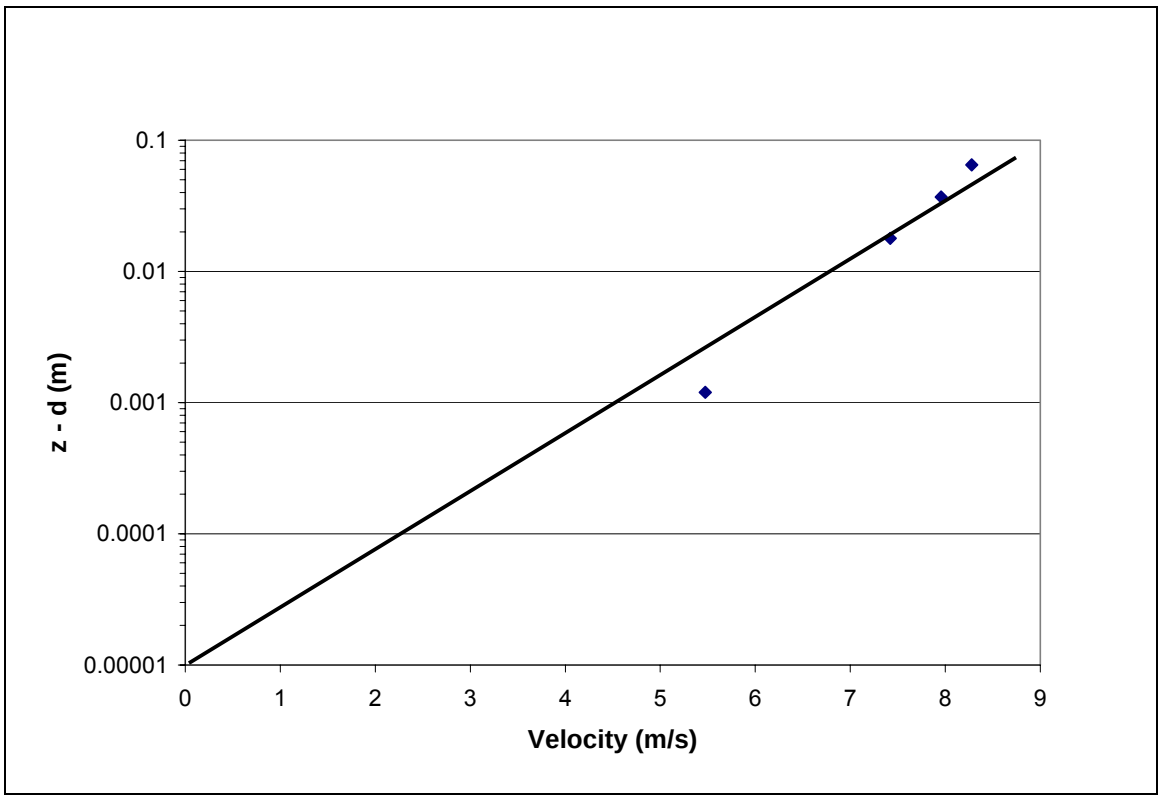

Figure 4.1 Determination of canopy roughness (z_{0c}).